POLITECNICO DI TORINO

Master's Degree in Biomedical Engineering
Address: Biomechanics
A.A. 2022/2023

Master's Thesis

How predictions of medial and lateral knee contact forces during walking, stair ascent and stair descent are affected by tibiofemoral alignment and contact locations in patients with knee osteoarthritis: a musculoskeletal modeling analysis

Graduation session: March 2023

Advisor:
Prof.ssa Cristina Bignardi
Co-advisor:
Ing. Giovanni Putame, PhD
External advisor:
Ing. Giordano Valente, PhD

Candidate:
Giulia Grenno

To my family

Abstract

Onset and progression of knee osteoarthritis and the cartilage degenerative process are related, among biological and mechanical factors, to the knee contact forces of the medial compartment, where the major percentage of the total contact force is transferred. Musculoskeletal modeling represents a state-of-the-art tool to predict knee contact forces, which are affected by two major geometric parameters: tibiofemoral alignment and contact point locations. Recent research show that medial contact force has a controversial level of correlation with tibiofemoral alignment and a marked correlation with contact points. However, there are limited and controversial data on osteoarthritis subjects, and few studies analyzing activities different from walking and without the inclusion of the geometric parameters. Therefore, the aim of this thesis is to evaluate how medial and lateral knee contact forces during walking, stair ascent and stair descent are affected by the inclusion of personalized tibiofemoral alignment and contact points in knee osteoarthritis patients, and to analyze the relationship between the knee contact forces and the geometric parameters.

Fifty-one knee osteoarthritis patients participated in this study. Weight-bearing radiographs were acquired to measure tibiofemoral alignment and contact points by using in-house developed software. Motion capture data including 3D marker trajectories, ground reaction forces and EMG activities were recorded according to the established IORgait protocol. A validated full-body musculoskeletal model was used to calculate knee contact forces during the different motor activities by implementing an inverse-dynamics and static optimization workflow in OpenSim. We created four sets of models with increasing level of personalization in geometric parameters for each patient and performed the simulations of motion. To analyze the effect of geometric parameters, we evaluated statistically significant differences in knee contact forces among models across the activity cycles (statistical parametric mapping with non-parametric paired t-tests), and statistically significant differences among the force peaks

(Mann-Whitney U-tests). To analyze the relationship between force peaks and geometric parameters, we performed a linear regression analysis (R, p).

We found significant differences in knee contact forces among all models in most of the activity cycles during all motor activities. The largest difference was found between the tibiofemoral alignment and contact point personalized models, which could reach a 1.2 body-weight mean difference in the medial force during walking and stair ascent, and 1.3 body-weight mean difference in the lateral force during stair descent. Almost all force peak distributions were found statistically significant different among models. Mild significant correlations were found between medial contact force and tibiofemoral alignment during stair descent only, while more marked correlations were found between medial and lateral contact forces and medial contact points during walking and stair descent ($p < 0.05$). Finally, an indirect model validation showed marked correlation between predicted muscle activations and recorded EMG activities.

This study demonstrated the large impact of the geometric parameters, mostly contact points, on the medial and lateral contact forces during different motor activities via musculoskeletal modeling. There is a lateral shift of the knee loads when introducing the contact point personalization, more marked in more complex motor activities (e.g. stair descent). Contact point locations had a more significant effect on the medial and lateral contact forces than tibiofemoral alignment in knee osteoarthritis patients. Further investigation will evaluate how the effect of contact point locations can be included in clinical scenarios to reduce medial loads and slow down osteoarthritis and how high tibial osteotomy affects knee contact forces and their relationship with the geometric parameters.

.

Contents

Chapter 1

Introduction

Knee is one of the main joints in the lower limb and its proper functioning is essential for an effective deambulation. For this reason, it is crucial to study and better understand its biomechanics.

Like all joints, also the knee suffers from pathologies affecting the progressive degradation of the cartilage. Among these, one of the most widespread is certainly osteoarthritis (OA), a chronic and degenerative joint disease that involves damage to the cartilaginous tissue as well as to the surrounding ones. It causes pain, stiffness and progressive loss of motor functions bringing many people into a condition of disability, which refers to a limitation in carrying out the usual task activities that are considered typical and socially expected [1]. The increase in the average age, in the cases of obesity in global population an in the numbers of joint injuries has meant that this pathology is taking hold even more than the past decades [2]. In addition to being a progressively disabling disease for the patient, it's therefore also proving to be an important burden for health systems and at a socio-economic level [3]

In cases where the disease presents severe and disabling traits the gold standard for treating this condition, as well as some knee fractures, is total knee arthroplasty [4]. This surgery operation allows to restore the possibility of carrying out activities such as climbing stairs or taking a simple walk. Primary hip and knee arthroplasty rank among the most performed surgeries and also among those with the fastest growth rate in the recent years in the United States [3] and a further increase is also expected in the years to come. Prevention and early detection plans are essential to detect the disease in its early stages to slow its course. It is also crucial to understand what factors most influence it.

Tibiofemoral varus malalignment appears to be related to the onset of OA of the medial compartment which is a common condition in patients after the age of 30. In fact, this condition affects the load distribution in the medial and lateral compartments of the knee. The best approach to characterize the biomechanical environment of the knee is multibody modeling of the musculoskeletal system, personalized with features obtained from clinical imaging. Computational techniques offer a non-invasive solution that does not modify the knee's biomechanics and have the advantage of being applicable to a greater number of subjects when compared to the calculation of joint contact forces in vivo. Creating musculoskeletal models that can reliably and accurately predict joint contact forces and muscle forces during movement is challenging for the complexity and amount of data needed, and for the sensitivity of the different parameters involved. The major geometric parameters of the knee that influence the predictions of medial and lateral KCF via musculoskeletal modeling include tibiofemoral alignment in the frontal plane (TFA) and contact point (CP) locations, i.e. the centers of pressure between femur and tibia [5], [6]. Most studies calculating knee contact forces (KCFs) and their distribution involve subjects with total knee replacement and there are limited and controversial data on healthy and OA subjects with limited sample sizes. Additionally, the few studies analysing activities different from walking, such as stair ascent and descent, did not include the effect of the geometric parameters [7], [8]. Therefore, it is unclear how variable are KCFs and their distribution when the personalized geometric parameters are considered during different activities in knee OA subjects, and so is the consequent relationship between KCF distribution and the geometric parameters.

A clinical trial started in 2021 at the Rizzoli Orthopaedic Institute in Bologna involved 50 patients with genu varum deformity and medial compartment OA, to study the effect of High Tibial Osteotomy (HTO) in slowing down the course of the disease by avoiding total knee arthroplasty or unicompartmental arthroplasty operations. HTO represents a surgery that involves the modification of the joint biomechanics allowing to preserve the actual joint. HTO modifies the tibiofemoral alignment which allows to change the distribution of joint loads leading to clinically significant improvements in the quality of the cartilage and subchondral bone, slowing down the course of OA itself. In the context of this project, one objective is to characterize the distribution of the knee contact forces via musculoskeletal modelling before and after the treatment. To the purpose, data from gait analysis during different motor activities as well as clinical imaging data were acquired for all the patients involved, and consequently used for the present master's thesis.

The main purposes were to evaluate: 1) how predictions of medial and lateral knee contact forces during daily activities are affected by tibiofemoral alignment and contact locations in patient with early-stage knee osteoarthritis, 2) what is the relationship between medial and lateral contact forces during daily activities and the knee geometric parameters. Since in vivo measurements of joint contact forces and muscle forces are not possible, estimations of load distributions were performed using musculoskeletal models. These models, customized with the anthropometric characteristics of each patient, enable the estimation of moments and forces in the medial and lateral compartment of the knee and allowed us to understand how the geometric parameters of interest affect the forces estimated among the models.

The introductory part of this work is written to provide the reader with both clinical and modeling background. There is a brief anatomical description of the bony segments of the knee and all those structures that allow it to function properly. OA is introduced highlighting its risk factors and the main techniques implemented for its containment. Finally, it is briefly explained what is meant by musculoskeletal modeling, what software is used to perform the simulations with an explanation of the workflow steps and what the state of the art is based on a literature review.

In Chapter 3 we aim to describe in detail what materials and methods were used to carry out this thesis. A description is given of the cohort of patients involved by the clinical study and the data available to carry out the simulations. The process by which it was possible to determine TFAs and CPs is explained. The reference musculoskeletal model is described, and it is explained what models were made based on the customization parameters estimated by imaging. The workflow used to perform the simulations is described in detail. There are two sections in which the post-processing of the contact forces and EMG/Activations signals is discussed in the first section, it is explained how, from the data coming out of the simulation process, the joint forces and muscle activations are estimated, and it is described what statistical analysis was carried out to go on to characterize the differences between the models and the correlations between the estimated forces and the personalization parameters. Instead, in the second one explains how the post-processing of the activations (an output of our simulations) and EMG signals was done and how they were treated to make it possible to compare them.

Chapter 4 contains the results of the analyses performed on the post-processed data in each task and for each model made. The first section reports the results obtained through Statistical Parametric Mapping ($\alpha = 0.05$), the differences between the averages of the forces estimated through the four models, the boxplots, medians, and interquartile ranges associated with the distributions of the first and second peak forces, and the results of the Wilcoxon signed-rank test ($\alpha = 0.05$) to make their differences explicit. This chapter also includes the outcomes of the correlations between the geometric parameters used to customize models and the two force peaks obtained using the two models personalized with that parameter. In support of the indirect validation of the models used, temporal correlation and RMSEs obtained between the EMG signals and the predicted muscle activations are reported.

The answers to the research questions and interpretations of the data are contained in the last two chapters. The results obtained were compared with those in the literature, and an attempt was made to understand which geometric parameter was most impactful for the estimation of the joint loads acting on the two knee compartments. A brief analysis was made regarding the limitations associated with the model used and possible future developments.

Chapter 2
Background

2.1 Anatomical references

Before introducing the anatomical part of interest, it could be useful to make a quick description of the anatomical planes and the respective axes taken as reference. Anatomical planes are nothing more than hypothetical planes used to describe the position of the various body segments. The most used are certainly:

- *The sagittal plane* - Runs in anteroposterior direction and allows the body to be divided into right and left parts.
- *The coronal plane* – Is the vertical plane that passes perpendicular to the sagittal plane and allows the body to be divided into anterior and posterior sections.
- *The transverse plane* - Corresponds to the horizontal plane. It is perpendicular to the previous two planes and allows to divide the body into an upper and a lower section.

The axes are identified as straight lines around which a body segment can rotate. Each joint movement corresponds to a rotation around an axis. Starting from the previously described planes, it is possible to derive 3 corresponding axes:

- *Sagittal axis*, formed by the intersection of the sagittal plane and the transverse plane.
- *Frontal axis*, formed by the intersection of the frontal and the transverse plane.
- *Vertical axis*, formed by the intersection of the sagittal and the frontal plane.

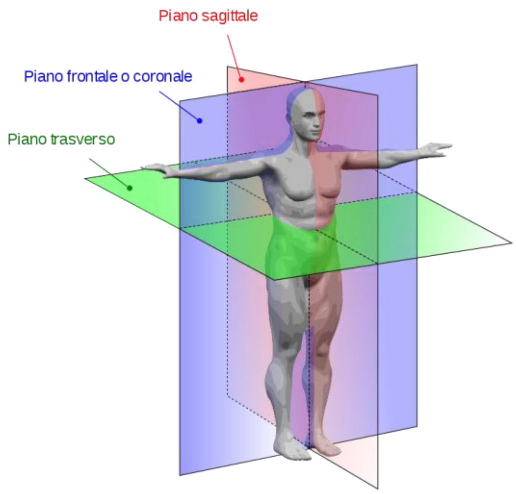

Figure 1: Anatomical planes

2.2 Knee anatomy

If not cited elsewhere consider the book “Anatomia Umana, basi anatomiche per la semeiotica” [65] as the reference for this section.

The knee is one of the largest, most complex and stressed synovial joints in the body. It takes care of supporting the weight of the body in an upright position, allows walking and can cushion the stresses due to the interaction with the support surfaces. It is composed of two different joints. The tibiofemoral one articulates femur and tibia, the patellofemoral articulates femur and patella. Stability is achieved by collaboration of muscles and tendons, which allow the movement of the bone segments in the sagittal plane and, to a small extent, rotation. As a diarthrosis joint it is bathed in synovial fluid which is contained inside the synovial membrane called the joint capsule.

2.2.1 Articular bodies

The bones primarily involved in the knee joint are femur, tibia and patella. Their articular surfaces are covered by a cartilaginous layer which, in addition to the presence of synovial fluid, further lowers the friction between the bone components.

The femur

The femur is the longest, heaviest and strongest bone in the human body which main function is weight bearing and stability of the gait. It is an essential component of the lower kinetic chain. Consists of two epiphyses, one proximal and one distal, and the diaphysis that is interposed between them. The distal epiphysis has two condyles: one medial and one lateral, convex in shape and covered by articular cartilage. These condyles are physically separated from each other posteriorly and inferiorly by the intercondylar fossa, femoral attachment site for the intracapsular ligaments. The medial condyle has a uniform thickness while the lateral one is wider in the front and narrower in the back. The patella articulates with the femur in the intercondylar groove, giving rise to the patellofemoral joint. The femoral condyles articulate with glenoid cavity of the proximal epiphysis of the tibia to form the tibiofemoral joint. Above the condyles, the femoral epicondyles can be found. These are important sites for the insertion of the collateral ligaments.

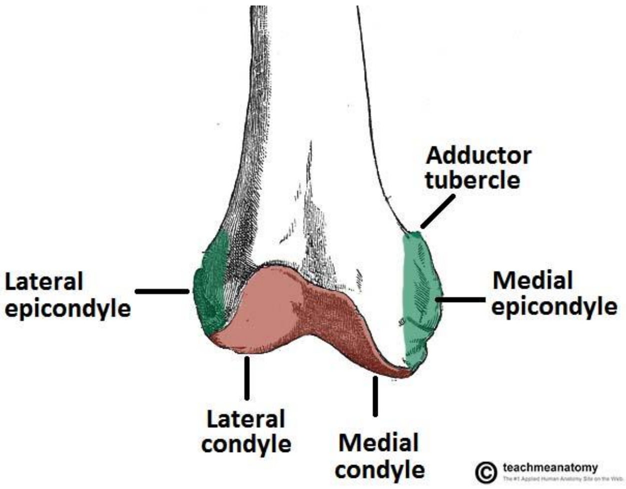

Figure 2: Distal femur anatomy [https://teachmeanatomy.info/lower-limb/bones/femur/]

The patella

The patella is a protruding, palpable bone that resides in the front of the knee joint. It is a sesamoid bone and often has the shape of an inverted triangle (the apex of the kneecap points downwards). It has an important anterior and posterior surface. The base is rough and is the site of insertion of important tendon structure, as the quadriceps femoris. The connection with the tibia is guaranteed by the patellar ligament. The back is smooth and covered with cartilage. It is properly located when it resides withing the femoral intercondylar groove. Worthy of note are its functions in view of the movement of the knee: it allows the proper extension of the leg, optimizes the work done by quadriceps and guarantees protection for the articular elements of the knee.

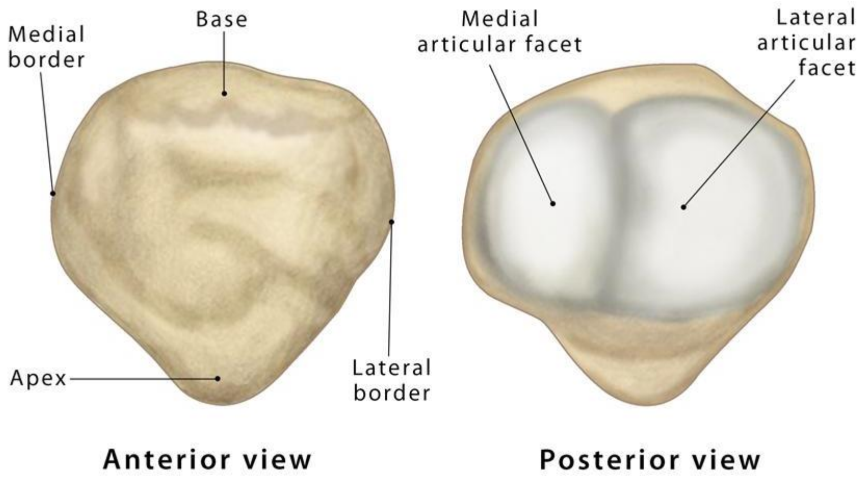

Figure 3: Patella anatomy [https://www.theskeletalsystem.net/wp-content/uploads/2021/12/Patella-Bone-Labeled.jpg]

The tibia

The tibia is the main bone of the lower leg, the second largest bone in the body and it is a key weight-bearing structure. It expands at its proximal and distal ends, articulating the knee and ankle joints respectively. Like the femur, the tibia also has a medial and a lateral condyle, anatomically asymmetrical to each other. They are mostly flat, which is why they are known as tibial plateau. The upper surface of the condyles, covered by cartilage, forms the articular face that is in contact with the femoral condyles. On the midline are located two tubercles, one medial and one lateral. These are two bony spines that, during the flexion-extension movement, they lodge in the intercondylar notch of the femur giving stability to the joint. Despite their presence, it can be said that the joint itself is relatively unstable. For this reason, other accessory joint structures such as menisci, muscles and tendons are essential.

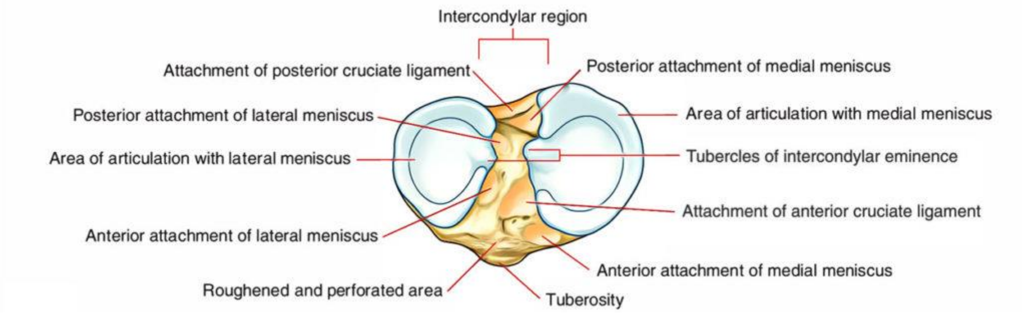

Figure 4: Tibial plateau [https://www.earthslab.com/anatomy/tibial-plateau/]

The fibula

The fibula is located next to the tibia but does not directly take part in the tibiofemoral joint, so it is not a weight-bearer. Despite this, this bone has a great (?) importance because it's the anchoring site for numerous muscles and ligaments that play fundamental roles for the correct joint function.

2.2.2 Articular capsule

The joint capsule is made of mostly fibrous tissue generated by the tendon endings and their extensions and of an inner synovial membrane. It is a relatively weak material. It is loose and broad, of variable thickness. Laterally it lies deep in relation to the tendon of the quadriceps femoris muscle. Posteriorly, the capsule contains fibres extending from the articular edges of the femoral condyles, the intercondylar notch and the proximal tibia. On the anterior side of the capsule, the ligaments mainly have the function of stabilizing the patella.

2.2.3 Synovial membrane

The synovial membrane of the knee is very extensive and particularly complex. On the anterior side it extends upward passing behind the tendon of the quadriceps femoris muscle, forming the suprapatellar bursa. The synovial membrane lines the inner surface of a fibroadipose pad called the infrapatellar body. On the sides, this membrane descends from the femur to the menisci but does not cover them. The anterior cruciate ligament is surrounded by the synovial membrane while the posterior ligament is only partially covered. In the posterior side two expansions of the membrane form the bursae of the gastrocnemius muscle. They serve as protection of the proximal attachment site of these muscles. The bursae, in fact, are structures filled with fluid that are located between the skin and the tendon or between the tendon or the bone [9].

2.2.4 Cartilage

Cartilage is an elastic tissue with considerable resistance to pressure and traction. It has a pearly white color and coats the joint bone ends to protect them from friction. Another important role is certainly the structural one. Thanks to its rigidity, in fact, the cartilage is used to keep open tubes such as the trachea one. There are 3 types of cartilage:

1. The hyaline cartilage, it's the type that can be found at an articular level. It helps lower friction between bone ends and to distribute weight properly. It can be in contact with menisci or other articular disks, but it is considered as an independent structure. Its extracellular matrix has a high specialized architecture and for this reason is possible to divide in different zones: the superficial zone is rich of collagen II fibers while the deep zone is structured to absorb compressive loads.
2. The elastic cartilage is more flexible than the previous one.
3. The fibrocartilage is tough and inflexible.

2.2.5 Menisci

The menisci are intracapsular structures of a fibrocartilaginous nature which have the aim of increasing the tibial articular surface. They have a half-moon shape, and their ends are fixed on the anterior and posterior intercondylar areas of the tibia and by the ligament expansions. The side that lies on the upper surface of the tibia is flat, the upper one, which is in touch with the condyles, is concave. One of the main functions performed by menisci is to increase the surface are assigned to absorb force. They compensate the poor congruence existing between both surfaces of femur and tibia, also due to their different curvature. They also contribute to distributing joint pressure and therefore to uniformly stress the tibiofemoral joint.

2.2.6 Ligaments and Muscles

The knee is a hinge joint ad it allows only a limited range of movements:

- Flexion – Allows to bring the knee towards the hip. Is limited to 135-140° in the average.
- Extensions – Allows to straighten the knee. It occurs when the knee is moved from a flexed position back.
- Rotations – In addition to flexion and extension, the knee joint can also perform a small amount of rotation. Rotation is allowed when the foot is lifted off the ground, in that case the tibia can rotate relative to the femur.

Any active movement that is made by the joint is the result of cooperation between muscle groups acting at its ends.

The muscles involved in flexion are:

1. Hamstrings (Semitendinosus, Semimembranosus, Biceps femoris)
2. Gastrocnemius
3. Gracilis
4. Sartorius
5. Popliteus

The muscles involved in extension are:

1. Quadricep femoris (rectus femoris, Vastus lateralis, Vastus medialis, Vastus intermedius)
2. Tensor Fascia Lata

The muscle involved in lateral rotation is:

1. Biceps Femoris

The muscles involved in rotation are:

1. Semitendinosus
2. Semimembranosus
3. Gracilis
4. Sartorius
5. Popliteus

However, not all muscles act with the same forces on the joint. In fact, some can exert greater forces than others. This depends on the amount and type of muscle fibers of which it is composed and on geometric characteristics of insertion on the bone segments of interest.

In tibiofemoral joint, the stability and the movements are also guaranteed by a complex system of intra and extra-articular ligaments. These ligaments work together to provide stability and support for the knee joint, allowing it to move smoothly and without pain. Injuries to these ligaments can occur through a variety of mechanisms, such as a sudden twisting motion or a direct blow to the knee. Among these we find:

- The *anterior cruciate ligament* and the *posterior cruciate ligament* are two ligaments located in the center of the knee. They are also called cruciform ligaments because they have a crossed conformation. In fact, the anterior cruciate ligament crosses the posterior cruciate ligament, forming an x. They are made from strong fibrous tissue and are responsible for managing the correct alignment between the femur and tibia.

- The *medial* and the *lateral collateral ligament* are located on the outside of the knee. They serve to hold the joint in place and support it during movement. The medial collateral connects the femur and tibia together. The lateral collateral connects the femur and fibula together.

- The oblique *popliteal ligament* originates near the posterior aspect of the tibia and then goes toward the lateral condyle of the femur. It can be seen as an expansion of the semimembranosus muscle.

2.3 Osteoarthritis

Degenerative diseases of the joints, especially osteoarthritis (OA), are among the most common disabling diseases in the world. OA itself occurs in particularly overloaded joints. The knee is the most common site of OA, followed by the hip and the hand [2]. Nowadays 1 adult in 4 has diagnosed OA in at least one joint and more than 1 in 8 has diagnosed OA of the knee [10]. Being a widespread disease and with further growth prospects, it constitutes an important burden for people’s lives, as regards health systems and due to socio-economic implications. In addition to the costs related to treatment, there is also the possibility of premature withdrawal from the workplace for those affected.

2.3.1 Pathogenesis

The cause of osteoarthritis is complicated and involves many factors such as mechanical stress, inflammation and metabolic changes that ultimately lead to the breakdown of the synovial joint. The condition is not simply a result of degeneration or normal wear-and-tear but rather a dynamic and active process in which joint tissue repair and destruction are out of balance [2]. Secondary arthritis develops almost exclusively based on poor biomechanical performances, such as mismatch between the joint surfaces. One of the important factors is the incorrect load that occurs, for example, in post-traumatic deformities, dysplasia and un presence of deviations of the axes. In this context the growing number of sports injuries should be mentioned. Obesity and lack of physical exercise and a poor diet can favor the onset of the pathology. The main cause of the osteoarthritis is an imbalance of factors acting on the articular cartilage. Mechanical wear involves a progressive destruction of the cartilage. When the cartilage is overloaded for a long time, it is possible that alterations take place not only in elasticity but also in metabolism of the joint tissue.

Kellgren-Lawrence classification

Beginning in 1957, Kellgren and Lawrence carried out studies aimed at finding parameters for classification of OA from radiographic images [11]. The scheme they proposed consists of 5 grades and is currently used as research tool in studies involving mainly knee OA [12]. For each x-ray is associated a grade from 0 to 4 according to the severity of the pathology:

- Grade 0: x-rays show no obvious signs of OA.
- Grade 1: x-rays show joint space narrowing that could be imputed to pathology (doubtful) but there is no pain.
- Grade 2: x-rays present possible joint space narrowing and osteophytes.
- Grade3: x-rays present definite joint space narrowing. Moderate osteophytes, sclerosis and bone irregularity can be present.
- Grade 4: x-rays show marked joint space narrowing, major sclerosis and definite bone deformities.

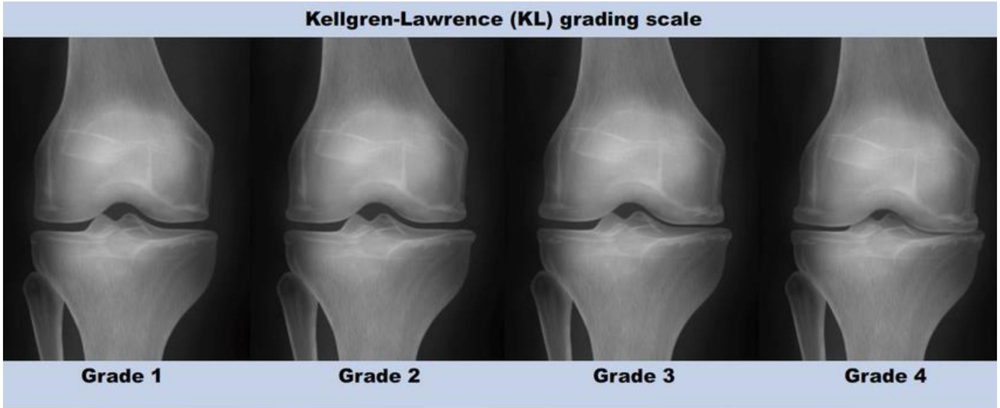

CLASSIFICATION	Normal	Doubtful	Mild	Moderate	Severe
DESCRIPTION	No features of OA	Minute osteophyte: doubtful significance	Definite osteophyte: normal joint space	Moderate joint space reduction	Joint space greatly reduced: subchondral sclerosis

Figure 5: The Kellgren and Lawrence grading system to assess the severity of knee OA [http://www.adamondemand.com/clinical-management-of-osteoarthritis]

Risk factors

The risk factors regarding osteoarthritis are various. The incidence of the disease increases with age and is a condition imposed by several other factors and age related variations in the biological functioning of the cartilage [2]. Among the main risk factors, we can find:

1. *Obesity* – Studies on OA showed how overweight people have an higher risk to develop knee OA than the others [13]. An overweight individual, in addition to having increased mechanical stresses at the joint, may exhibit structural changes in cartilage because of increased adiposity, the presence of certain hormones and growth factors.
2. *Genetics* – Can lay a role in the development of osteoarthritis, although the exact mechanisms are not fully understood.
3. *Gender* – Women in fact are more likely to develop the condition than men. There are many explanations for this fact: among all it could be because women have higher proportion of body fat, that leads to higher stresses on the joints. Reached menopause women often gain weight and have hormonal changes that can lead to variations in bone density.

4. *Occupation* – Heavy workers and people who have to do repetitive motions every day are at a high risk of developing localized osteoarthritis.
5. *Sport*
6. *Joint injuries*
7. *Overuse*
8. *Altered joint biomechanics* – Knee OA occurs mostly in the medial compartment, increased loads in this portion of the joint are thought to be an important factor in its pathogenesis [14]. Excessive mechanical load can also be linked to subchondral bone remodelling that will induce more stresses on the cartilage, resulting in a reduction of its capability of absorbing shocks and leading to a development of localized damages [15].

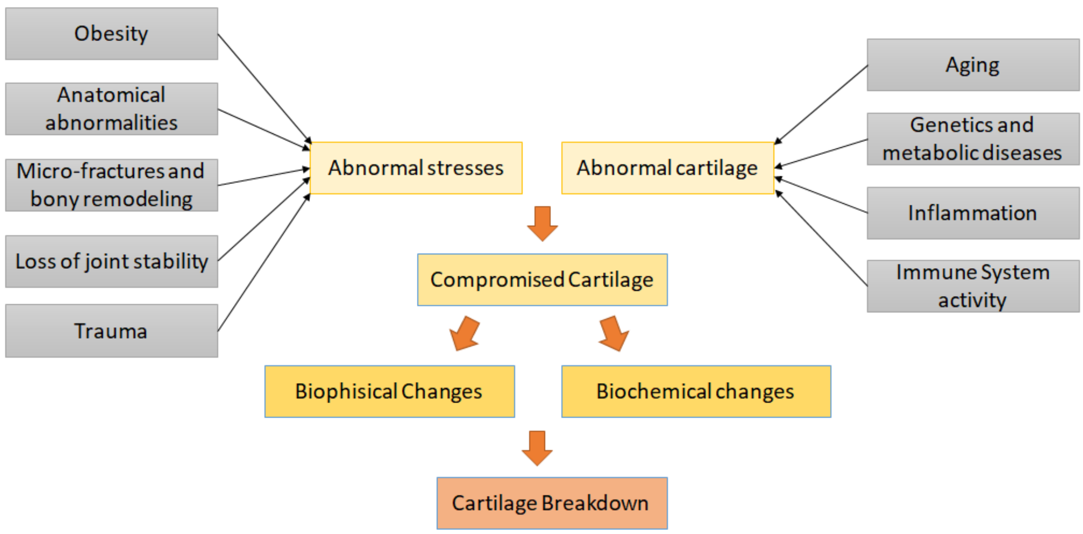

Figure 6: risk factors for knee OA

Genu varum

Is an alteration of the axis of the lower limbs that appear like round brackets. The distance between the knees is increased as opposed to the valgus knee, which has an x-shaped appearance, for this reason can also be referred to as bow-leggedness. The varus deformity can affect only one limb or both. Since the mechanical axis of the lower limb, in normal situations, passes through the center of the knee, this deformation changes the joint forces distributions. The degree of varus deformity can be quantified thanks to the hip-knee-ankle angle [16]. Some studies show that tibiofemoral alignment angle is also associated with increasing wear of the polyethylene placed on the tibial plateau. This indicates that it is important to take this parameter into consideration as well when going for TKA surgery [17],[18]

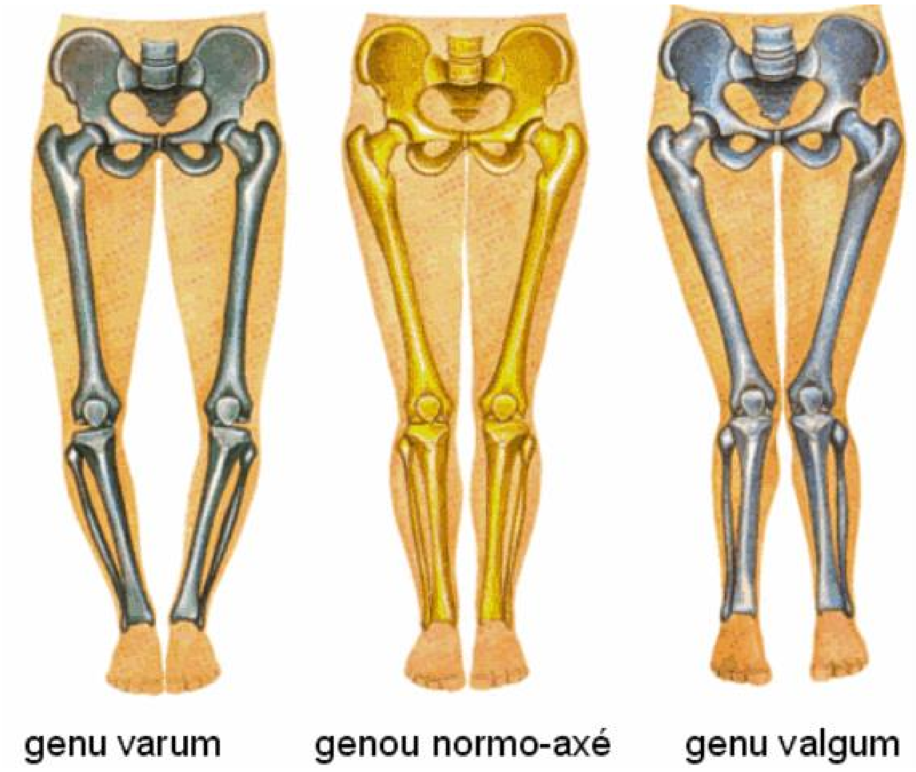

Figure 7: differences among normal, varus and valgus lower limb [https://www.cabinetpodologie.fr/details-gonalgies+femoro-tibiales+sur+genu+valgum+et+genu+varum-55.html]

Unicompartmental Osteoarthritis

Medial unicompartmental OA is a type of knee OA that involves deterioration of cartilage focused on the medial compartment. It is one of the most common forms of OA and can be associated with a varus malalignment condition which involves excessively high and unphysiological mechanical stresses that can lead to wear and tear of joint structures. Other factors that can lead to the development of unicompartmental OA are damage (or excision) of the internal meniscus and necrosis of the internal femoral condyle. This condition contributes to a narrowing of the joint space especially in the medial compartment of the knee.

Symptomatology evolves over time in a progressive manner, the pain worsens and generally increases by carrying on heavy physical activities. Another frequent symptom is the progressive increase in stiffness of the joint. Just as with other forms of osteoarthritis, medial unicompartmental OA is a permanent condition. Once joint structures are degraded, it is no longer possible for them to heal. For this reason is important to act in a preventive way for the treatment of this pathology searching for solutions that allow to improve the quality of life of patients and maintain knee function as much as possible [19].

Figure 8: OA in medial knee compartment [https://www.sori.org.au/index.php/patient-information/osteoarthritis/]

2.4 Pathology treatment

2.4.1 Conservative treatments

The goal of a therapeutic process due to a pathology is to improve the patient's quality of life. Several studies have focused on how to determine the presence of OA even during its early stages, to perform restraining maneuvers and to reduce structural damage as much as possible before it is too late. Prevention results crucial for this type of disease but it is not always easy to be able to notice the early alarm bells. [19]

During the initial stages of the disease, a conservative treatment can be applied, treating, monitoring pain and trying to preserve the affected person's motor abilities as much as possible. Therefore, focus is on pharmacological, weight control and physiotherapy treatments, resorting to a surgical operation only if the conservative treatment was not effective in some way [20].

2.4.2 Knee arthroplasty

Each year in Western countries tens of thousands of knee prostheses are implanted. However, many experts believe that these procedures often occur too early. The prosthetic replacement of an arthritic joint should in fact represent the last option. These are highly invasive procedures, but are able to provide excellent results in terms of functional recovery and pain symptoms [21]. Knee prostheses are divided into total or unicompartmental prostheses. Total knee replacement or total knee arthroplasty surgery involves replacing all the joint surfaces damaged by osteoarthritis and a small amount of femoral and tibial bone. The prosthetic components can be made of different types of materials such as titanium, cobalt-chrome or titanium-cobalt alloys and ultra-high molecular weight polyethylene (UHMWPE). On the other hand, unicompartmental prostheses replace only one compartment of the knee, either the medial or lateral one. Here, as in the previous case, the damaged parts of the knee are reconstructed using an implant often made of titanium alloy and UHMWPE. They have the advantage of being less invasive, preserving more bone, and having faster recovery times after surgery. However, their use is rather limited compared to total replacement, not being indicated for all types of patients.

2.4.3 High tibial osteotomy

Genu varum, as previously said, is a condition characterized by an inward curvature of the knee that cause the lower leg to angle away from the thigh. It can be caused by various factors, including genetic predisposition, growth disturbances and joint disease. In some cases, it may cause knee pain, instability or difficulty in walking. Treatment for genu varum may include physical therapy, bracing or, in severe cases, surgeries as high tibial osteotomy. High tibial osteotomy (HTO) is a surgical procedure that aims to realign the lower limbs and is intended for patients with medial knee compartment arthrosis who have nonadvanced OA, young age and special physical demands. Correcting the tibiofemoral alignment axis, an attempt is made to unload the medial compartment by going to stress the lateral one, preventing worsening in the compartment most affected by OA. Among the surgical ones, this is considered a conservative technique as it allows to preserve the total joint surface, redistributing the loads on the joint by realigning the tibio-femoral axis of the leg. There are two main types of HTO:

1. *Medial opening wedge osteotomy* – Most common type of HTO, where a wedge of bone is placed in medial (inner) side of the tibia in order to correct alignment of the knee.
2. *Lateral closing-wedge osteotomy* – This type of HTO involves removing a wedge of bone from the lateral (outer) side of the tibia and repositioning the tibia to improve alignment. This type of osteotomy is less commonly performed and is used where medial opening-wedge osteotomy is not suitable.

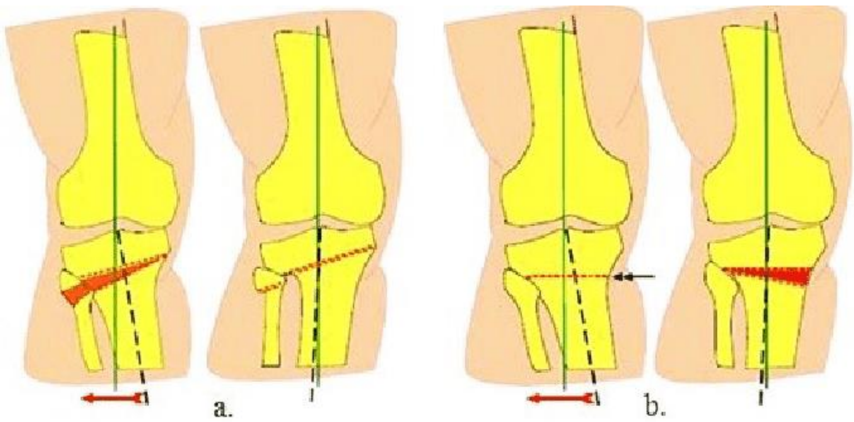

Figure 9: High tibial osteotomy a) with closing wedge b) with opening wedge [https://www.researchgate.net/publication/319012421_Experimental_modular_stand_used_for_studies_of_the_High_Tibial_Osteotomy]

Both types of HTO aim to correct knee alignment and reduce the load on the damaged part of the joint, helping to relieve pain and improve joint function. The degree of correction is assessed through careful preoperative planning by examination of the patient's radiographs.

Rehabilitation after HTO can take several months and weight bearing activities should be limited for a period to allow a proper bone healing. Usually after a period of about 1 month, the patient stops using crutches; after a couple of months, it is possible to return to drive a car.

HTO is a surgical procedure performed for over 40 years which allows a benefit from pain and a good recovery of mobility and muscle strength. One of the most advantageous aspects of this surgery is that it allows to preserve all the patient's joint structures, only changing the tibiofemoral alignment. Since OA is a degenerative disease, with the aging there is a progressive worsening of the joint situation. HTO surgery allows a delay of several years for a total knee arthroplasty intervention.

2.5 Basics aspects of motion capture and Gait Analysis

Gait analysis consists in various possible exams where the patient has to walk or do any other motor task freely within a room to reconstruct kinematics and dynamics associated at body segments, to study the forces produced by the muscles during the walk and many other things. It is a completely non-invasive practice that can be requested for patients who present alterations in walking, to provide additional consideration and data in situations where diagnosis is not possible with just clinical observation, to test the effectiveness of rehabilitation therapies, do research about physiology or pathology of the movement and also to understand the effects on the walking of devices such as prosthesis, orthosis etc. It is a relatively easy and economic approach. It is not necessary to do a live analysis and this allows to compare different repetitions of the same task recorded months apart or compare different repetition of the same task even for different patients. The analysis is also wriggled away from the constraint and allows the evaluation of minimal movement.

2.5.1 Gait cycle

Deambulation refers to the regular and repetitive sequence of movements involved in walking. This movement pattern is based on the gait cycle (GC), which is the basic building block of walking. The GC encompasses the time between two consecutive contacts of the same foot with the ground. To enable appropriate comparison with tasks performed in different repetitions and evaluated by different patients, it is useful to normalize this period into 0% and 100%.

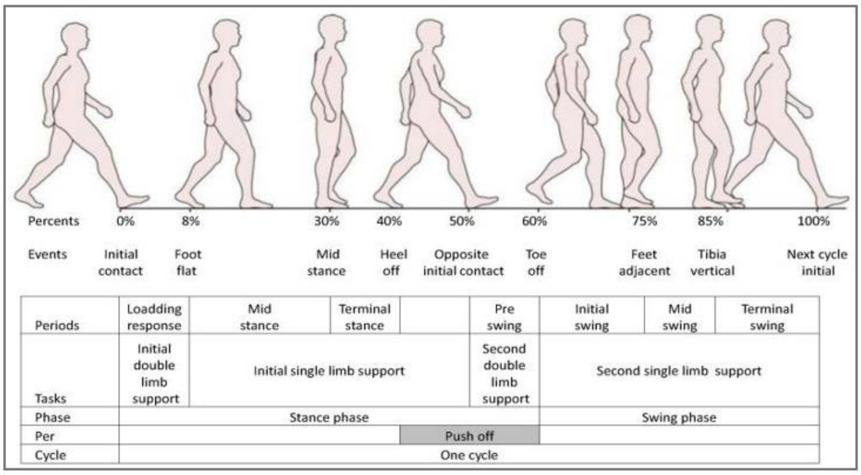

Figure 10: Gait cycle and its subphases [https://fisioheroes.altervista.org/ciclo-del-passo/]

GC consists of two main phases, named *stance* and *swing,* which can be divided also into sub-phases. During the stance phase, the foot is in contact with the ground and corresponds to about 60 percent of the total cycle, begins with the impact of a foot with the ground and ends with the detachment of the same foot. The swing phase, on the other hand, occupies about 40 %, starts with the detachment of the foot and ends when the same foot subsequently impacts the ground. It is possible to subdivide these two main phases into 8 sub-events. These phases are useful to determine the presence of pathology when they are altered from normal walking. In 20% of the time weight is exchanged on both limbs simultaneously, in the remaining 80% we have weight supported on only one limb.

2.5.2 Instrumentation of a gait analysis laboratory

In a gait analysis laboratory in addition to optoelectronic systems, it is possible to find:

1. *Force platforms* – Also known as dynamometer, provide as output a signal that is proportional to the force applied to them. Applying a weight above a force platform, in fact, induces a deformation of the sensor or transducer inside it. The deformation generates a voltage change proportional to it, which is then converted into an output signal. Knowing the relationship between strain and tension change, it is possible to be able to derive the applied force. Dynamometer platforms can be single or tri-axial, allowing force to be measured in one or more directions.

2. *Electromyographs* – these are indispensable instruments for gait analysis. They are mostly analogical and wired instruments, but telemetric models are commercially available to facilitate their use during gait testing. During recording, the electromyograph, in addition to taking EMG signals, takes care of an initial post-processing phase of the taken EMG signal. It goes in fact to apply detrending and filtering between 40 and 400 Hz.
3. *Videorecording systems* – allow physicians to be able to consult the patient's gait even some time after the examination. This is a facilitation for the diagnosis.

Figure 11:Representation of a gait analysis laboratory [https://optitrack.com/applications/movement-sciences/]

Motion capture technologies

Many types of motion analysis systems can be found on the market nowadays. This large family of technologies can be divided into two subgroups: *optical* (or optoelectronic) and *non-optical* motion capture systems.

Non-optical systems include electro-mechanical, electro-magnetic and inertial systems.

Optoelectronic systems are based on the use of markers placed at anatomical landmark points on the patient and cameras that allow their detection over time, necessary for the three-dimensional reconstruction of the motor task in the computational domain. The placement of these markers is "normed" by validated and tested protocols to minimize reconstruction errors and artifacts. A further subdivision can be introduced according to the use of markers of different nature:

- *Active markers* can generate light themselves, being composed of bright LEDs. They are recommended for recordings in which proper illumination of the room where the survey is done is not always guaranteed. However, the markers must be powered, which implies a cable connection that can annoy the patient during movement.
- *Passive markers* are considered the gold standard in gait analysis. These are markers made of materials that can reflect wavelengths between 780 and 820 nm so that they can be picked up by special cameras working in the infrared. The lights are emitted by illuminators coaxial with the cameras. The latter, in the former case work in the visible, in the latter in the near infrared. To make a correct recording and reconstruct the three-dimensional kinematics in the virtual environment, it is necessary that there are several cameras and that they are properly calibrated and arranged in the recording environment. The number of cameras needed is related to the type of motion that is to be analysed and the complexity of the biomechanical model used to go and do the analysis, the minimum possible number is 2. The data used for the simulation of the models realized in this thesis were obtained through passive optoelectronic systems.

Data from motion capture trials are stored in .c3d format files. This is a single file in which all the information obtained during the experimental trial is stored, in this way it can all be exchanged together more easily. There is no limit on the amount of data that can be stored in this structure.

2.6 Musculoskeletal modeling approach

Motion is essential for humans as it allows us to access sources of sustenance and basic needs. In the field of biomechanics, understanding the internal forces exchanged between joints during various motor activities is of great interest. This knowledge has applications in clinical, sports, and safety settings. However, measuring in vivo internal and muscular forces is challenging since it involves implanting sensors inside the human body. Furthermore, this approach allows only a limited number of joints to be investigated.

Patient-specific musculoskeletal models are a tool developed specifically to answer this type of question. It has emerged from the need for precise, detailed, and quantitative information to improve the treatment of patients with gait pathologies [22].

Musculoskeletal models can be used in conjunction with data obtained during gait analysis sessions to estimate the forces acting on each modeled joint. These forces include joint reaction (or contact) forces and the corresponding muscle forces that primarily contribute to them.

Musculoskeletal models are multi-body models designed to simulate the dynamics of the musculoskeletal system. They consist of rigid bodies connected by joints, allowing for a certain number of degrees of freedom, as well as modeled musculotendon actuators. The aim is to accurately replicate the behaviour of the human body during motor tasks. To create an appropriate musculoskeletal model, a deep understanding of both Newtonian mechanics (dynamics) and fundamental anatomical properties is necessary. The process is thus situated at the intersection of medicine and mechanical engineering.

2.7 Musculoskeletal modelling and Simulations in OpenSim

If not otherwise stated, refer to the OpenSim Documentation [https://simtk-confluence.stanford.edu:8443/display/OpenSim/Documentation] for this section.

In the early 1990s, Delp and Loan developed a musculoskeletal modeling environment called SIMM, which allowed for the creation of musculoskeletal structures and models, as well as the evaluation of simulations based on gait analysis data. SIMM stands for "Software for Interactive Musculoskeletal Modeling."[22], [23]. OpenSim was first introduced in 2007 and has since been widely used by biomechanics researchers to explore and gain a better understanding of movement mechanics. The software offers access to a vast amount of information, models, and experimental data that have been shared with the scientific community, as well as a range of computational tools accessible through a user-friendly graphical interface (GUI). Users can analyze and modify musculoskeletal models, visualize 3D movements, and view simulation results through the interface. OpenSim is an open-source software program written in ANSI C++ and can be interfaced with programming software such as C++, MATLAB, and Python using the application programming interface (API). The use of external programming environments helps to automate the simulation process, reducing computational time and minimizing errors when setting parameters of interest.

2.7.1 Musculoskeletal models

The OpenSim project's primary aim is to establish a unified platform for constructing and exchanging musculoskeletal system models. An OpenSim model is a critical element of any analysis, enabling the resolution of muscle forces and joint forces and moments resulting from virtual movement. It is possible to model specific parts of the body in detail. For the study of the lower limb, for example, it is not necessary to model the upper part in the same detail as the lower limb. The main components of a musculoskeletal model are:

1. *Reference frames*
2. *Bodies* – in musculoskeletal models the rigid bodies refer to bone segments and are described by their mass, moment of inertia, and center of mass position. It is assumed that the body segments cannot change during simulations. A Cartesian reference system is associated with each body segment, which is located at its center of mass and aligned with the standard anatomical directions of the segments (proximodistal, anteroposterior, mediolateral) [24].
3. *Joints* – They correspond to the points of junction between two adjacent rigid bodies and determine how they connect each other and the degrees of freedom associated with those joints. Different joint types can be modeled, such as: weld joints, pin joints, slider joints, ball joints, ellipsoid joints, free joints, custom joints. They are defined as frictionless and nondeformable, in this way the forces exchanged through the joints are equal and opposite in the two rigid bodies involved. [24]
4. *Constraints* – kinematic constraints are used in models to avoid movements. There are three kinds of constraints: Point constraints, weld constraints and coordinate coupler constraints.
5. *Muscular forces* – To define a muscle model, the minimum information required includes its geometry and a parameter indicating its maximal strength. The geometric parameters must include the coordinates of origin and insertion within the musculoskeletal model and pennation grade. To describe the force with which the muscle reacts if it is maximally activated, one can also rely on more complex models such as Hill's. Although every muscle has the same baseline, different types of

muscle can be modeled by varying associated parameters (i.e. activation, muscle fiber length…).

6. *Contact Geometry*
7. *Geometry*
8. *Virtual Marker Set* – Is a marker set placed on virtual model and used to perform scaling and inverse dynamic steps of the workflow. They are necessary for match the experimental marker used during the motion capture data collection. To ensure accurate reconstruction of 3D trajectories, at least one virtual marker must be assigned to each experimental marker placed on the patient. Virtual markers are placed on the rigid body of interest and are defined according to its reference system. Optimal trajectory reconstruction requires at least 3 markers per rigid body. During recording, it is crucial to ensure that these markers are always clearly visible to the cameras.
9. Controllers

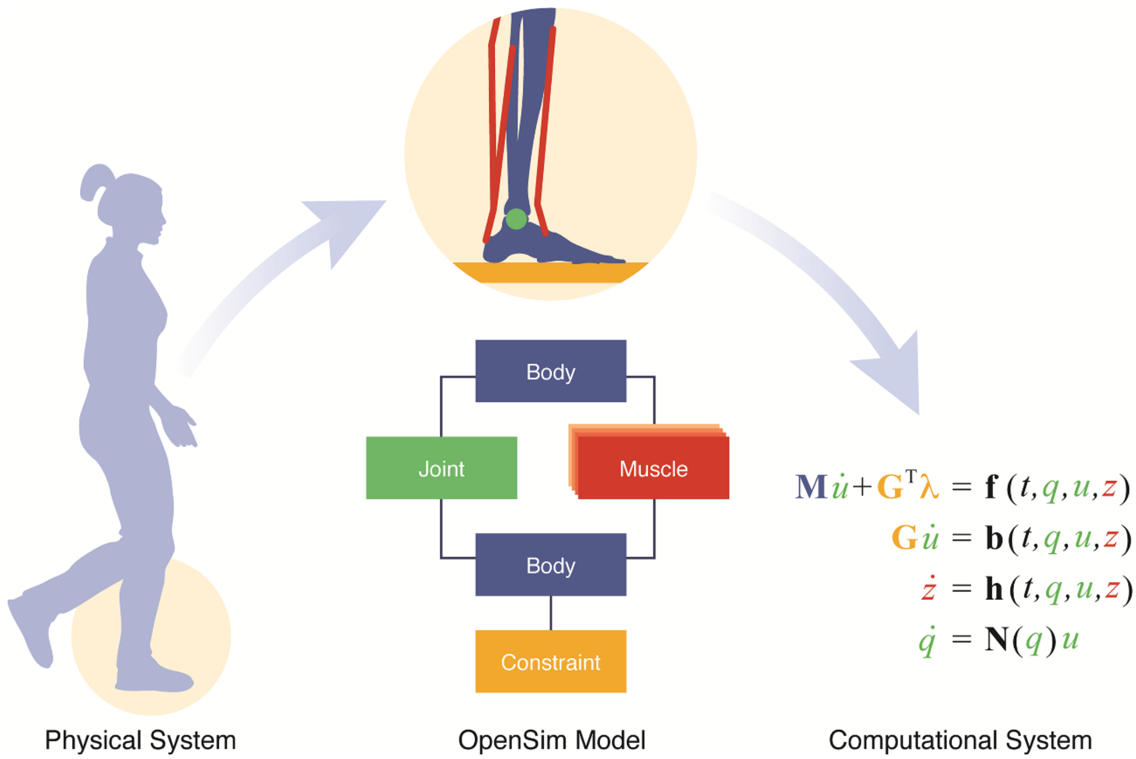

Figure 12: Musculoskeletal modeling approach

2.7.2 Experimental data necessary for simulations

To conduct a simulation, in addition to a musculoskeletal model, it is necessary to have two other fundamental elements:

1. *Marker trajectories data* – These are files in .trc format, within them it is possible to find stored the sampled trajectories of each marker belonging to the protocol. Each row in the table corresponds to a frame, each column instead is associated with a marker component, as indicated in the header.
The header consists of the first three rows of the document and contains important information regarding the acquisition system, the units of measurement used, the start and end times of the simulation and the number of markers. This information is necessary for OpenSim to correctly interpret the data contained in the file.

DataRate	CameraRate	NumFrames	NumMarkers	Units	OrigDataRate	OrigDataStartFrame	OrigNumFrames	
100	100	202	214	mm	100	370	202	
Frame#	Time	RA			LA			RBAK
		X	Y	Z	X	Y	Z	X
370	3.7	176.123	-81.6911	1371.73	-185.146	-64.5289	1367.76	110.299
371	3.71	177.659	-72.2667	1370.23	-183.6	-55.126	1366.55	111.756
372	3.72	179.237	-62.5808	1368.77	-182.012	-45.4994	1365.42	113.274

Figure 13: an example of a .trc file used in our study. It is possible to see a part of the header.

This file format is needed to perform the first two steps of the OpenSim workflow: scaling and inverse kinematics (IK).

2. *External force data* – This is the type of file in .mot format selected to store data from the force plates. Just as the format described above, there is a header where are stored some information about the acquisition performed. Each row corresponds to a sampled frame and each column instead corresponds to a component of ground reaction forces, points of application, torques exerted.

version=1							
nRows=3640							
nColumns=19							
inDegrees=yes							
endheader							
time	ground_force_vx	ground_force_vy	ground_force_vz	ground_force_px	ground_force_py	ground_force_pz	1_ground_force_vx
3.75	0	0	0	0	0	0	0
3.7505	0	0	0	0	0	0	0
3.751	0	0	0	0	0	0	0

Figure 14: An example of a ground reaction force .mot file

2.7.3 OpenSim Workflow

Over the years, various simulation workflows have been developed to address different clinical questions. The aim of the workflow we employed was to determine the joint reaction forces acting on the medial and lateral compartment of the knee using 3D marker trajectories obtained during gait analysis sessions. This required solving an inverse kinematics and dynamics problem.

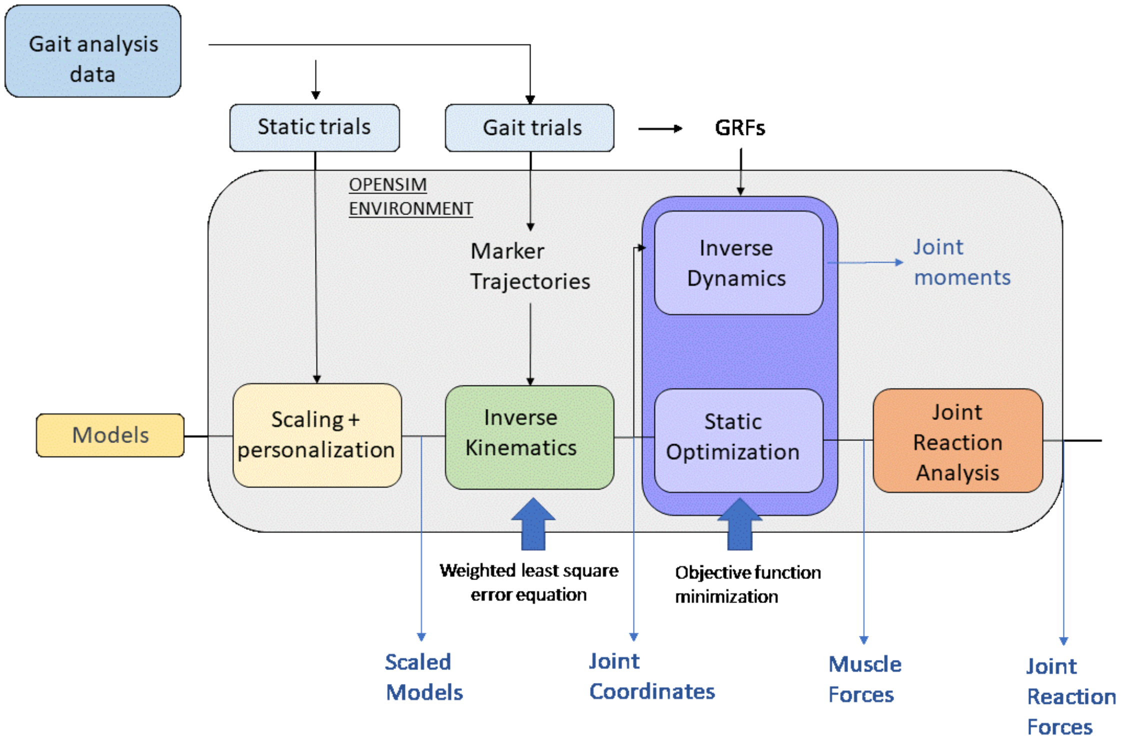

Figure 15: Schematization of the OpenSim's workflow used.

2.7.4 Scaling

The simulations are usually performed using generic models, but before proceeding with the workflow, it is crucial to adjust the model to fit the experimental data obtained during gait analysis sessions. This process is called scaling, and it involves altering the dimensions of the rigid bodies in the generic musculoskeletal model to match the measurements obtained during the experimental protocol. Additionally, the mass properties of the model, such as mass and inertia tensor, are also adjusted. To scale the rigid segments, input data from a static acquisition is required, and to adjust the mass properties, the patient's mass must be provided as input to OpenSim.

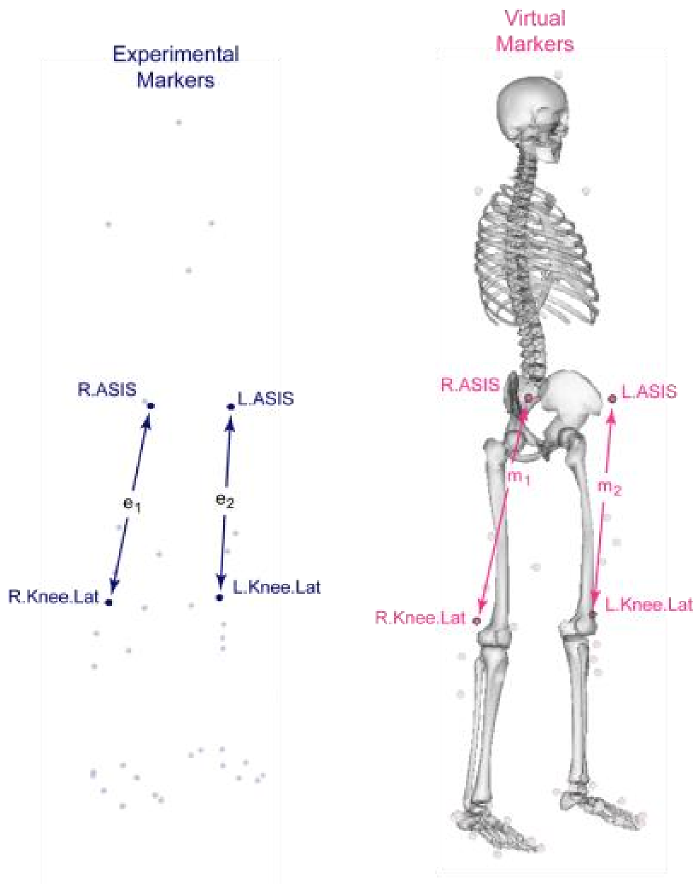

Figure 16: e1 (and e2) represents the distance evaluated between two experimental markers associated at one segment. Scaling allows to minimize the difference between e1 (and e2) and its correspondent distance between markers located on the virtual model. [https://simtk-confluence.stanford.edu:8443/display/OpenSim/How+Scaling+Works]

The scaling process involves two types of scale factors: manual scale factors based on anthropometric analysis and measurement-based scale factors based on differences in distance between the 3D coordinates of motion capture markers and virtual markers. The measurement-based scale factors are computed by comparing the distances between selected virtual markers and their experimental counterparts in each frame and averaging them over the scaling process. The scaling factor for each segment is then calculated as the average of the scale factors obtained for each pair of markers on the segment. Additionally, markers can be assigned weights to control their influence on the scaling process. The aim of this procedure is to minimize the discrepancies between experimental and virtual markers.

This step has a fundamental importance because the following ones are sensitive to the errors committed here. It may be necessary to perform this step iteratively to find out which combination of scale factors is the most functional to reach the better performances. It is possible to assess how similar the virtual model is to the experimental data by estimating errors (total squared error, RMS marker error and max marker error) that are provided to us by the OpenSim “messages” window.

The virtual markers, after scaling, are placed in different positions from the starting ones to perform the next steps with a marker set more similar to the one used by the experimental setup.

Input and output files

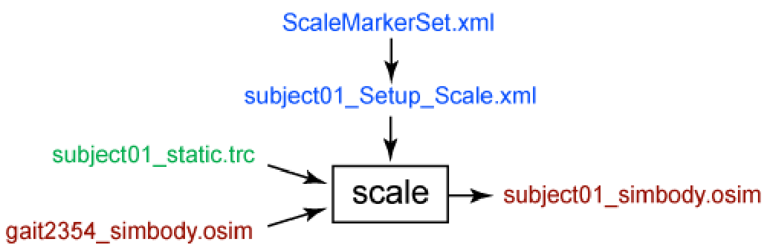

Figure 17: Schematization of the input/output files of the Scale Tool

To perform the scaling process optimally, a whole series of files and settings must be provided as input. The easiest way to provide OpenSim with everything it needs to perform this step is to give it as input a setup. The setup is an .xml format file that contains all the parameters needed to perform properly a scaling. It stores:

- The patient mass.
- The generic model that must be scaled and its path.
- A file containing the marker set.
- The marker pairs against which to calculate the scaling factors.
- The anthropometric scaling factors.
- The wights associated with the markers.
- A file containing the static experimental recording (.trc).
- The time range of the simulation.
- The output model with associated its respective folder where you wish to save it.

2.7.5 Inverse Kinematics (IK)

Solving an inverse dynamics problem requires the evaluation of both angular and linear accelerations, which is done by solving an inverse kinematics problem. The primary goal of inverse kinematics is to accurately replicate the patient's motion in the virtual environment by computing the optimal generalized model coordinates. To achieve this, OpenSim uses a weighted least squares optimization method to minimize the differences between the virtual markers and the experimental markers.

$$\min_q \left[\sum_{i \in markers} w_i \left\| (x_i^{exp} - x_i(q))^2 \right\| + \sum_{j \in coordinate} w_j (q_j^{exp} - q_j)^2 \right]$$

Where w_i represents weights associated with the marker error, x_i^{exp} the position of an experimental marker and x_i the position its corresponding virtual marker. For the other factor w_j represents weights associated with the generalized coordinates error, q_j^{exp} the experimental generic position and q_i its experimental generic position in virtual environment.

Two sources of error are considered:

- *The marker error:* corresponds to the difference in position between the experimental marker and the corresponding virtual marker.
- *The coordinate error*: corresponds to the difference between the experimentally measured coordinate and the one calculated by OpenSim for the virtual marker. This is a type of information not strictly necessary for the IK tool functioning.

The weights assigned to markers and coordinates are critical as they dictate the degree to which the error associated with a specific marker or coordinate contributes to the overall error. By increasing the weight, greater constraints can be placed on the errors associated with these markers.

For each simulation frame, OpenSim returns as output the model configuration that can minimize the sum of the weighted least squares errors of the coordinates and markers.

To ensure the accuracy of the subsequent tools, the inverse kinematics (IK) step must be performed with precision. It is important to iterate this step until acceptable errors are achieved. A good inverse kinematics solution should have errors below certain standards. The maximum marker error should be below 4 cm, and the root mean square (RMS) marker error should be below 2 cm [25].

Input and output files

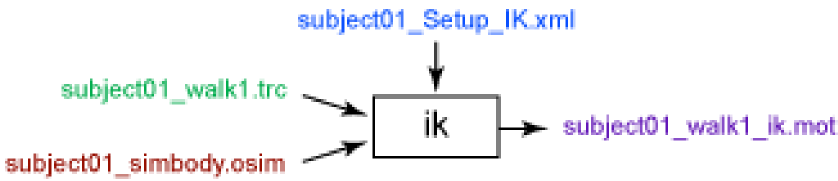

Figure 18: Schematization of the input/output files of the IK Tool

To perform the IK process optimally, a whole series of files and settings must be provided as input. The easiest way to provide OpenSim with everything it needs to perform this step is to give it as input a setup which it stores:

- The directory in which to save the results. The results are saved in a .mot format file.
- The scaled model that must be used in this step.
- The weights associated with the markers.
- A flag associated with whether or not the coordinates will be considered in the minimization problem.
- The weights associated with the coordinates.
- The .trc file containing the data recorded during the gait session for the motor task being evaluated.
- The time range of the simulation

2.7.6 Inverse Dynamics (ID)

The inverse dynamics tool is responsible for calculating the forces and torques acting on every joint in each frame. This is done by using the accelerations obtained from the previous step in the workflow and the external forces applied to the model, which are typically ground reaction forces. The relationship between masses and accelerations is governed by Newton's second law of motion:

$$\vec{F} = m\vec{a}$$

ID is responsible for solving the inverse dynamics problem of the kinematic chain formed by the musculoskeletal model under consideration expressed according to the following equation:

$$M(q)\ddot{q} + C(q, \dot{q}) + G(q) = \tau$$

q, $\dot{q}$, $\ddot{q}$, are respectively position, velocity, and generalized accelerations, M represents the mass matrix of the system, C corresponds to the vector of Coriolis and centrifugal forces, and G represents the vector of generalized forces.

Because of the movement of the model is determined only by generalized positions, velocities, and acceleration this means that all the left-hand side of these equations of motion are already established while the right-hand is unknown.

Input and output files

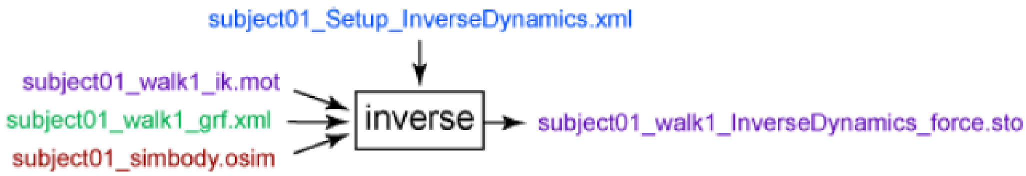

Figure 19: Schematization of input/output files of the ID Tool

To perform the ID process optimally, a whole series of files and settings must be provided as input. The easiest way to provide OpenSim with everything it needs to perform this step is to give it as input a setup which it stores:

- The directory in which to save the results. The results are saved in a .sto format file.
- The scaled model that must be used in this step.
- Il time range of the simulation.
- The external loads file.
- The inverse kinematics file obtained at the previous step.
- The low pass cutoff frequency needed to filter the coordinates of the kinematics file before starting to solve the inverse kinematics problem.

It is important to clarify the contents of the external loads file, which contains information about the ground reaction forces, the moments in three directions, and the position of the center of pressure. To correctly evaluate inverse dynamics, it is necessary to specify the point at which these external forces are applied, typically the heel. This is because the external forces are assumed to act as point forces.

As output, we get a .sto file containing all the forces and moments estimated during the simulation.

2.7.7 Static optimization

Static optimization (SO) is a technique used to determine the individual muscle forces that contribute to the overall net joint moments at each time frame. This step uses rigid multibody dynamics to model how the muscle forces produce motion in body segments [24]. The kinematics associated with the model are known thanks to the previous IK step. The SO Tool solves the equations of motion for the generalized forces and moments, which are subject to muscle-force activation conditions imposed during model construction. When muscles are modeled as ideal force generators, we have this kind of generalized equation of motions:

$$\sum_{m=1}^{M} (\mathrm{a_m}\ F_m^0)\mathrm{r_{m,j}} = \tau_j$$

When muscles are modeled as force generators but constrained by force-length-velocity properties, the generalized equation of motion are described as below:

$$\sum_{m=1}^{M} \left(\mathrm{a_m}\ f(F_m^0, l_{m,} v_m)\right)\mathrm{r_{m,j}} = \tau_j$$

In each model these variables are defined as follows:

- *n* represents the total number of the muscles present
- a_m stands for level of activation of a given muscle at a specific moment.
- F_0 is the maximum force that can be generated isometrically by the same muscle.
- l_m is the muscle length and v_m is its shortening rate.
- f(F0m,lm,vm) is the force-length-velocity surface associated.
- $r_{m,j}$ is muscle's moment at the j^{th} joint axis.
- τj is the generalized force acting about the j^{th} joint axis.

We must notice that there are more muscles than necessary acting and cooperating with each other to make certain body segments move. This leads to a redundant inverse dynamics problem; the system to be solved is therefore indeterminate because there are more unknowns than available equations. To address this, the SO tool applies a minimization criterion to find the most efficient solution. This criterion is applied frame-by-frame to calculate the muscle forces required to produce the observed joint torques while minimizing the total muscle effort.

$$J = \sum_{m=1}^{N} (a_m)^p$$

Where p is constant specified by the user. Optimization methods assume that the human nervous system minimizes a cost function subject to constraints to produce motion. This is critical in determining reliable and accurate contact forces. However, these methods have limitations, including uncertainty about the appropriate form of the cost function, unknown weight factors for individual terms in the cost function, and the possibility that the optimality assumption may not be applicable to individuals with joint pathology or neurological impairment [26].

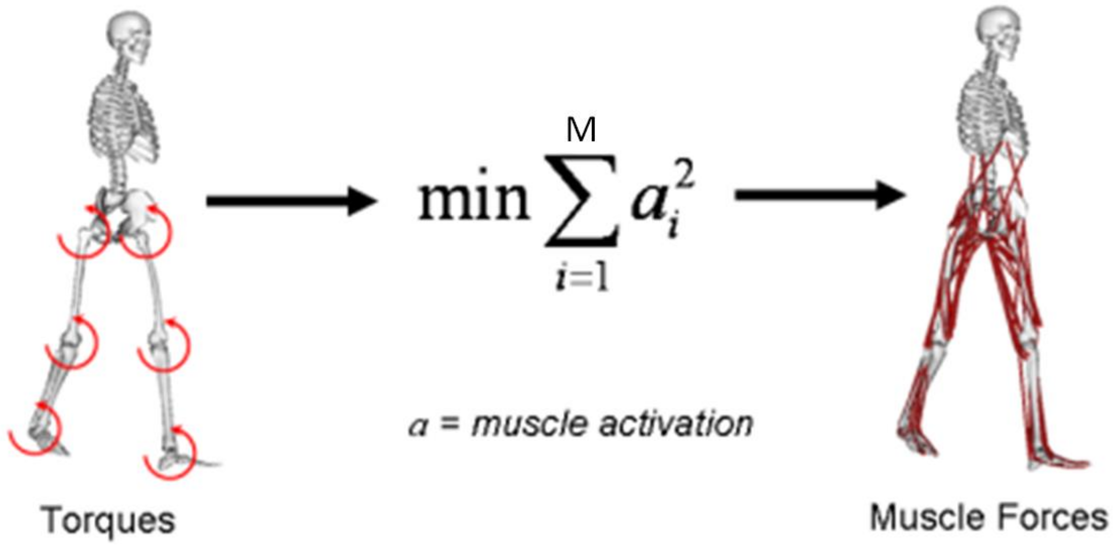

Figure 20: Solving of redundancy problem associated with Static Optimization

The use of reserve forces is necessary to ensure consistency between motion and applied forces. However, it is important to keep these forces and moments to a minimum to avoid any influence on the study's results. Specifically, it is advised that force discrepancies should be 5% or less (peak and RMS) compared to the net external force measured in the experiment. The reserve moments should be less than 1% of the COM height times the magnitude of the measured net external force [25]

Input and output files

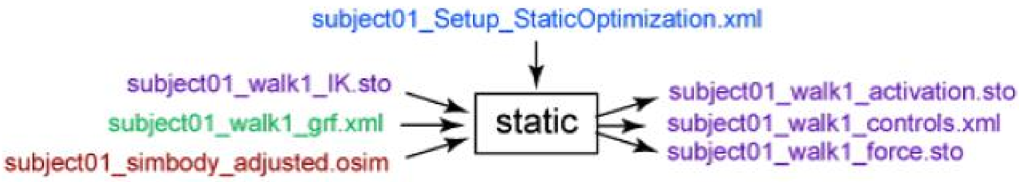

Figure 21: Schematization of the input/output files of the SO Tool

To perform the SO process optimally, a whole series of files and settings must be provided as input. The easiest way to provide OpenSim with everything it needs to perform this step is to give it as input a setup which it stores:

- The directory in which to save the results. The results are saved in a .sto format file.
- The scaled model that must be used in this step.
- The time range of the simulation.
- The external loads file.
- The inverse kinematics file obtained due to the IK
- The low pass cutoff frequency needed to filter the coordinates of the kinematics file before starting to solve the inverse kinematics problem.
- The file containing the actuators. The reserve actuators refer to additional torques applied to each joint to boost the force of the actuators, allowing the simulation to operate. Every degree of freedom (DOF) in the model should have an appropriate torque or force reserve actuator, including the six DOFs of the model's base segment, which are also known as the "residual actuators".
- The output precision
- The maximum number of integrator steps
- The maximum integration step size
- The minimum integration step size
- The integrator tolerance

As output, the SO returns 3 different files:

- the activations (.sto): The file in question contains estimated muscle activations for each muscle in the model, calculated during the simulation. These activations range from 0 to 1, representing normalized values with respect to the maximum force that the muscle can generate.
- Forces (.sto): this file contains estimated muscle forces associated for each muscle in the model, obtained during the simulation.
- The controls (.xml): this file contains the muscle controls implemented during the static optimization process.

2.7.8 Joint reaction analysis

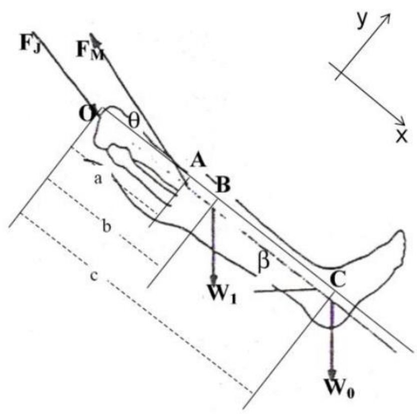

3

Figure 22: free body diagram used in estimation of KCFs

OpenSim provides a tool called Joint Reaction, which is used to calculate the forces and moments on body joints. This tool determines the joint forces and moments transferred between different body segments due to all the loads acting on the model, including those generated by the joint structure and other components that are not modeled but contribute to joint kinetics, such as contact with cartilage or ligaments that are not represented. The reaction load acts at the joint center (mobilizing frame) of both bodies, i.e., the parent and child segments. The resulting loads can be expressed in the child, parent or ground frames. By default, the force on the child is expressed in the ground frame.

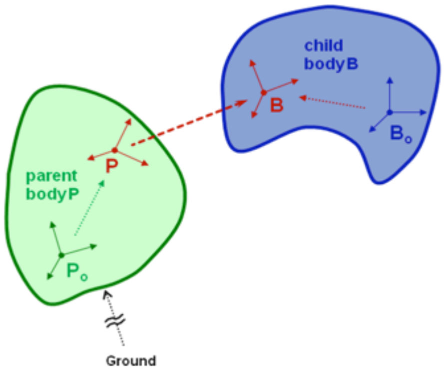

Figure 23: representation of parent and child bodies of a joint

Input and output files

To perform the Joint Reaction Analyses process optimally, a whole series of files and settings must be provided as input. The easiest way to provide OpenSim with everything it needs to perform this step is to give it as input a setup which it stores:

- The directory where save results. The results are saved in a .sto format file.
- The scaled model that must be used in this step.
- The time range of the simulation.
- The external loads file.
- The inverse kinematics file obtained because of the IK.
- The low pass cutoff frequency needed to filter the coordinates of the kinematics file before starting to solve the inverse kinematics problem.
- The file containing the actuators.
- The output precision.
- The maximum number of integrator steps.
- The maximum integration step size.
- The minimum integration step size.
- The joints where evaluate the reaction forces.
- On which bodies apply the forces (parent or child).
- In which frame express them (ground, parent or child).

The results are printed to a storage file in. sto format. This file contains as rows the simulation frames and as columns the data associated to the 3 force and moment vector components of the joint reaction load estimated at each selected joint of the model.

2.8 Prediction of knee contact forces and relationship with geometric parameters

The knowledge of the distribution of the joint contact forces of the medial and lateral compartment (MCFs and LCFs) of the knee during the time frames of a motor activity cycle, requires innovative experimental or computational techniques and technology. To directly measure the forces exchanged in vivo, it is possible to use instrumented prostheses that provide telemetric data transfer. It is a useful procedure, for example, regarding model validation but far too invasive to be adopted as a standard for evaluating joint loads, as they are currently implanted in patients requiring total joint replacements. In the absence of the possibility of having telemetric feedbacks [27], [28], predictions via musculoskeletal modelling can be used. Musculoskeletal models represent a state-of-the-art tool to predict KCFs and their distribution in the knee, although the complexity and amount of data required limit its applications. Creating computational models that faithfully replicate the musculoskeletal systems of the patient give also us the chance to investigate various alternative treatments and enhance clinical results [26]. One of the main goals is also to make motion analysis in the clinical field as objective as possible by providing customized models based on anatomical features of the patient and describing the problem in a more quantitative way.

The knee adduction moment (KAM) has often been used as an indirect measure of MCFs [15],[29],[30] . KAM corresponds, in motor activities, to the net torque acting around the knee joint and for this reason clinical practices aimed at reducing this entity to unload the medial compartment have also been introduced. Kumar et al. [29] have found that MCFs is increased in patients presenting with OA with K&L grade ≥ 2, but the role of KAM as an indicator of MCFs has been questioned. Therefore the level of correlation with MCFs is still controversial [31], [32], this suggests that the KAM is not able to explain the variability in the MCFs that determines the onset and progression of knee OA.

Another method used was to divide the total force acting on the knee into MCFs and LCF by defining a knee center and their respective lever arms [33]. The total force here was evaluated using an instrumented prosthesis. This study aims to go to investigate how TFA goes to influence mediolateral load distribution. It was seen that varus malalignment leads to increased load in medial compartment but there is little correlation between varus malalignment and medial contact force intensity [33]. Previous studies based on measurements taken on patients with total knee replaced showed a marked correlation instead [34].

Other studies, on the other hand, have focused on the development of musculoskeletal models capable of providing both MCFs and LCFs as outputs [35]–[38]. Prediction of medial and lateral knee contact forces are influenced not only by TFA in frontal plane but also by another important parameter of the knee: the locations of contact points (CP).

To determine the geometric parameters of interest properly, it is necessary to use imaging techniques. To obtain TFA it is necessary to measure by how much the tibiofemoral axis is deviated from its neutral position The gold standard for determining this parameter is to join the hip, knee and ankle joint centers using weight-bearing anteroposterior radiographs. The hip center can be easily identified as the center of the femoral head, and for the other two joint centers it is not easy to find an unambiguous way to determine them. The determination of CPs is difficult even using advanced imaging techniques. They are defined as the points at the shortest distance between the femur and tibia in the medial and lateral compartments of the knee and are typically calculated by imaging techniques. The Rosenberg view has proven to be an effective tool for their determination [39], [40] . This is a postero-anterior radiograph taken at the knee flexed 45° and in a weight-bearing condition that is used in the clinic to observe the joint space narrowing induced by the development of OA. Another way to measure CPs was introduced in a recent study [38], in which CPs were calculated using a bi-planar X-ray images in squat positions, and found medially located CPs in OA subjects, especially on the lateral compartment.

In general, varus TFA was suggested to increase MCF, although the level of correlation found between MCF and TFA is variable. Measurements on patients with total knee replacement showed both marked [34] and weak significant correlation between peak MCF and TFA during single-support activities [33], [41], and no significant correlation in double-support activities [33]. Lerner et al. [35], to investigate on load distribution among the two compartments of the knee joint, have developed a new type of musculoskeletal model (described in section 3.2) that can separately evaluate the medial and lateral components of the contact force on the knee. They customized it with several degrees of customization (TFA and CP) and performed a perturbation of these characteristics to understand how these would affect the prediction of the forces. For this study they used gait analysis data from a single patient with valgus malalignment who was provided with an instrumented prosthesis. It was through the telemetric prosthesis data that was possible for them to make a comparison between the outputs of the simulated models and the real distribution of forces occurring in the two compartments of the knee. They found out that the prediction accuracy increased by specifying each subject specific parameter, especially in the early stance of walking. This musculoskeletal modelling analysis showed an increase in peak MCF of 7.7% body-weight (BW)/deg in a total knee replacement patient. Another perturbation analysis carried out by Saliba et al. [36] aimed to quantify the sensitivity between knee contact forces predictions with TFA and CP errors under different dynamic conditions, using Lerner's validated musculoskeletal model. The project involved a perturbation of TFA between 10° to -10°. It was noted that for each degree of varus TFA perturbation, there was an increase in medial forces and a decrease in lateral forces between 3% and 6% bodyweight.

Regarding knee CPs, recent studies showed how CP locations have a significant effect on the prediction of KCF and their distribution. The two perturbation analyses described before investigating also on the role of CPs as a geometric parameter of personalization. The first [35] showed a decrease in MCF up to 6% BW/mm by shifting the CPs medially while maintaining a constant contact distance. The other one involved a perturbation of CPs among -10 mm to -10 mm and showed that there is an up to 4% BW/mm decrease in MCFs if CPs are moved medially [42]. In addition, a marked correlation between peak MCFs and CP locations was found in both knee OA and healthy subjects during walking [43], [44].

To sum up, most studies that compute KCFs and their distribution focus on individuals who have undergone complete knee replacement surgery. However, there is insufficient and conflicting information with limited sample sizes regarding healthy and OA individuals. Additionally, studies that examine activities other than walking, such as stair ascent and descent, have not considered the influence of geometric parameters [7], [45]. As a result, it remains uncertain how KCFs and their distribution vary when personalized geometric parameters are used in models to simulate different activities in knee OA individuals. The correlation between KCF distribution and geometric parameters is also unclear.

Chapter 4

Materials and Methods

The aim of this thesis is twofold. The first, of a modelling nature, aims to evaluate how prediction of the MCFs and LCFs of the knee in osteoarthritic patients during repetitions of walking, stair ascending and descending is influenced by the geometric parameters of varus malalignment and contact points between the femur and the tibia. The second aims to characterize the relationship between the lateral and the medial contact forces with these geometric parameters. To create the models and carry out the simulations, it was necessary to use imaging techniques and motion capture systems available within the Institute. The combination of this technology allowed the creation of a customized musculoskeletal model with characteristics that are as faithful to reality as possible. These models in OpenSim allowed us to estimate the forces generated at the knee joint by our patients during the motor tasks analysed. Batch processing of the OpenSim tools was performed by using external routines created in MATLAB to carry out all the simulations for each model created, and consequently automating the whole process and markedly reducing time.

3.1 Experimental data

A total of 50 patients (41 males, 9 females, mean age 52.9 ± 8.7 years, mean BMI 26.0 ± 4.4 kg/m^2) with medial knee OA (graded ≤ 3 Kellgren-Lawrence), no lateral knee OA nor patellofemoral compartment symptoms, and clear indication for high tibial osteotomy (varus malalignment > 4°), participated in this study. All participants showed an early OA located in the medial compartment, all of them led reasonably active lifestyle and could complete the five attempts needed for each motor task, except two of them (EV0 and RB0 who only completed the walking task). To have all the data available make this musculoskeletal analysis possible, it was necessary to subject patients to a day of data collection. All information was collected from:

1. *Radiographs* in weight-bearing anteroposterior extension view and posteroanterior 45° knee flexion view (i.e. Rosenberg view) that were acquired on each patient to measure TFA and CP locations, respectively, by using tools implemented in a software application (HTO-Rplus) developed in-house for a larger project. To obtain these geometric parameters accurately, imaging techniques are needed, but even with more advanced techniques, CP locations in particular are not easy to measure, and this affects how KCFs are distributed [35], [42]–[44].

2. *Marker trajectories* - .trc format files used within the scaling and inverse kinematics steps of our workflow.

3. *Ground reaction forces* – recorded from force plates, they are .mot format files necessary to solve the inverse dynamics problem

4. *EMG recordings* – recorded during gait analysis sessions, they are necessary in the process of indirect validation of our models.

In table 1, table 2 and table 3 it is possible to see the main information related to the patients.

Table 1: Table of subject characteristics

N°	Subject	Age [years]	Gender	Weight [kg]	Height [cm]	BMI [kg/m2]	Side Operated
1	AV0	59.7	M	81.0	174	26.7	Left
2	BA0	39.7	M	93.6	186	27.1	Right
3	BAM0	48.5	M	71.1	175	23.2	Right
4	BC0	60.8	M	83.3	174	27.5	Left
5	BCA0	60.2	F	58.0	163	21.8	Right
6	BN0	57.2	M	89.6	170	31.0	Left
7	BS0	46.5	M	66.2	168	23.5	Left
8	BSE0	47.0	M	88.1	184	26.0	Right
9	CA0	58.7	M	80.5	179	25.1	Left
10	CC0	62.0	M	66.9	162	25.5	Right
11	CE0	55.9	M	88.0	178	27.8	Left
12	CEM0	38.8	M	96.1	183	28.7	Left
13	CF0	60.8	M	72.7	170	25.2	Right
14	CG0	53.8	M	93.7	166	34.0	Right
15	CGC0	53.6	M	112.4	179	35.1	Right
16	CL0	52.9	M	97.7	187	27.9	Left
17	CM0	53.0	M	88.9	171	30.4	Left
18	CP0	60.9	M	75.9	177	24.2	Right
19	DCA0	44.1	M	79.5	189	22.2	Left
20	EA0	57.0	M	71.7	174	23.7	Left
21	EV0	62.2	F	74.1	150	32.9	Right
22	FF0	57.1	M	80.8	180	24.9	Left
23	FS0	50.5	M	72.4	170	25.0	Right
24	GA0	34.5	M	35.6	177	11.4	Right
25	GF0	61.6	M	65.1	173	21.7	Right
26	GN0	26.2	M	81.6	191	22.4	Right
27	LC0	52.0	F	70.9	167	25.4	Right
28	LE0	61.6	F	57.3	160	22.4	Right
29	LG0	55.0	M	82.7	170	28.6	Left
30	MD0	54.0	M	63.0	177	20.1	Right
31	MR0	46.3	M	80.1	173	26.7	Right
32	MT0	58.8	M	94.3	180	29.1	Right
33	OD0	51.9	M	78.9	170	27.3	Left
34	PF0	49.2	M	75.4	173	25.2	Left
35	PG0	62.8	M	65.7	187	18.8	Right
36	PL0	48.6	F	55.5	165	20.4	Left
37	PO0	59.3	F	61.7	166	22.4	Right
38	RA0	38.3	M	96.2	187	27.5	Right
39	RB0	67.4	F	75.7	158	30.3	Right
40	RD0	49.2	F	71.4	165	26.2	Left
41	RP0	67.2	M	102.3	173	34.2	Right
42	SA0	46.0	M	119.7	195	31.5	Left
43	SAA0	58.7	M	70.3	180	21.7	Right
44	SAO0	49.3	M	78.7	178	24.8	Right
45	SEA	38.1	M	67.4	170	23.3	Right
46	SOA0	58.7	M	80.3	171	27.5	Left
47	TM0	58.7	F	67.8	170	23.5	Right
48	UI0	47.4	M	105.6	172	35.7	Right
49	VA0	42.1	M	91.3	190	25.3	Left
50	ZL0	60.9	M	77.2	165	28.4	Right

Table 2: summary of estimated geometric parameters of customization.

					Contact Point Locations [mm]			
			Varus Angle [°]		Target		Controlateral	
N°	Subject	Side Operated	Target	Controlateral	Lateral	Medial	Lateral	Medial
1	AV0	Left	3.5	2.5	12.4	26	12.8	33.4
2	BA0	Right	3.7	6.9	12.9	38.7	15.1	40
3	BAM0	Right	9.4	8.5	13.6	39.6	12.4	37
4	BC0	Left	5.1	7	12.3	37.4	11.3	38.6
5	BCA0	Right	8	3.7	9.8	30.7	8.9	32.5
6	BN0	Left	11	10.1	10.4	29.4	10.5	35.3
7	BS0	Left	7.2	3.5	11.3	39.6	-	-
8	BSE0	Right	7	8.2	12	39.1	11	38.1
9	CA0	Left	9.5	5.3	9.6	40.7	12.6	38.8
10	CC0	Right	4.9	2.8	10.9	43.4	12.9	40.1
11	CE0	Left	4.7	6.5	11	39.8	14.4	31.7
12	CEM0	Left	10.3	10.6	10.5	31	-	-
13	CF0	Right	6.8	1.8	11.8	33.7	11.6	41.2
14	CG0	Right	11.9	5.9	12.4	37.4	12.1	36.2
15	CGC0	Right	1.3	3.3	11.8	41.3	-	-
16	CL0	Left	10.4	14.1	11.8	38.9	9.1	41
17	CM0	Left	5.5	5.2	13.4	32.2	12.7	29.9
18	CP0	Right	5.6	4.7	10.4	36.8	12.5	38.9
19	DCA0	Left	7.1	5.5	13.6	39.6	13.3	41.6
20	EA0	Left	9.3	7.7	12.5	31.7	12.4	28.2
21	EV0	Right	3.7	2.6	11.7	32.3	10	32.7
22	FF0	Left	6.8	2.8	12.9	38	10.9	35.6
23	FS0	Right	5.3	6.4	-	-	-	-
24	GA0	Right	15.8	9.9	11	26	11.4	30.2
25	GF0	Right	4.4	4.8	13.5	31.2	13.9	33.9
26	GN0	Right	8	6.9	12.6	35.5	13.9	34.1
27	LC0	Right	2.4	1.3	9	31.5	-	-
28	LE0	Right	11.1	13.7	9.1	28.2	11.3	24.4
29	LG0	Left	15.7	8.6	11.2	28.6	-	-
30	MD0	Right	4.2	3.9	11.5	38.4	16.3	37.2
31	MR0	Right	9.1	5.4	12.7	30.1	12.6	30.4
32	MT0	Right	5.2	7.2	14	39.4	13.8	39.4
33	OD0	Left	8.8	6.6	11	26.3	8.8	30.7
34	PF0	Left	3.1	3.1	13.1	33.2	12.7	32.9
35	PG0	Right	3.3	1.2	12	36.2	-	-
36	PL0	Left	7.1	4.2	10.4	24.8	11	27.4
37	PO0	Right	8.1	5.3	11.5	31.1	10.7	31.7
38	RA0	Right	9.6	3.4	13.8	31.6	12	39.4
39	RB0	Right	10.2	0.8	9.9	33.7	-	-
40	RD0	Left	9.3	5.1	11	34.2	10.9	33.2
41	RP0	Right	14.8	11.2	10.7	26.2	10.1	35.3
42	SA0	Left	13.4	6.5	12.3	31.4	9.5	38.5
43	SAA0	Right	11.7	8.4	14.1	35.7	11.6	32.4
44	SAO0	Right	13.3	10.3	11.7	29.4	14	30.6
45	SEA	Right	7.8	7.6	10.1	33.6	12	33.1
46	SOA0	Left	4.4	3.4	12.9	38.7	10	38.2
47	TM0	Right	7.1	0.2	11.2	33	13.1	37.4
48	UI0	Right	6.5	4.8	10.6	39.9	10.3	33.7
49	VA0	Left	10.9	5.1	12	35.5	11.3	38.3
50	ZL0	Right	6.8	2.1	10.3	33.3	10.8	35.5

Table 3: Summary of patient data

Mean (SD) partecipant characteristics	
Male	41
Female	9
Age[years]	52.9 (8.7)
Height[cm]	174 (9)
Weight[Kg]	79.1 (15.2)
BMI[kg/m2]	26.0 (4.4)
Varus Angle [°]	7.8 (3.5)
Lateral contact point [mm]	11.7 (1.3)
Medial contact point [mm]	34.2 (4.7)

3.1.1 Evaluation of TFA

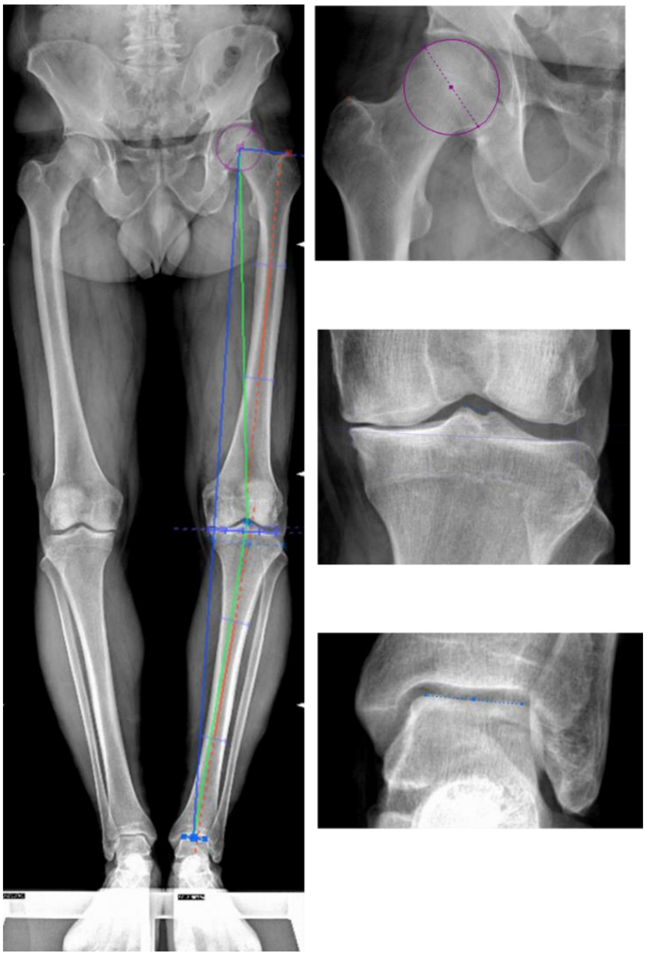

Figure 24: TFA evaluation from an antero-posterior x-ray using HTO-Rplus

To be able to determine the TFA, it was necessary to use antero-posterior X-ray images imported in HTO-Rplus, a software application developed in-house by the IT team of BIC lab, currently used for surgical planning of HTO by Rizzoli's surgeons.

The antero-posterior X-ray is a complete radiography of the lower limbs and pelvis under load. It is an orthopedic radiology examination useful to the study of the main joints in lower extremities. The patient must undress and stay barefoot on a platform to perform it. It is used an x-ray cassette that can acquire the entire limbs in a single projection. It is considered the primary tool for evaluating TFA in lower limbs because to define the necessary mechanical axes it is essential to know the relative position between hip, knee and ankle [46].

The TFA was calculated as the angle formed by the mechanical axis of the femur and the tibia's ones. The mechanical axis of these two bones is evaluated by tracing a line from the center of the proximal joint to the center of the distal joint. The mechanical axis belonging to the femur is determined by the union between the knee and hip centers, while the mechanical axis associated with the tibia connects the ankle center with the knee center. The hip center was defined as the center of the circle that best fitted the femoral head, the knee joint center as the mid-point of the centers of the tibial spines and the ankle center as the mid-width of the tibia and fibula at the level of the plafond.

For knee and ankle joints, it is not always easy to uniquely define their joint center and even on which X-ray images should be used to get a better definition of it. Several studies have proposed to give an unambiguous solution to this problem, but the debate is still open.

The distribution of TFA in the target and contralateral limbs are reported in the fig. 25 there is a wide range of values in both distributions. Measured angles had a mean value of $7.8° \pm 3.5°$ in the target limb and $5.7° \pm 3.2°$ in the contralateral limbs, and the two distributions were statistically different (Mann-Whitney U-Tests, $p = 0.0029$)

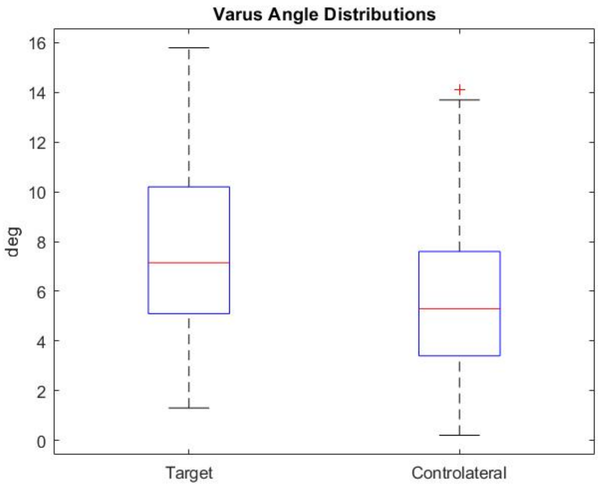

Figure 25: distribution of TFA among our patient cohort

3.1.2 Evaluation of CPs

Figure 26: contact point evaluation from a Rosenberg x-ray view, using HTO-Rplus

CPs are located at the minimum joint space width in the medial and lateral compartments of the knee and are typically measured via radiographs. The most widespread imaging technique for measuring joint space width and diagnosing OA is the Rosenberg view. This view of the knee is a specific projection used primarily to investigate limbs with suspected or stated osteoarthritis. It consists of a postero-anterior weight-bearing radiograph with a knee flexion of 45°. This flexion allows for a more sensitive determination of joint space thinning due to the course of pathology compared with the antero-posterior extension view [39], [40].

We calculated the CPs as the points on the minimum joint space width on the medial and lateral knee compartments. The minimum joint space width was calculated as the minimum Euclidian distance between the two splines defined on the femoral condyle and tibial plateau for each interpolated point along the two splines [47]. The corresponding CP was then located at the mid-point of the minimum joint space width.

This was possible thanks to a tool in HTO-Rplus implemented at BIC specifically to solve the problem of the position of the contact points. This procedure was carried out for each limb about both lateral and medial CPs.

Radiographs with Rosenberg view were available for all patients' target limbs but were absent for the contralateral limb in 6 different patients. Where the Rosenberg was not present, at the modeling level, it was decided to leave the involved limb with a CP customization of 20 mm both lateral and medial.

Distributions of medial and lateral CPs in target and contralateral are reported in the fig. 27 below. Measured medial CPs are overall higher than the lateral ones. A recent study [38] calculated knee CP locations of healthy and OA subjects by using bi-planar X-ray images in squat positions, and found medially located CPs in OA subjects, especially on the lateral compartment.

The mean CP locations medial and lateral of the knee joint center were respectively 34.2 ± 4.7 mm and 11.7± 1.3 mm in the target knees, and respectively 35.0 ± 4.1 mm and 11.9 ± 1.7 mm in the contralateral knees, which were not significantly different (Mann-Whitney U-Tests, $p = 0.45$ and $p = 0.65$).

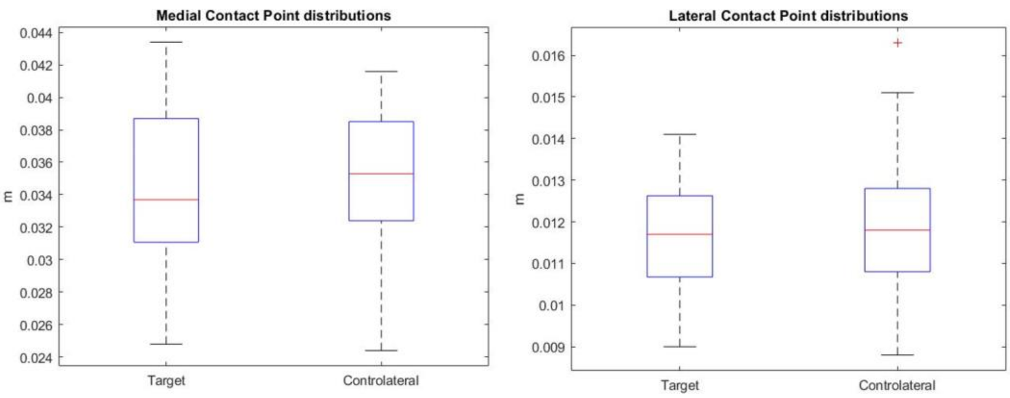

Figure 27:Boxplot representing a) medial and b) lateral contact point location distribution above our patient

3.1.3 Motion capture

The trajectories obtained from the markers and the ground reaction forces were recorded by 8-camera motion capture system (100 Hz, Vicon 612 Motion System, Oxford, UK), and two embedded force plates (2000 Hz, Kistler, Winterthur, Switzerland) for the three different motor activities. To perform this examination, subjects were undressed and were placed on their skin 10-mm-diamether spherical passive markers at precise body landmarks. This first phase was performed by an experienced physiotherapist who can accurately identify bony landmarks by palpation. What allows reconstructing the movement of the subject in the virtual environment is the continuous comparison between the markers placed on the patient under examination and the markers placed on the virtual model. Erroneous positioning can lead to errors in scaling and IK that will then affect the final outputs of our simulations.

When conducting gait analysis, it is important for protocols to prioritize both accurate reconstruction of segment and joint kinematics based on the individual's anatomical references, as well as fast and convenient methods for data collection [48]. In some cases, being able to find the appropriate point for marker placement is not easy. In overweight subjects there is a thick layer of adipose tissue between the bony landmark and the marker, which results in an initial placement error and decreases the reliability of reconstructing the position over time of that anatomical point. Fat tissue causes the marker to shift over time from its resting position (soft tissue artifact). This type of inaccuracy during acquisition cannot be eliminated entirely, only limited. To optimize application position and reconstruction efficacy, several positioning standards were tested and validated. The one adopted for the acquisitions performed in this clinical study is the one assessed by Leardini et al. [48], also known as the IOR gait protocol. This positioning protocol is designed specifically for the study of lower limb motion and can provide a complete description of the three-dimensional motion of body segments and joints based on anatomy. It involves the placement of 30 markers over the entire body giving representation priority regarding the lower body.

- markers placed on the upper part of the body:
  1. A – Acromion (both right and left)
  2. C7
  3. L5
- markers placed on the pelvis:

1. PSIS – posterior iliac spine (both right and left)
2. ASIS – Anterior iliac spine (both right and left)

- markers placed on the inferior limbs:
  1. GT – Great trochanter (both right and left)
  2. LE – Lateral epicondyle (both right and left)
  3. ME – Medial epicondyle (both right and left)
  4. HF – Proximal tip head fibula (both right and left)
  5. TT – Tibial tuberosity (both right and left)
  6. LM – Lateral malleolus (both right and left)
  7. MM – Medial malleolus (both right and left)
  8. CA – Tendon insertion on calcaneus (both right and left)
  9. FM – First metatarsal head (both right and left)
  10. SM – Second metatarsal head (both right and left)
  11. VM – Fifth metatarsal head (both right and left)

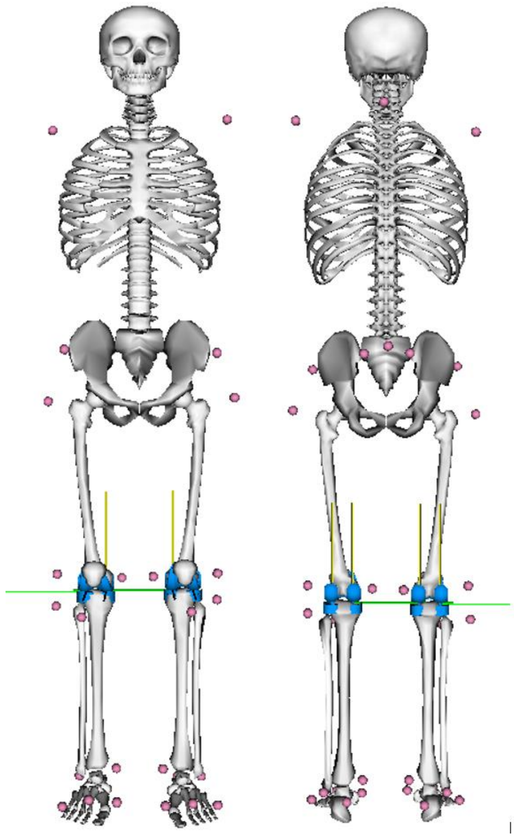

Figure 28: IOR gait Marker set placed on one of our scaled models.

The motor tasks of interest for this clinical study were 3: walking, stair ascending and stair descending, which are motor activities that most individuals need to perform daily. Stairs ascending and descending are tasks not sufficiently investigated in studies concerning OA and in general in studies involving musculoskeletal analysis, that's why it was decided to include them within this study. Stair ascending requires a greater range of motion of the lower limbs, there are greater moments acting on the knees and in general there is a greater overall muscle action **[7]**. Indeed, this is a motor task that the elderly and patients with advanced forms of OA have difficulty performing. Five repetitions of each task were recorded for each subject and patients were asked to move at their normal speed. Stair ascending and descending were performed step-over-step on a staircase with four steps, each 16 cm high, 28 cm deep and 86 cm wide, with no railings nor banisters, and with two force plates under the second and third step.

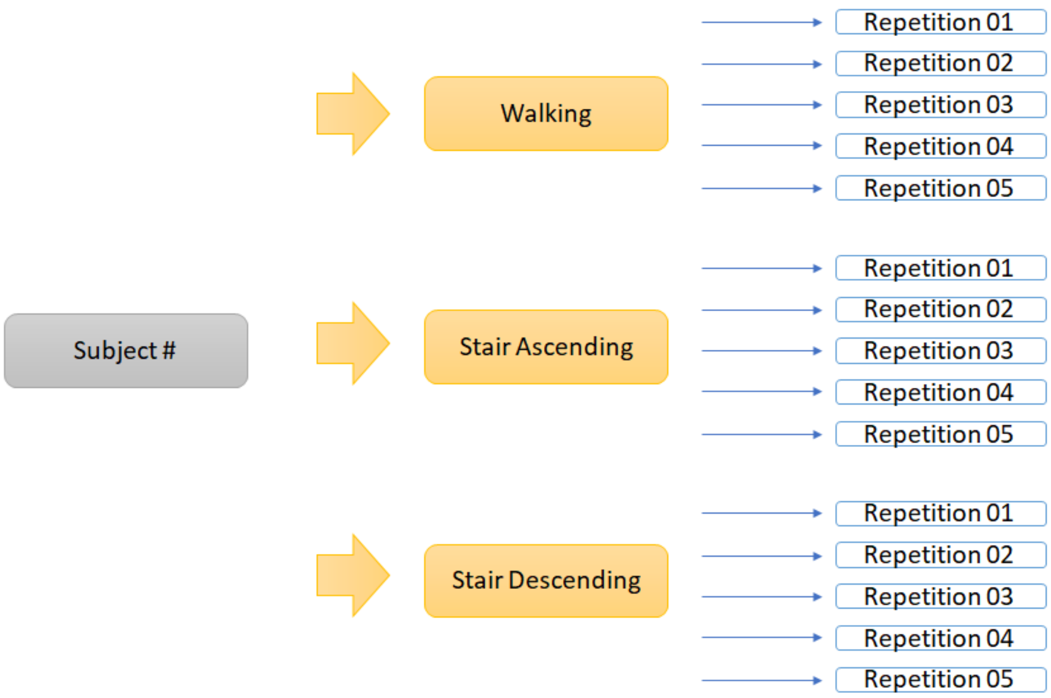

Figure 29: Schematization of motor tasks performed by patients

Static acquisitions necessary for marker calibration and scaling, were also performed in two ways. The first required to have the patient positioned with one foot on each force platform. The second involved positioning the patient with both feet on the same force plate. From this acquisition it was possible to derive the actual weight associated with the patients.

3.1.4 EMG recordings

EMG signals refer to a set of electrical signals from muscles which are the manifestation of control by the central nervous system. They represent a method to understand the behaviour of the human body under both physiological and pathological conditions. In this study, surface EMG signals were recorded through a non-invasive sampling system (2000 Hz, Wave Wireless, COMETA, Milan, Italy). Pre-amplified adhesive surface electrodes were placed parallel to the muscle fibers according to SENIAM recommendations. There were 16 recording channels, i.e. 8 muscles per leg, described as follows:

1. *GMED – Gluteus Medius*: extends and tilts pelvis laterally when prefixing fixed point on femur, abducts thigh, aids in upright standing.

2. *ES – Erector Spinae*: is part of the muscles of the vertebral showers, extends the column by going against the force of gravity to maintain an upright position.
3. *RF – Rectus Femoris*: Is a bi-articular muscle located in the anterior position of the thigh. It acts as a hip flexor and knee extensor.
4. *VML – Vastus Medialis*: One of the four heads of the quadriceps. It is an extensor of the knee and stabilizes the patella. It is the most active muscle during leg extension.
5. *BFLH – Bicep Femoris Long Head*: Acts in both hip and knee movements.
6. *STEND – Semitendinosus*: Positioned postero-medially in the thigh. Allows flexion and intrarotation of the leg and adducts the thigh.
7. *GASTMH – Gastrocnemius medial head*: superficial and posterior muscle of the leg. Allows extension of the foot by rotating it internally and participates in flexion of the leg.
8. *TA – Tibialis anterior*: Dorsiflexes, rotates and adducts the foot.

Ideally, we would like the signals recorded to exactly match the EMG signal generated at the muscle level. In practice noise and interference due to disparate reasons (network interference, environmental noise, motion artifacts, crosstalk etc) are superimposed on the recorded signal. To limit these noises it is necessary to apply filters [49]. The first filtering was done before the digitalization process, applying a band-pass filter with cutoff frequencies of 40 Hz and 200 Hz. In this way was possible to eliminate low-frequency trends, possible offsets due to DC voltage, motion artifacts… as well as superimposed high-frequency noise and to avoid aliasing phenomena.

Electromechanical delay

To eventually compare EMG signals with their respective activations, it was necessary to consider the phenomenon of electromechanical delay (EMD). Electromechanical delay can be defined as the delay between electrical activity arriving in the muscle and a measurable change in muscle tension [50]. This happens since muscle response can be slowed down due to many factors. In particular, EMD is believed to be caused by: the position of body segments, how motor units are recruited, characteristics of the tissue involved by signal conduction, speed of conduction etc. [51], [52]. EMD values reported in the literature vary widely but different studies observed it from a minimum of 8 ms to a maximum of 100 ms during voluntary contractions [53], [54], [55].

Then, to account for physiological electromechanical delay, in our study time-shifting in a range of 10-100 ms was applied to the EMG envelopes corresponding to the highest cross-correlation coefficient between EMG signals and Activation evaluated during our simulations [56]

3.2 Baseline musculoskeletal model

One of the most important keys to the development of this thesis was the choice of the musculoskeletal model to use as a baseline. The most logical choice would be to create a model of the patient's musculoskeletal system using advanced imaging techniques that can replicate every feature in a virtual environment [57]. According to the data available, the best starting model was a generic model capable of predicting MCFs and LCFs, allowing us to optimize the model customization time and perform the simulations of the three motor activities. The choice fell on the validated model developed and introduced by Lerner et al. [35], which is based on the full-body model developed by DeMers et al. [58] consisting of 18 body segments and 92 muscle-tendon actuators. They incorporated a tibiofemoral joint capable of returning both MCFs and LCFs as output of the Joint reaction analysis.

This model includes a series of joints to simulate and describe the behaviour of the lower body. Among these we find a ball-and-socket joint between the third and fourth lumbar vertebra, three translations and three rotations of the pelvis, ball-and-socket joints at each hip, and revolute ankle and subtalar joints.

The tibiofemoral joint was developed with additional components to allow the frontal-plane alignment of the knee and for resolving distinct medial and lateral tibiofemoral forces. To achieve this, they introduced a distal femoral component and a tibial plateau body evaluated CAD techniques with the geometry of the instrumented implant, with orientation parameters for configuring frontal-plane alignment in the femur (θ_1) and tibia (θ_2). A series of joints were then defined between the femoral component and the tibial plateau to characterize the tibiofemoral kinematics and medial/lateral load distribution.

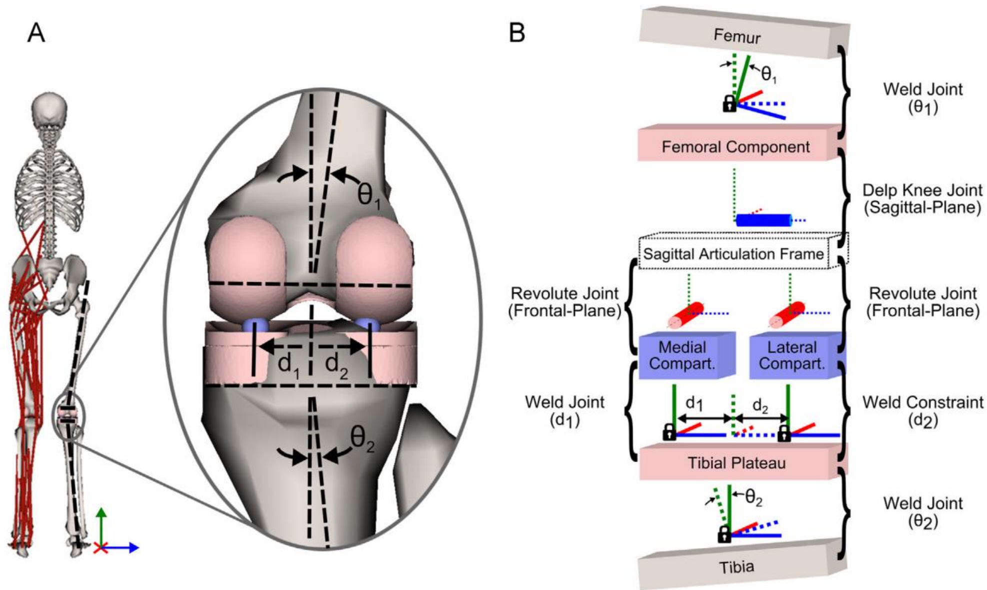

Figure 30: Graphical (A) and schematic (B) description of the medial/lateral compartment of joint structure in Lerner's model [35]

The knee joint was defined according to previous research [22], which specified the sagittal-plane rotations and translations of the knee between the femoral component and the sagittal articulation frame of reference. Two revolute joints were also connected to the sagittal articulation frame to represent the medial and lateral tibiofemoral compartments. These joints had axes perpendicular to the frontal plane, and the medial and lateral compartments were welded at the anteroposterior mid-point of the tibial plateaus, allowing them to articulate with the surface of the femoral component during flexion-extension. These revolute joints cannot resist to the frontal-plane moments individually but acting in parallel they share all the loads transmitted between the femur and tibia and resolve them as the medial and lateral contact forces. The patella segment was also included in the model and articulated with the femoral-condyle segment according to previous research.

Overall, the knee remains a joint with a single degree of freedom with movement allowed only and exclusively in the sagittal plane.

This type of model lends itself to being customized with both parameters which, from what emerges from the study of the literature, have a strong influence on the distribution of forces in the knee compartments: TFA and CPs. TFA can be implemented by modifying the orientations of the weld joints that are found respectively on the femur and on the tibia (i.e. θ_1 θ_2, TFA default= 0°) while the CPs can be modified by changing the position of the weld joints on the tibial plateau (default distance from knee center: 20mm).

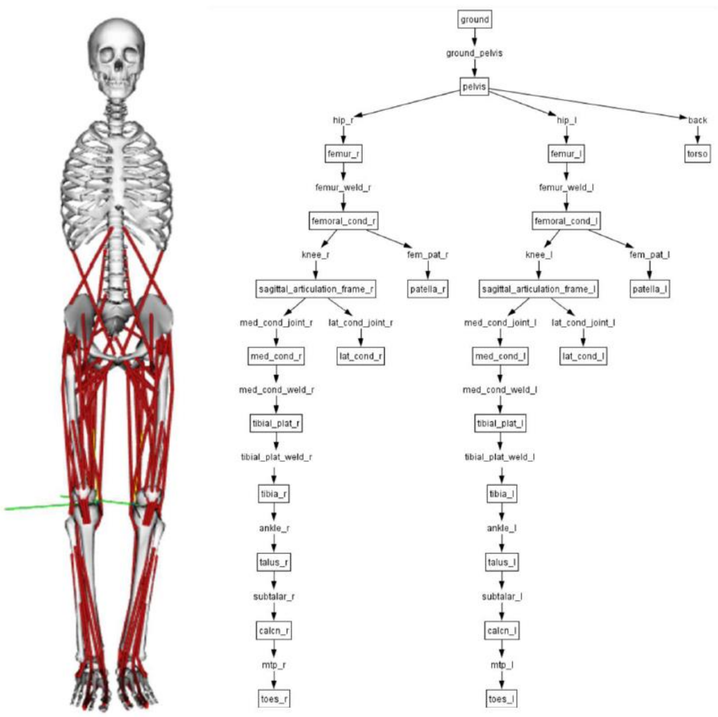

Figure 31: Topology window of Lerner's musculoskeletal model

3.3 Modeling and simulation workflow in OpenSim

Four different OpenSim musculoskeletal models were scaled and then built with four different levels of customization for each patient, with the aim of isolate the effects of each of these parameters on the predictions of the forces.

- *Uninformed (UI):* Just as the one used in Lerner's study [35], this model is built based on data recorded from an instrumented prostheses, contact model for a neutrally aligned lower extremity[27] and matching assumptions for an artificial knee implant made previously [5]. CPs in the frontal plane of the medial and lateral compartment were placed 20 mm medial and lateral from the knee joint center. As the model is the UI, TFA was set as 0°.
- *Tibiofemoral alignment – informed (TFAI):* This model had subject specific TFA but uninformed CPs.
- *Contact point – informed (CPI):* This model had subject specific CPs but uninformed TFA.
- *Fully – informed (FI):* This model had subject specific TFA and CPs informed through radiographic analysis

To answer the questions of our interest and to estimate joint reaction forces in knee compartments, a workflow in OpenSim based on an inverse dynamics and static optimization approach was adopted, as summarized in the figure below.

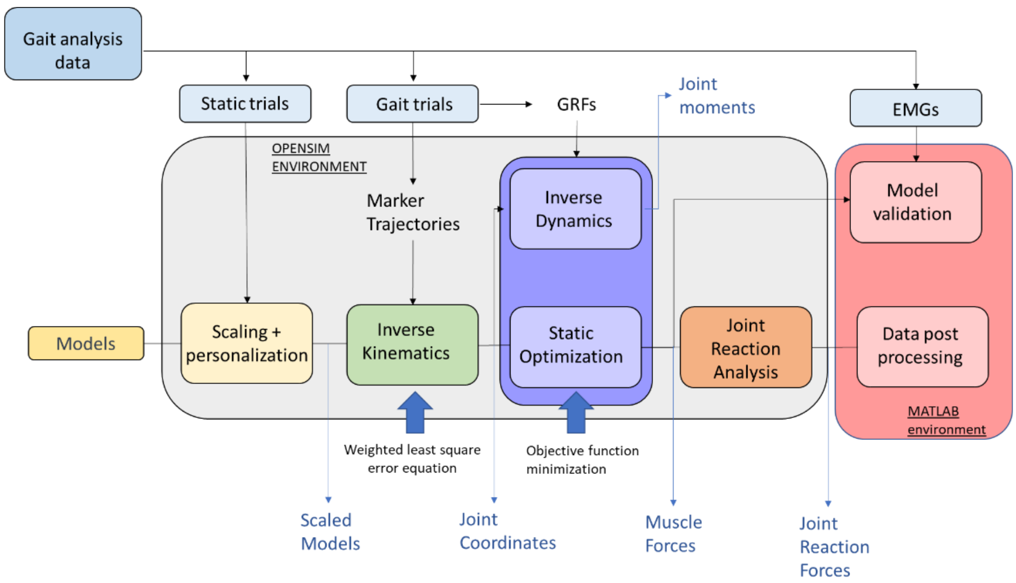

Figure 32: Inverse dynamics and static optimization approach used to solve joint reaction forces in OpenSim.

To perform all the steps of our workflow for each patient, model, and task, MATLAB routines were implemented that could generate setups to be provided as input to OpenSim. The workflow steps were run directly in the MATLAB environment, to totally bypass the OpenSim interface and loop through the simulations involved in our study. It was decided to proceed in this way to be able to complete the large number of simulations required to obtain all the data for the patients involved in the study.

To save time and computational work, the IK, ID and SO steps were performed only for the UI and TFAI models since the introduction of CPs goes to affect only the estimation of forces but not the inverse kinematics and inverse dynamics processes.

3.3.1 Files opening

The data from the Vicon system present in the laboratory were available in .c3d format. Firstly MATLAB routines, capable of separating all the information contained here into separate files, have been implemented. These allowed us to split contents of the .c3d files and obtain in the desired format the files of:

- *The marker trajectories* - recorded by the Vicon system.
- *The ground reaction forces* – recorded from the force platforms.
- *The EMG recordings* – recorded during motor tasks.
- The information regarding the gait events

In these experimental files resides everything necessary to solve the inverse kinematics and dynamics problem that allowed us to estimate the joint reaction forces.

3.3.2 Models customization

The only step in the non-automated workflow was the model customization. We decided to perform this before starting the OpenSim workflow. This, at the modeling level, corresponds to the actual starting point of the simulation process. As described above, the customization parameters were TFA and CPs where former was set in radiant, while the latter was expressed in meters.

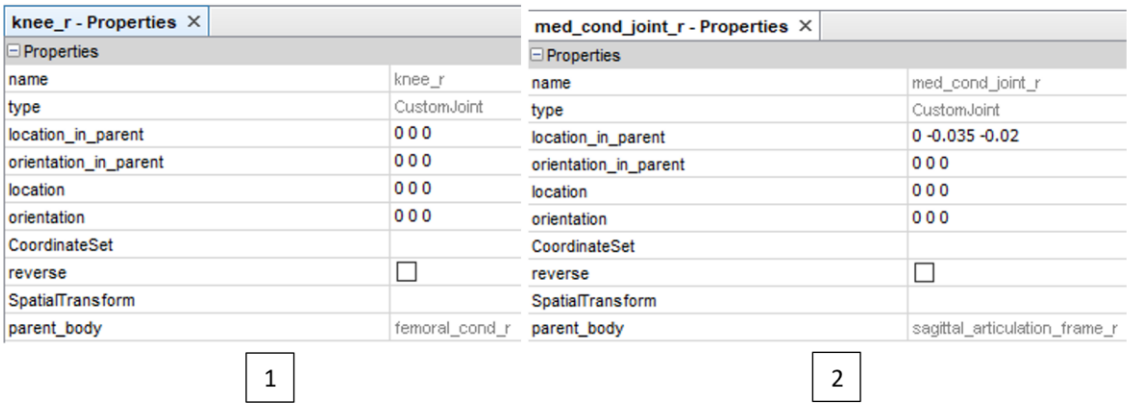

knee_r - Properties

Properties	
name	knee_r
type	CustomJoint
location_in_parent	0 0 0
orientation_in_parent	0 0 0
location	0 0 0
orientation	0 0 0
CoordinateSet	
reverse	☐
SpatialTransform	
parent_body	femoral_cond_r

1

med_cond_joint_r - Properties

Properties	
name	med_cond_joint_r
type	CustomJoint
location_in_parent	0 -0.035 -0.02
orientation_in_parent	0 0 0
location	0 0 0
orientation	0 0 0
CoordinateSet	
reverse	☐
SpatialTransform	
parent_body	sagittal_articulation_frame_r

2

Figure 33: OpenSim's property windows where it is possible to modify the model with our geometric parameters of interest 1) TFA 2 B) CPs

From the generic UI model, it was possible to obtain the models described above using the OpenSim GUI to modify its structure. To customize the model with TFA, it was necessary to act on the knee joint (in fig. 33, knee_r) by entering the parameter measured as the first component in the orientation_in_parent section of the properties window. To obtain a CPs informed models (i.e., CPI, FI), it was necessary to enter the parameter of interest as the third component in the location_in_parent section of the med_cond_joint and med_cond_weld joints with regard to the medial contact point, while acting on the lat_cond_joint and lat_cons_contraint joints to model the lateral contact point.

Customizations were made for both the target and contralateral limb.

Once the models of interest were obtained, they were ready to enter the actual workflow of OpenSim.

3.3.3 Scaling

The first step of the OpenSim's workflow is scaling. Here the markers belonging to the previously described IORgait marker set were applied to the virtual model to be used during the process. This process scales the generic model to minimize differences between the real model of the patient (acquired through orthostatic registration) and the virtual one. As described in Section 2.7.3, a custom setup was provided to OpenSim for each Scaling performed, in this way the correct parameters were set.

The exact body weight of the subjects was obtained from the static task recording with both feet on one single platform: the weight was then calculated as the mean value of the Euclidean norm of the three components evaluated by the force plate.

The type of measurement-based scale factors and the manual scale factors used are given below.

Measurements	Marker Pairs					
Pelvis_X	LASIS	LPSIS	RASIS	RPSIS		
Pelvis_z	RPSIS	LPSIS	RASIS	LASIS		
Trunk_Y	C7	L5	RA	RASIS	LA	LASIS
Trunk_Z	RA	LA				
Thigh_R	RASIS	RLE				
Thigh_L	LASIS	LLE				
Shank_R	RHF	RCA				
Shank_L	LHF	LCA				
Foot_R	RCA	RVM	RCA	RSM	RCA	RFM
Foot_L	LCA	LVM	LCA	LSM	LCA	LFM

Figure 34: Measurement-based scale factors used for scaling

Body Name	Measurement(s) Used			Applied Scale Factor(s)		
ground	Unassigned					1.0
pelvis	Pelvis_X	Unassigned	Pelvis_z	1.257633	1.0	1.062340
femur_r	Thigh_R					1.003537
femoral_cond_r	Unassigned					1.0
sagittal_articulation_frame_r	Unassigned					1.0
med_cond_r	Unassigned					1.0
lat_cond_r	Unassigned					1.0
tibial_plat_r	Unassigned					1.0
tibia_r	Shank_R					1.102630
patella_r	Unassigned					1.0
talus_r	Foot_R					1.073892
calcn_r	Foot_R					1.073892
toes_r	Foot_R					1.073892
femur_l	Thigh_L					0.998354
femoral_cond_l	Unassigned					1.0
sagittal_articulation_frame_l	Unassigned					1.0
med_cond_l	Unassigned					1.0
lat_cond_l	Unassigned					1.0
tibial_plat_l	Unassigned					1.0
tibia_l	Shank_L					1.069121
patella_l	Unassigned					1.0
talus_l	Foot_L					1.061178
calcn_l	Foot_L					1.061178
toes_l	Foot_L					1.061178
torso	Unassigned	Trunk_Y	Trunk_Z	1.0	0.978776	1.290213

Figure 35:Manual Scale factors used for scaling

To achieve the best possible match different weights can be associated with the markers, to make a certain marker important (or not) for the scaling process. We decided to set all weights equal to 1. It is possible to decide to disable one or more markers thus opting whether or not to consider them during the scaling process. This option can be useful in the presence of patients with high BMI. Indeed, in these situations, the errors achieved on markers as RGT or LGT could be high and affect the scaling process.

Enabled	Marker Name	Value	Weight
☑	RA	From File	1.0
☑	LA	From File	1.0
☑	C7	From File	1.0
☑	L5	From File	1.0
☑	RASIS	From File	1.0

Figure 36: A part of our Static pose weight set used for Scale Tool

Each step described from here on was performed for each repetition of all 3 motor tasks and for each model made per patient.

3.3.4 Inverse Kinematics

Once the model was scaled, it was ready to enter the IK step. In this step, the kinematics associated with all body segments in the model were estimated by comparing the real model to the virtual model. The goal in IK was to minimize the distances between virtual and experimental markers, as described in section 2.7.4 of this thesis.

All the parameters necessary for the correct performance of IK were provided to OpenSim through the setups constructed with the previously described routines. It was decided to set as the first simulation instant the first right heel strike, as the last one the second left heel strike.

To solve the minimization problem, the kinematic data from the Vicon system were disregarded, and only the errors between virtual and experimental markers were used. To succeed in minimizing errors on markers it is possible to go disable some markers or associate specific weights to markers of greatest interest and at the same time "loosen" the restrictions associated with less important markers. In this study, all markers provided by the marker set were considered, and the weights associated with them were set to 1. This approach was chosen to ensure that all markers were given equal importance in the analysis.

Enabled	Marker Name	Value	Weight
☑	RA	From File	1.0
☑	LA	From File	1.0
☑	C7	From File	1.0
☑	L5	From File	1.0
☑	RASIS	From File	1.0
☑	RPSIS	From File	1.0
☑	RGT	From File	1.0
☑	RLE	From File	1.0
☑	RHF	From File	1.0

Figure 37: A part of our weight set used for IK Tool

3.3.5 Inverse Dynamics

The .mot file that was obtained as output from the IK was then used as input here. All the parameters required for the successful execution of the ID step were supplied to OpenSim through the custom setups created using the routines described earlier. ID is the first step in the workflow involving the external forces file. External forces were defined as a point forces, with the heel chosen as the point of their application. It was necessary to implement these settings for both the right and left limbs.

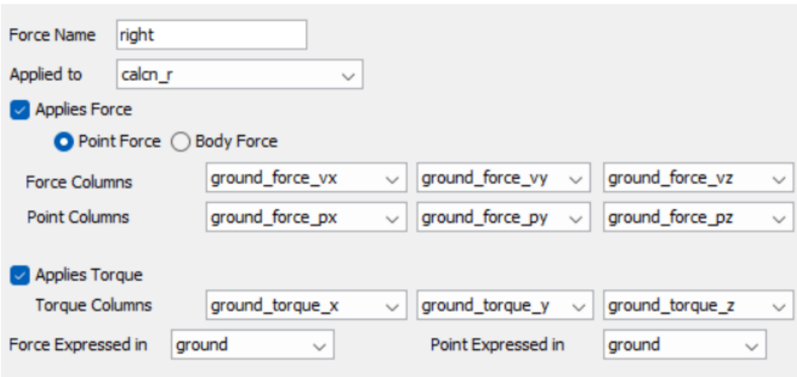

Figure 38: GRF settings necessary for the ID Tool

The ID Tool plays a crucial role in determining the generalized forces acting on each joint based on the kinematics of the body segments and external forces. Newton's generalized second law is used to derive the forces from the kinematics. However, due to experimental errors, Newton's second law may not always hold true. To account for this inconsistency, residual forces and moments are applied to the pelvis. For a simulation to be considered accurate, the magnitude of these residual forces must not exceed 5% of the maximum external force [59]

3.3.6 Static Optimization

The next step in the workflow, which requires inputs from both the IK and external forces (.mot) files, is Static Optimization. This step calculates the muscular forces starting from the moments that act on the joints. These muscular forces are obtained by carrying out a process of minimization of the sum of the squares of the muscular activations. In our case study it was necessary in this phase to introduce reserve actuators. All the parameters necessary for the correct performance of the SO were provided to OpenSim via the specially constructed setups thanks to previously described routines.

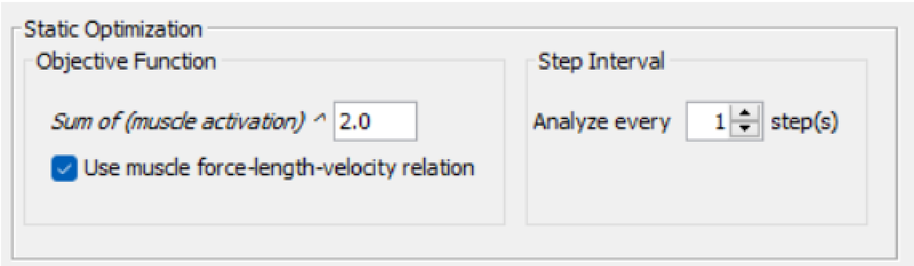

Figure 39: objective function selected for our simulations.

3.3.7 Joint Reaction Analysis

The Joint Reaction Analysis tool was employed to determine the joint reactions of all joints within the model. Although the forces acting on the child body are typically expressed in the ground frame, we chose to express them in the child frame. Our aim was to resolve both MCFs and LCFs. All the parameters necessary for the correct performance of this step were provided to OpenSim via the specially constructed setups thanks to the previously described routines.

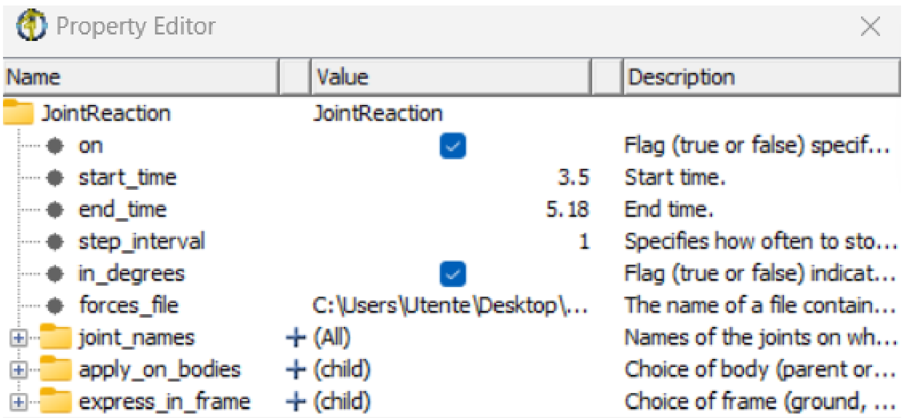

Figure 40: an example of property editor. Important settings of the simulation must be inserted here.

The outputs from this tool are different from those obtained by performing Inverse Dynamics. ID allows obtaining the generalized net forces in each degree of freedom of the model. It considers only the applied external forces (GRFs) and the kinematics of the model, completely ignoring the contribution due to the muscles, motors and actuators. Through Joint Reaction Analysis, on the other hand, it is possible to calculate the resulting forces and moments in the joint structures present in the model while considering the contribution from muscles, motors and actuators.

3.4 Post-processing of the knee contact forces

In the following sections we aim to describe schematically the steps taken to post-process the output files obtained from the SO and the OpenSim Joint Reaction Analysis Tool, to answer the questions that prompted us to pursue this thesis project. It was decided to focus only on the target limb and not to consider the contralateral limb, considered the most affected by OA. What is described next was performed for each repetition of each task and for each model constructed and basis on the anthropometric characteristics of each patient.

The whole post-processing phase was performed in MATLAB R2021b, and as a first step all KCFs were normalized to the percentage of stance phase of motor activity cycle and to each subject body-weight (BW). To reply to our first research question, i.e. the effect of geometric parameters on KCFs, statistical parametric mapping (SPM) and an analysis on the peak force distributions were performed to evaluate the differences among the models. To reply to our second research question, i.e. the relationship between the KCFs and the geometric parameters, a linear regression analysis was performed to evaluate how the KCFs correlated with the TFA and CPs.

3.4.1 Contact forces

OpenSim Joint Reaction Analysis outputs were imported in MATLAB from files in .sto format and saved within memory structures. The .sto files contain the estimated force reactions for each joint present within the model in the form of a single large matrix having as rows the simulation frames and as columns the components of the acting forces and moments.

This file contains the reaction forces and moments
applied to the specified body of a joint pair and expressed in the specified reference frame.

Units are S.I. units (seconds, meters, Newtons, ...)
endheader

time	ground_pe	ground_pe	ground_pe	ground_pe	ground_pe	ground_pe	ground_pe	ground_pe	ground_pe	hip_r_on_	hip_r_on_	hip_r_on_	hip_r_on_	hip_r_on_	hip_r_on_
3.86	0	0	0	0	0	0	0	0	0	-64.9349	-127.42	68.36885	-0.19443	-0.25545	0.266485
3.87	0	0	0	0	0	0	0	0	0	34.92986	-205.288	65.66456	0.163813	-0.20505	-0.03057
3.88	0	0	0	0	0	0	0	0	0	75.94486	-528.628	87.89823	0.230435	-0.27938	-0.11835
3.89	0	0	0	0	0	0	0	0	0	99.89337	-778.029	94.09867	0.201141	-0.29243	-0.22986

Figure 41: example of a .sto file, output of the Joint Reaction Analysis Tool

The components of the total force acting on the knee, MCF and LCF estimated in the target limb were derived for each repetition analysed. The Euclidean norm of the three components of each force considered was performed to derive the total forces.

It was decided to focus the attention of the analyses on the behaviour that the forces exhibited during stance. For this reason, the signals were isolated in this portion of the GC. It was necessary to resample the signals to have 100 samples between the instant of beginning and end of the interval considered, so that different repetitions of the same motor task could be made comparable with each other. The magnitude of the estimated forces was normalized with respect to the weight (N) associated with the patient, thus obtaining the forces expressed no longer in Newtons but in body weight (BW).

The averages and standard deviations associated with each complete task (5 repetitions) of each model performed for all the patients considered were stored in special memory structure to be then used in the statistical analysis and peak finding process.

Figure 42: an example of a TOTAL force pattern evaluated as a mean of 5 repetition. for the walking task. It is possible to see that has a double peak pattern.

The force patterns during stance present a first and a second force peak. The study of the distributions of these peaks is important both to understand how much the predictions of the models differ and to understand how well the geometric parameters correlate with the actual force values. To determine the locations of the peaks, it was necessary to search for the maximum value of the function associated at the total force in two separate intervals, to correctly find them. Then, were evaluated the peaks of the lateral and medial forces by going to obtain the value of the function associated with the positions (sample) of the peaks in the total force.

3.5 EMGs and Activations post processing

Validation of these models is a crucial step and remains one of the most challenging aspects to manage. Like any model, they are subject to uncertainties that arise during design and simulation. Since direct information cannot be obtained through instrumented prostheses, the validation of the models developed for this thesis relied on comparing the EMG signals recorded during motor tasks with the activations obtained as output from Static Optimization.

However, it is not entirely appropriate to compare these two types of signals because the activations obtained from OpenSim correspond to the estimated EMG signals normalized to the maximum muscle activation value set during the creation of the corresponding muscle model. In contrast, the EMG signals recorded in the laboratory correspond to the electromyographic signal, not normalized for the maximal muscle activation value (which was not available in our study). To make a comparison possible, the EMG signals were normalized to the maximum value of the corresponding activation signals assessed with the TFAI models.

3.5.1 Activation post processing

What is described in this section was done for each activations file obtained from the simulations performed with the TFAI and UI models.

The outputs of the OpenSim SO were imported in MATLAB from files in .sto format and saved within memory structures. The .sto files contain estimated muscle activations for each muscle of the model which are normalized against their maximal force value. They are organized in one large matrix having as rows the simulation frames and as columns estimated muscle activations during the simulation.

time	glut_med1	glut_med2	glut_med3	glut_min1_	glut_min2_	glut_min3_	semimem_	semiten_r	bifemlh_r	bifemsh_r
3.8	2.32E-05	0.107252	0.307107	8.51E-05	0.014519	0.112361	9.8E-06	3.59E-05	1.37E-05	0.12881
3.81	1.79E-05	0.026599	0.204084	6.84E-05	0.000561	0.051321	1.43E-05	5.32E-05	2.17E-05	0.076889
3.82	1.21E-05	4.84E-05	0.060341	4.17E-05	5.19E-05	0.000121	3.71E-05	0.000165	0.000132	0.005513
3.83	1.41E-05	5.07E-05	0.036006	4.81E-05	5.56E-05	0.000101	0.00194	0.004376	0.051449	0.00307
3.84	1.66E-05	6.49E-05	0.042914	5.49E-05	6.23E-05	0.000109	0.090243	0.024334	0.128618	0.003126
3.85	2.21E-05	0.000111	0.055602	7E-05	7.94E-05	0.000151	0.165748	0.042755	0.186176	0.002363

Figure 43: example of an Activation .sto file obtained as output of SO

A whole GC of muscle activations for each muscle of interest of the target limb was isolated. For the Gluteus Medius Muscle, the Euclidean norm of the three modeled muscle components was performed. The signals were then resampled to obtain 100 samples between the beginning and end of the GC. This allowed for the activations estimated during different simulations to be compared.

Next, the mean and standard deviations of the five repetitions of each simulated motor task associated with the models were calculated and stored in appropriate memory structures. These signals were used to make the comparison with EMGs during the indirect validation process.

3.5.2 EMGs post processing.

Experimental EMG files were provided within .c3d format files. After extracting the signals in the appropriate way, only the muscles of interest in the target limb were analyzed. To obtain EMG envelopes, a 6th order Butterworth low-pass filter with a cutoff frequency of 6 Hz was applied, followed by rectification.

To properly compare EMGs and activations, it was necessary to handle the EMD problem. A GC associated with the signals of interest was taken into analysis. 100 samples within the GC were resampled and then the new sampling rate was calculated. The average of the repetitions of the analysed task estimated with the TFAI model of the patient under investigation was extracted. Normalization of the EMG signal to the maximum value of the Activations signal was performed. The delay between the two signals was calculated assessing the cross-correlation them and searching the lag where correlation was maximum. A threshold was set on the maximum delay to be consistent to what has been found in the literature: If the estimated delay was greater than 0.1 s, then a time shift of the EMG signal equal to 0.1 s was implemented. Otherwise, the signal was delayed by a factor equal to the estimated delay. The signal was then resampled to obtain 100 samples within the GC. Averages and standard deviations were calculated for each complete task performed by each model of each patient.

3.6 Statistical Analysis

The term statistical analysis refers to the collection and interpretation of data to determine trends and patterns. It helps us describe the nature of the data that have been obtained and processed and explore the relationships that exist in a population or those between stand-alone populations. Statistical analysis is also useful to prove the validity of evaluated models. Specifically, for this thesis, we relied on statistical analysis to determine and quantify the difference existing between the outputs obtained from the four models used for the simulations. It was also used to be able to understand the correlations between the force outputs and the geometric modeling parameters and to make and indirect validation of our model.

Effect of geometric parameters on KCFs

To quantify the difference between evaluated models and answer the first research question, we used statistical parametric mapping (SPM). SPM refers to that whole set of spatially extended statistical methods that have been developed to test hypotheses concerning functional imaging data [60]. This technique can analyze smooth changes in topology associated with experimental interventions, and it can be applied in multiple dimensions [61]. The SPM package we use was developed do an analysis of brain imaging sequences, but nowadays they are also optimized for fMR, EEG... In biomechanics, SPM can be seen as a topological methodology to understand whether there is variation in n-dimensional quantities [61]. In our case these correspond to the averages of repetitions obtained patient by patient, for each model.

At the end of post processing on joint reaction forces we have 4 matrices per task: of M rows (100 samples) and N columns (patients considered). Each column corresponds to the average of repetitions done for a specific task, obtained from simulations of one of the four models. SPMs were used to be able to quantify whether the differences between the 4 models (the four matrices) were statistically significant and at which instants of the GC.

For each task, for both lateral force and medial force, 6 different combinations were determined to perform the SPMs: UI-TFAI, UI-CPI, UI-FI, TFAI-CPI, TFAI-FI, CPI-

FI. SPM is a nonparametric two-tailed paired t-tests ($\alpha = 0.05$), evaluated by using the SPM1D package v 0.4.8 for MATLAB [62].

During post-processing, peak distributions for medial and lateral forces for each task were derived for each simulated model.

A whole series of parameters such as mean, standard deviation, median and interquartile range were defined for these distributions, and it was decided to represent them by boxplots. Wilcoxon sign-rank tests ($\alpha = 0.05$).) were also performed to determine any statistically significant differences among distributions. For each task, for both LCFs and MCFs peak distributions, 6 different combinations were determined to perform this test: UI-TFAI, UI-CPI, UI-FI, TFAI-CPI, TFAI-FI, CPI-FI.

Relationship between geometric parameters and KCFs

Linear correlations (R, p-value) between the model customization parameters and the two peaks of the MCFs and LCFs estimated during the motor tasks were also evaluated. Specifically, it was decided to correlate the TFA with the peaks obtained from the TFAI and FI models and to correlate the medial and lateral CPs with the force peaks obtained using the CPI and FI models.

Indirect validation: EMG vs Activations

Since it is not possible to have direct measurements by instrumented prostheses, model validation was performed by comparing estimated muscle force patterns and between EMG signals taken during gait analysis sessions.

Temporal correlation (R value=1 perfect correspondence) between activations obtained by static optimization in the UI and TFAI models and the EMG signals was calculated, first applying an EMD to the electromyographic signals in accordance with what was reported in the previous chapter.

The similarity between EMG signals and activations was assessed by RMSE. A lower value of RMSE corresponds to a higher correspondence between the analyzed signals.

Chapter 4

Results

4.1 Effect of geometric parameters on KCFs

MCFs and LCFs were significantly different among the four models with different level of personalization in geometric parameters during the three motor activities. In particular, the comparisons of the forces between models showed significant differences in most of the stance phase of the gait cycles in almost all cases. The largest differences always occurred between TFAI and CPI, which could reach a mean difference in MCF of 1.2 BW during walking at the second force peak (fig. 45). In all motor tasks the patterns of total force acting on the knee are characterized by the typical double bumped trend among the stance phase. Walking and stair ascent show a second force peak greater than the first one in the MCFs while during stair descent the trend is reversed. LCFs estimated during walking by the TFAI model have a counterphase trend compared to what is observed for estimates forces obtained with the other models. In the remaining tasks instead LCFs present the same pattern, although of different intensity, for all four models considered. During descent, the first peak of the LCFs estimated by all models disappears, while the second peak is very pronounced.

In general, the introduction of TFA led to an increase in MCF and a decrease in LCF, while the introduction of CPs decreased MCF and increased LCF. Customization by CPs has such an effect that it results in portions of stances in which MCFs are even lower than those estimated in the lateral compartment. TFAI and UI models, on the other hand, have higher MCFs than LCFs in each task analyzed. In particular, the introduction of CPs led to more marked variations in KCFs compared to TFA. In fact, going from UI to CPI led to more marked differences than going from UI to TFAI, and CPI showed closer values to FI than TFAI to FI.

Focusing on the peaks of KCFs, we found that almost all distributions were significantly different among the four models, where the exceptions included only differences in LCF between UI and TFAI.

We found the largest differences between TFAI and CPI, whose medians of MCF distributions showed a difference of 1.2 BW during all the motor activities.

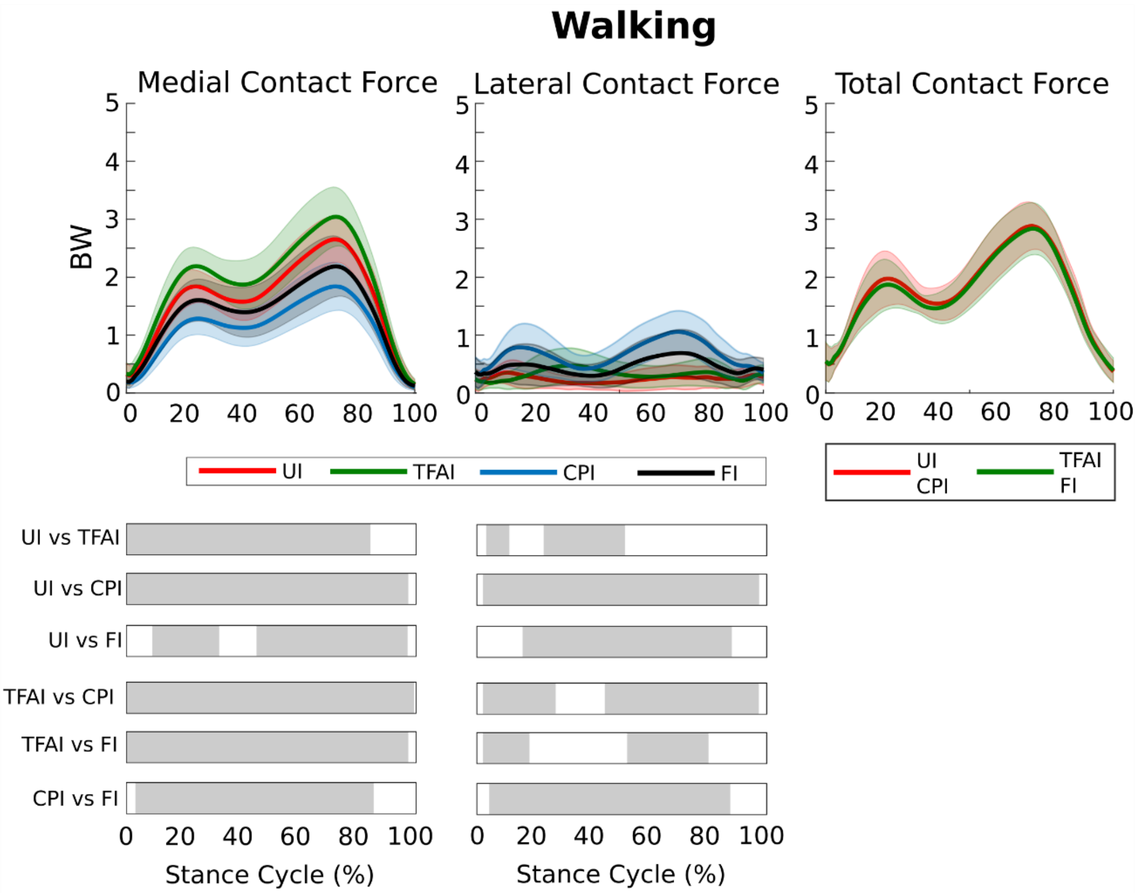

Figure 44: Mean ± SD of MCF and LCF predicted during walking stance using: UI (red, solid line), TFAI (green, solid line), CPI (blue, solid line), FI (black, solid line) models. Mean ± SD of total contact forces in the knee predicted during walking stance using: UI-CPI (red, solid line), TFAI-FI (green, solid line). Statistically significant differences between the trends obtained according to the type of customization used were evaluated with SPM and shown in the figure. Each bar corresponds to a comparison of estimated forces between two different models. Where differences were found to be statistically significant, the corresponding step phase was colored in gray.

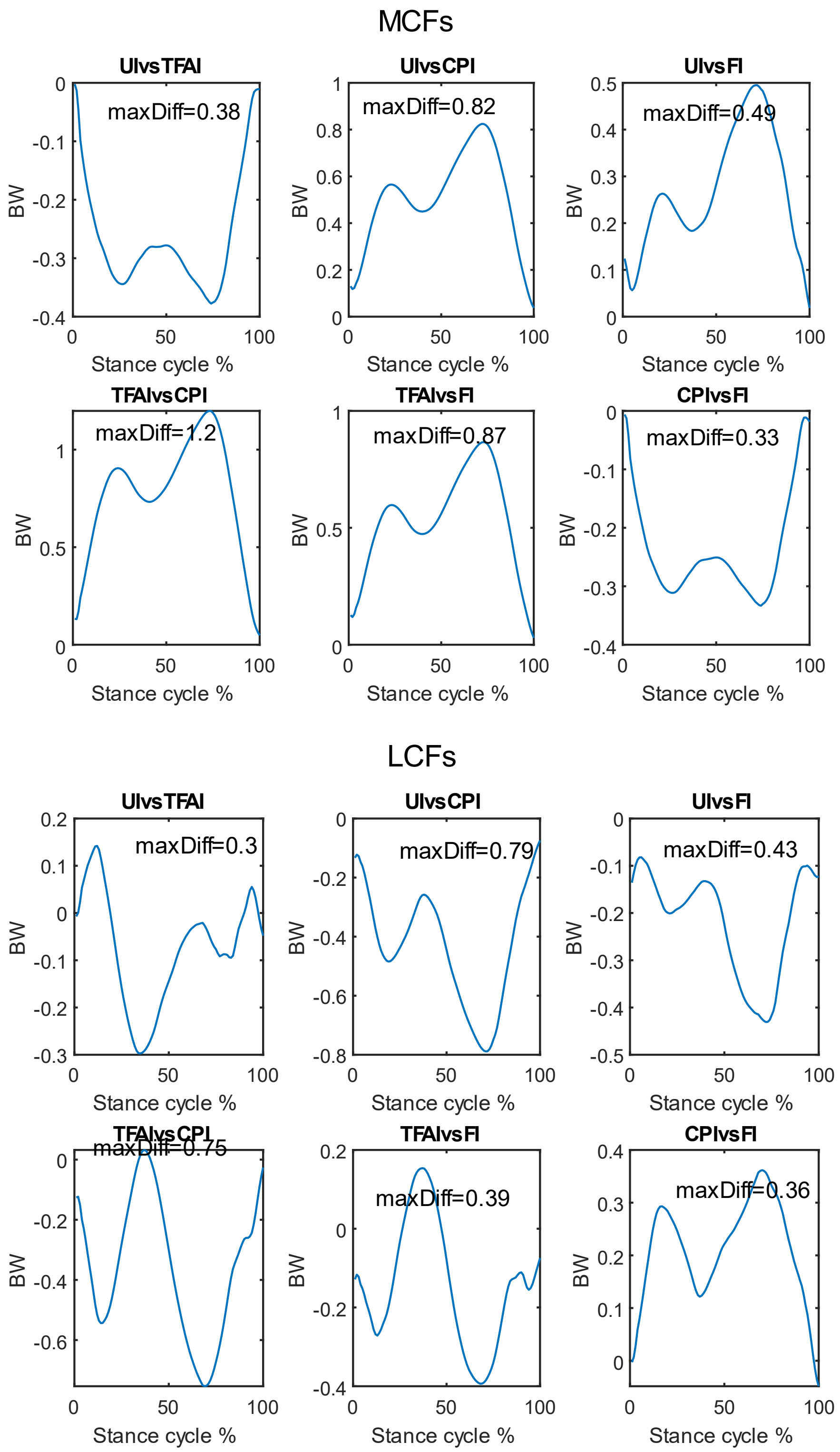

Figure 45: Mean differences among models during walking

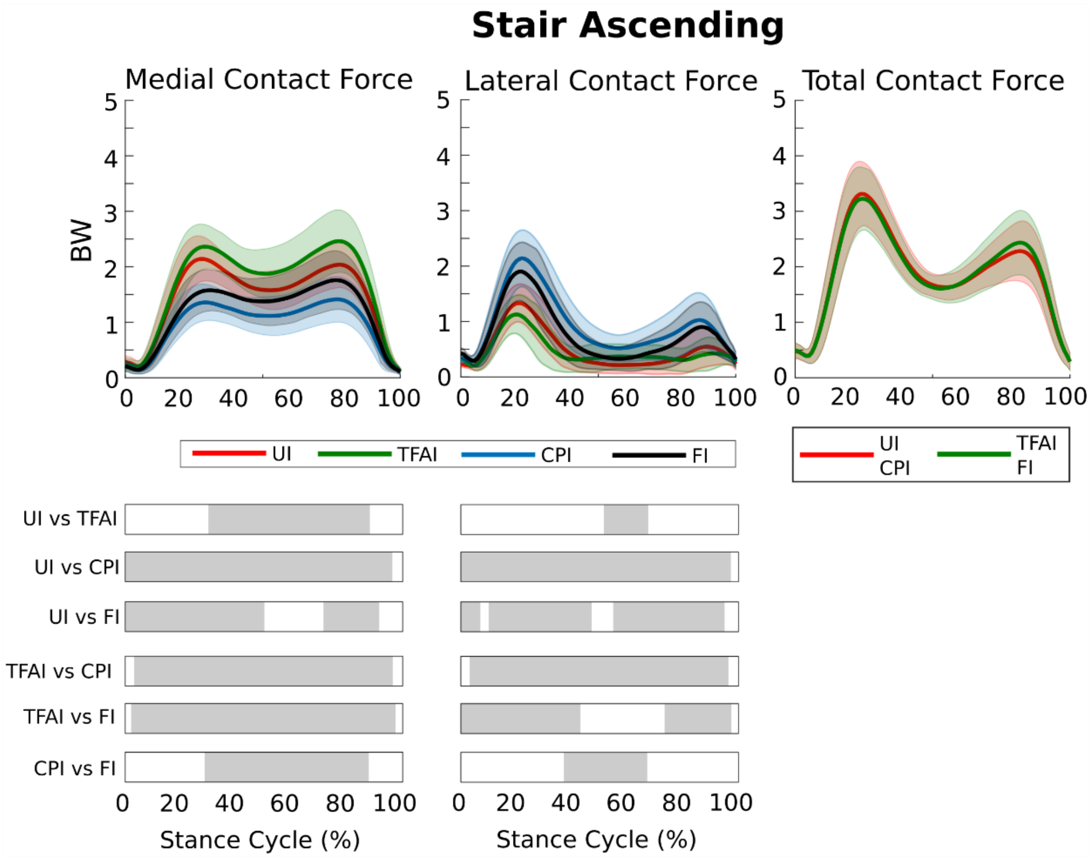

Figure 46: Mean ± SD of MCF and LCF predicted during stair ascending stance using: UI (red, solid line), TFAI (green, solid line), CPI (blue, solid line), FI (black, solid line) models. Mean ± SD of total contact forces in the knee predicted during stair ascending stance using: UI-CPI (red, solid line), TFAI-FI (green, solid line). Statistically significant differences between the trends obtained according to the type of customization used were evaluated with SPM and shown in the figure. Each bar corresponds to a comparison of estimated forces between two different models. Where differences were found to be statistically significant, the corresponding step phase was coloured in gray

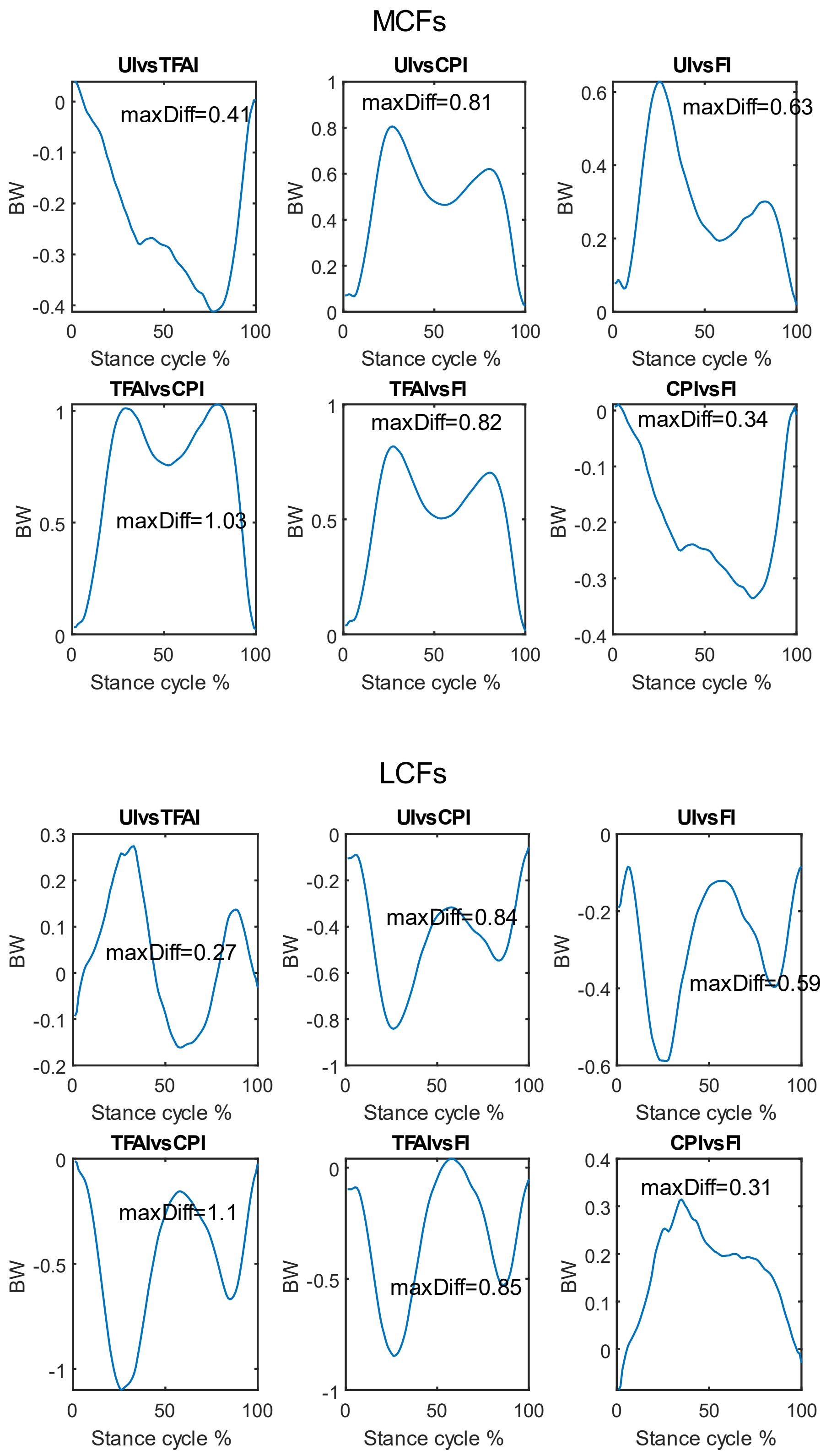

Figure 47: Mean differences among models during stair ascending.

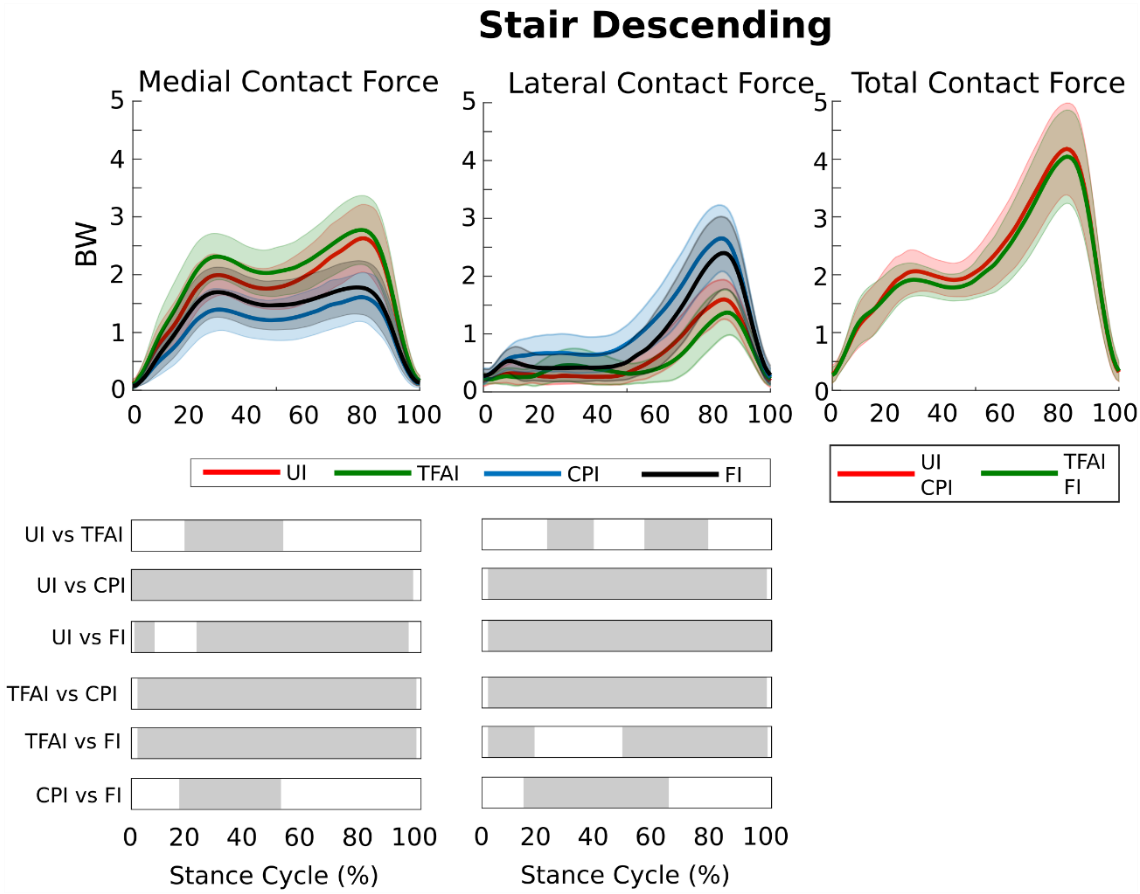

Figure 48: Mean ± SD of MCFs and LCFs predicted during stair ascending stance using: UI (red, solid line), TFAI (green, solid line), CPI (blue, solid line), FI (black, solid line) models. Mean ± SD of total contact forces in the knee predicted during stair ascending stance using: UI-CPI (red, solid line), TFAI-FI (green, solid line). Statistically significant differences between the trends obtained according to the type of customization used were evaluated with SPM and shown in the figure. Each bar corresponds to a comparison of estimated forces between two different models. Where differences were found to be statistically significant, the corresponding step phase was coloured in gray.

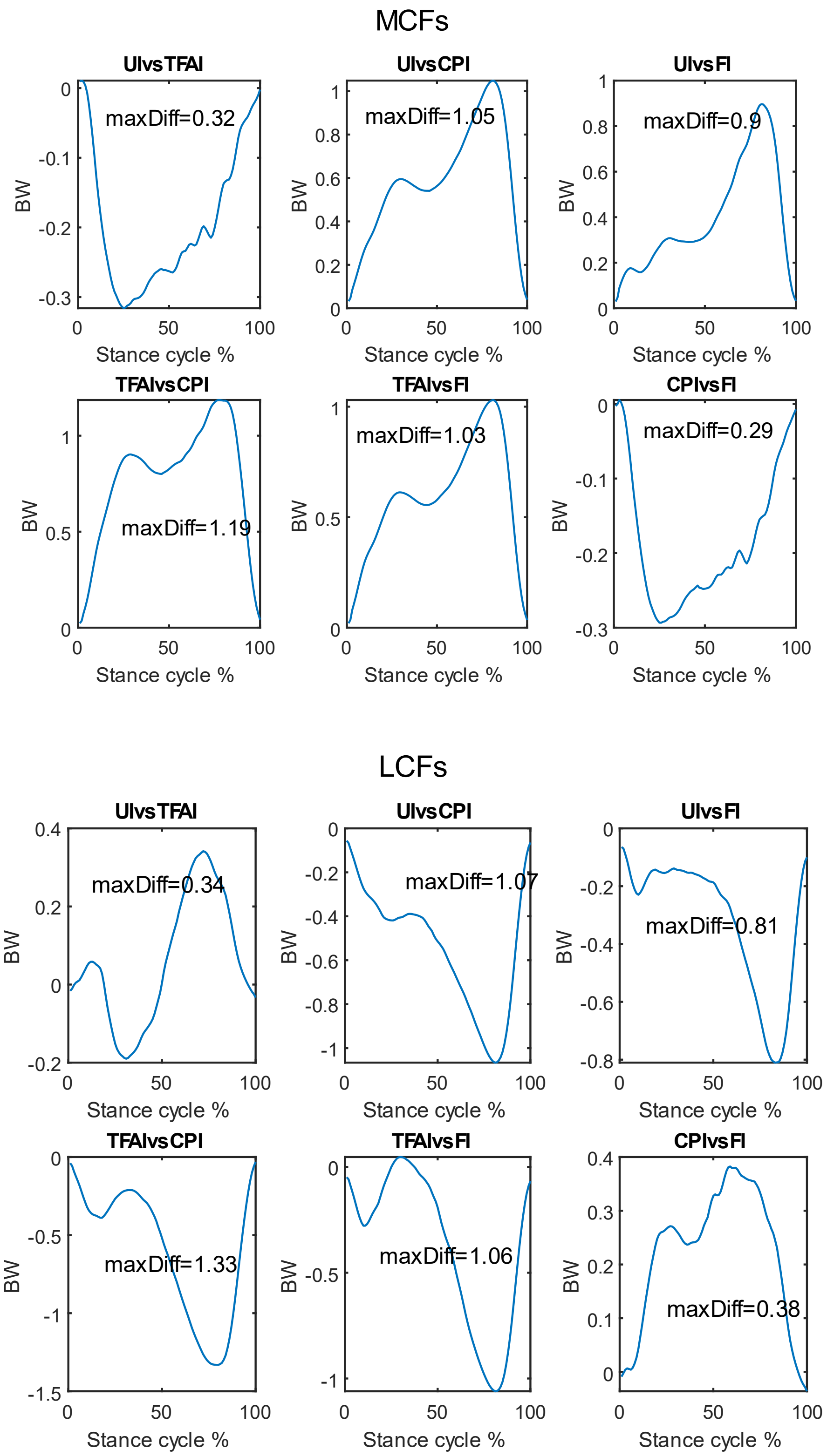

Figure 49: Mean differences among models during stair descending.

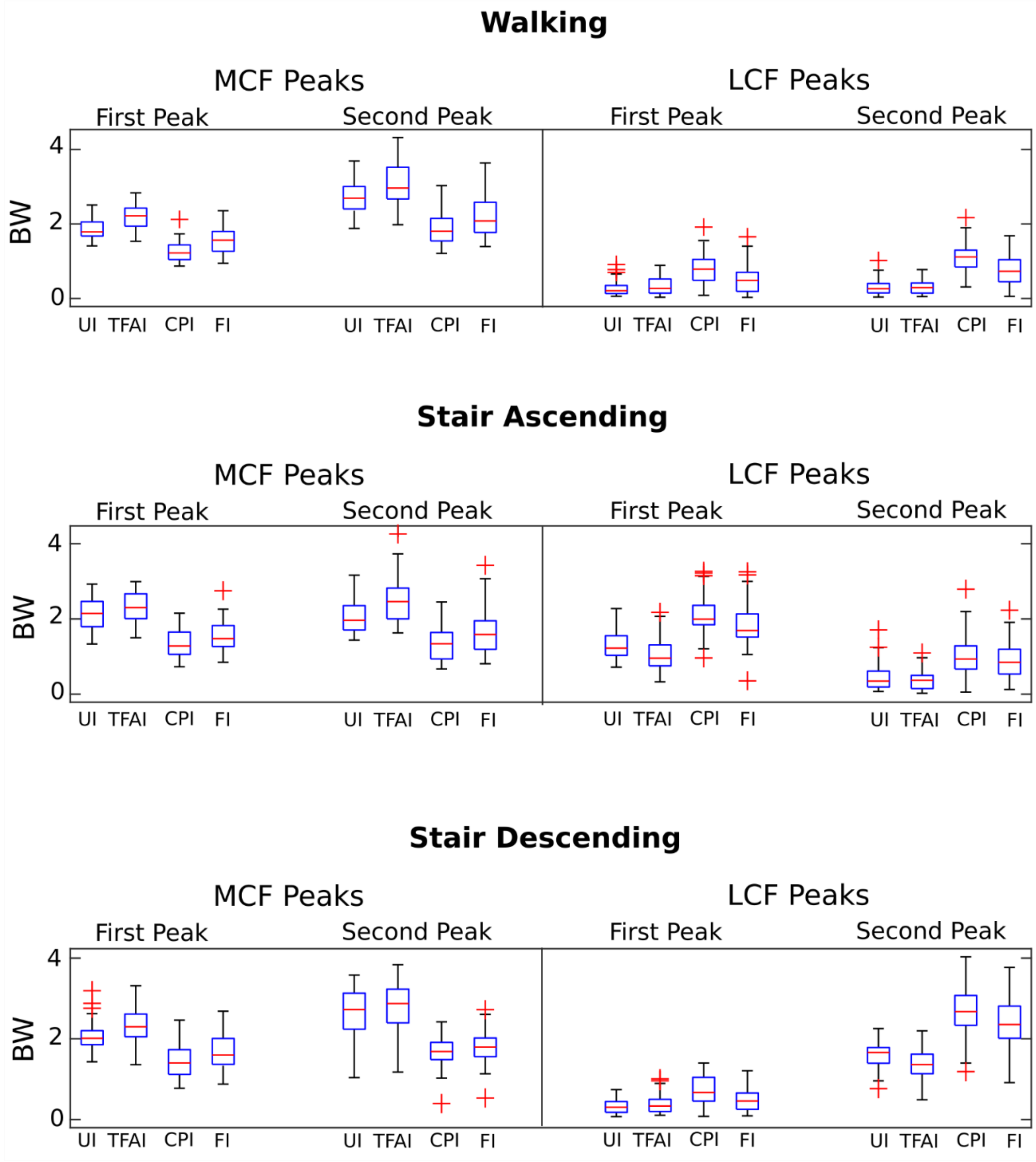

Figure 50: boxplot representation of the distributions of the first and second peak of MCFs and LCFs predicted by the 4 models for all motor tasks analyzed The plot shows the minimum, maximum, lower and higher quartiles and the median of the distributions considered. Outliers are shown as + marks.

Table 4: The values of the medians and the interquartile range associated with the distributions of the first and second force peaks of the MCFs and LCFs for all 3 tasks considered are reported here.

Walking

	Medial Contact Force				Lateral Contact Force			
	First Peak		Second Peak		First Peak		Second Peak	
	Median	IQR	Median	IQR	Median	IQR	Median	IQR
UI	1.79	0.38	2.69	0.60	0.21	0.22	0.26	0.25
TFAI	2.22	0.48	2.96	0.85	0.27	0.38	0.29	0.27
CPI	1.22	0.39	1.80	0.61	0.79	0.56	1.11	0.45
FI	1.57	0.53	2.08	0.81	0.48	0.51	0.73	0.59

Stair Ascending

	Medial Contact Force				Lateral Contact Force			
	First Peak		Second Peak		First Peak		Second Peak	
	Median	IQR	Median	IQR	Median	IQR	Median	IQR
UI	2.14	0.67	1.97	0.65	1.22	0.52	0.35	0.42
TFAI	2.30	0.66	2.46	0.82	0.95	0.56	0.37	0.35
CPI	1.28	0.59	1.34	0.70	1.99	0.51	0.93	0.62
FI	1.47	0.56	1.59	0.76	1.69	0.62	0.85	0.66

Stair Descending

	Medial Contact Force				Lateral Contact Force			
	First Peak		Second Peak		First Peak		Second Peak	
	Median	IQR	Median	IQR	Median	IQR	Median	IQR
UI	2.01	0.35	2.72	0.89	0.30	0.27	1.66	0.39
TFAI	2.30	0.56	2.87	0.84	0.34	0.30	1.36	0.48
CPI	1.40	0.61	1.69	0.42	0.67	0.59	2.67	0.74
FI	1.60	0.64	1.79	0.46	0.46	0.40	2.35	0.80

Table 5: p-values evaluated by Wilcoxon sign-rank test among all model pairs considered.

Walking

	Medial Contact Force		Lateral Contact Force	
	First Peak	Second Peak	First Peak	Second Peak
	p-values	p-values	p-values	p-values
UI vs TFAI	**0.000**	**0.001**	0.327	0.577
UI vs CPI	**0.000**	**0.000**	**0.000**	**0.000**
UI vs FI	**0.000**	**0.000**	**0.001**	**0.000**
TFAI vs CPI	**0.000**	**0.000**	**0.000**	**0.000**
TFAI vs FI	**0.000**	**0.000**	**0.014**	**0.000**
CPI vs FI	**0.000**	**0.002**	**0.001**	**0.000**

Stair Ascending

	Medial Contact Force		Lateral Contact Force	
	First Peak	Second Peak	First Peak	Second Peak
	p-values	p-values	p-values	p-values
UI vs TFAI	0.050	**0.001**	**0.002**	0.437
UI vs CPI	**0.000**	**0.000**	**0.000**	**0.000**
UI vs FI	**0.000**	**0.000**	**0.000**	**0.000**
TFAI vs CPI	**0.000**	**0.000**	**0.000**	**0.000**
TFAI vs FI	**0.000**	**0.000**	**0.000**	**0.000**
CPI vs FI	**0.014**	**0.004**	**0.013**	0.202

Stair Descending

	Medial Contact Force		Lateral Contact Force	
	First Peak	Second Peak	First Peak	Second Peak
	p-values	p-values	p-values	p-values
UI vs TFAI	**0.003**	0.339	0.655	**0.003**
UI vs CPI	**0.000**	**0.000**	**0.000**	**0.000**
UI vs FI	**0.001**	**0.000**	**0.026**	**0.000**
TFAI vs CPI	**0.000**	**0.000**	**0.000**	**0.000**
TFAI vs FI	**0.000**	**0.000**	0.094	**0.000**
CPI vs FI	**0.009**	0.128	**0.001**	0.032

Table 6: Differences between the medians of the distributions

Walking				
	Medial Contact Force		Lateral Contact Force	
	First Peak	Second Peak	First Peak	Second Peak
	Diff	Diff	Diff	Diff
UI vs TFAI	-0.43	-0.27	-0.06	-0.03
UI vs CPI	0.57	0.89	-0.58	-0.85
UI vs FI	0.22	0.61	-0.28	-0.47
TFAI vs CPI	0.99	1.16	-0.52	-0.83
TFAI vs FI	0.65	0.88	-0.21	-0.44
CPI vs FI	-0.34	-0.28	0.30	0.38

Stair Ascending				
	Medial Contact Force		Lateral Contact Force	
	First Peak	Second Peak	First Peak	Second Peak
	Diff	Diff	Diff	Diff
UI vs TFAI	-0.16	-0.49	0.27	-0.02
UI vs CPI	0.86	0.63	-0.77	-0.59
UI vs FI	0.67	0.38	-0.47	-0.50
TFAI vs CPI	1.02	1.12	-1.04	-0.57
TFAI vs FI	0.83	0.87	-0.74	-0.48
CPI vs FI	-0.19	-0.25	0.30	0.09

Stair Descending				
	Medial Contact Force		Lateral Contact Force	
	First Peak	Second Peak	First Peak	Second Peak
	Diff	Diff	Diff	Diff
UI vs TFAI	-0.29	-0.15	-0.03	0.30
UI vs CPI	0.61	1.04	-0.37	-1.01
UI vs FI	0.41	0.93	-0.15	-0.69
TFAI vs CPI	0.89	1.19	-0.33	-1.31
TFAI vs FI	0.70	1.08	-0.12	-0.99
CPI vs FI	-0.20	-0.11	0.21	0.32

4.2 Relationship between geometric parameters and KCFs

Regarding the relationship between TFA and MCFs, we found no significant correlations during walking and stair ascending, and weak significant correlations at both force peaks estimated by FI models during stair descending (R_{1st} = 0.309, R_{2nd}=0.312, fig. 51). Regarding TFA and LCFs, we found weak significant correlations only at the second force peak estimated by TFAI models during walking (R = -0.3) and stair ascending for both types of models considered (R_{TFAI} = -0.32, R_{FI}=-0.323).

Conversely, regarding the relationship between medial CPs and KCFs, we found moderate significant correlations with MCFs during walking and stair descending (-0.44 < R < -0.58), and weak to moderate significant correlations with LCFs during walking and stair descending (0.33 < R < 0.49), fig 52. We found no significant correlations between lateral CPs and KCFs (fig. 53).

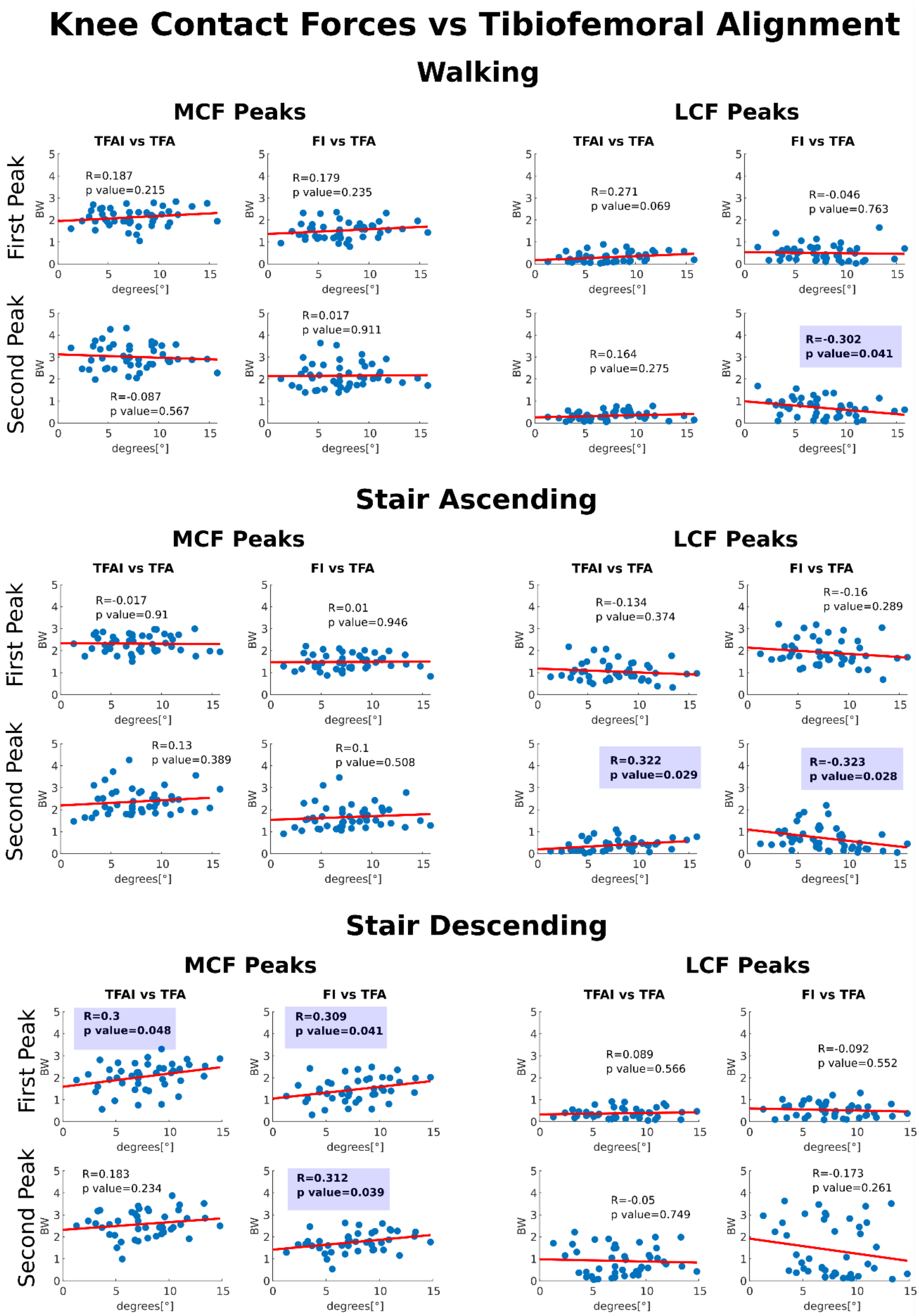

Figure 51: Relationship between TFA and MCFs in TFA informed models. R and p-values are reported as legends in the subplots. Significant correlation, when present, is marked with boldface type.

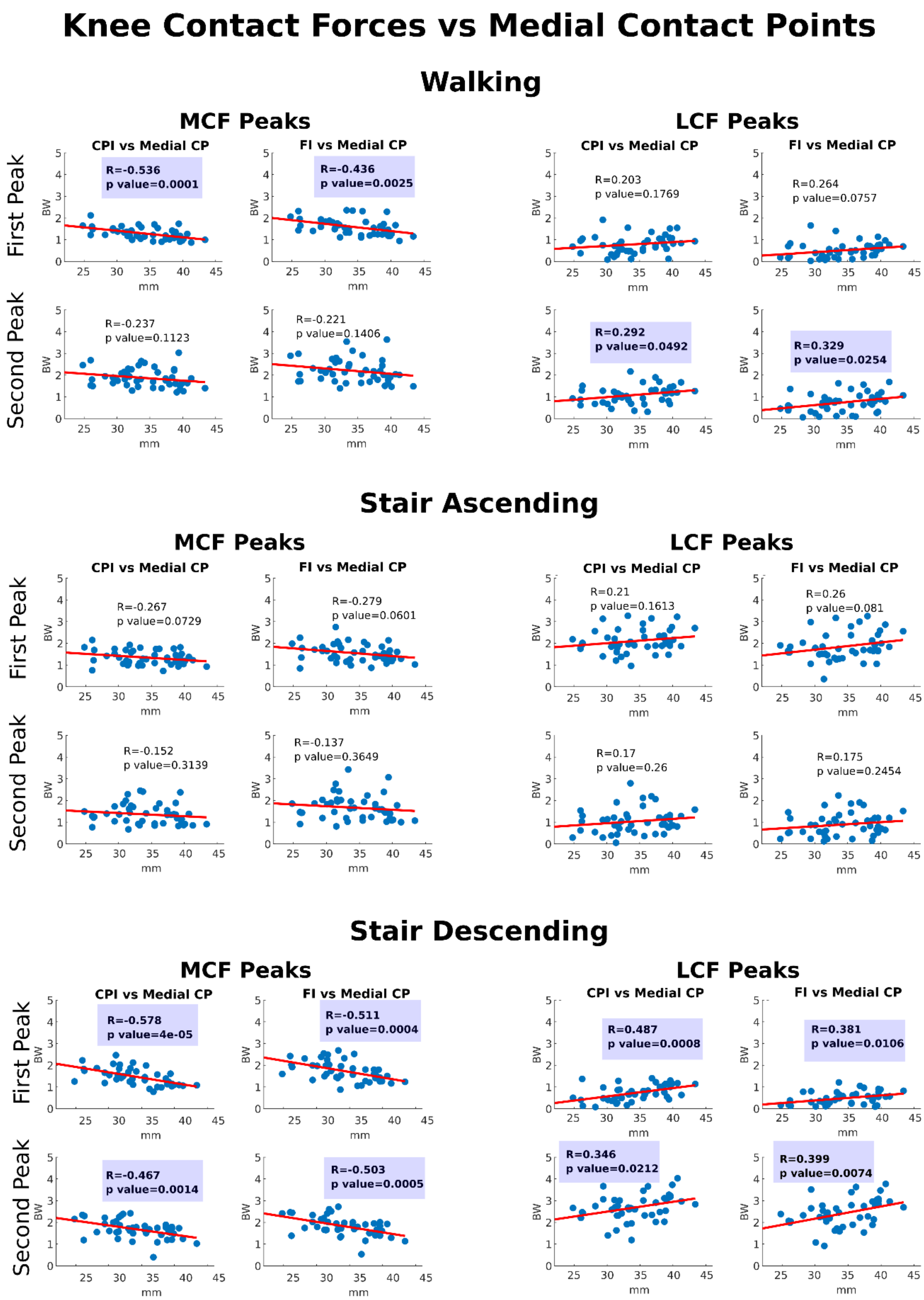

Figure 52: Relationship between both MCFs and LCFs and medial CPs location in CP informed models. R and p-values are reported as legends in the subplots. Significant correlation, when present, is marked with bold type.

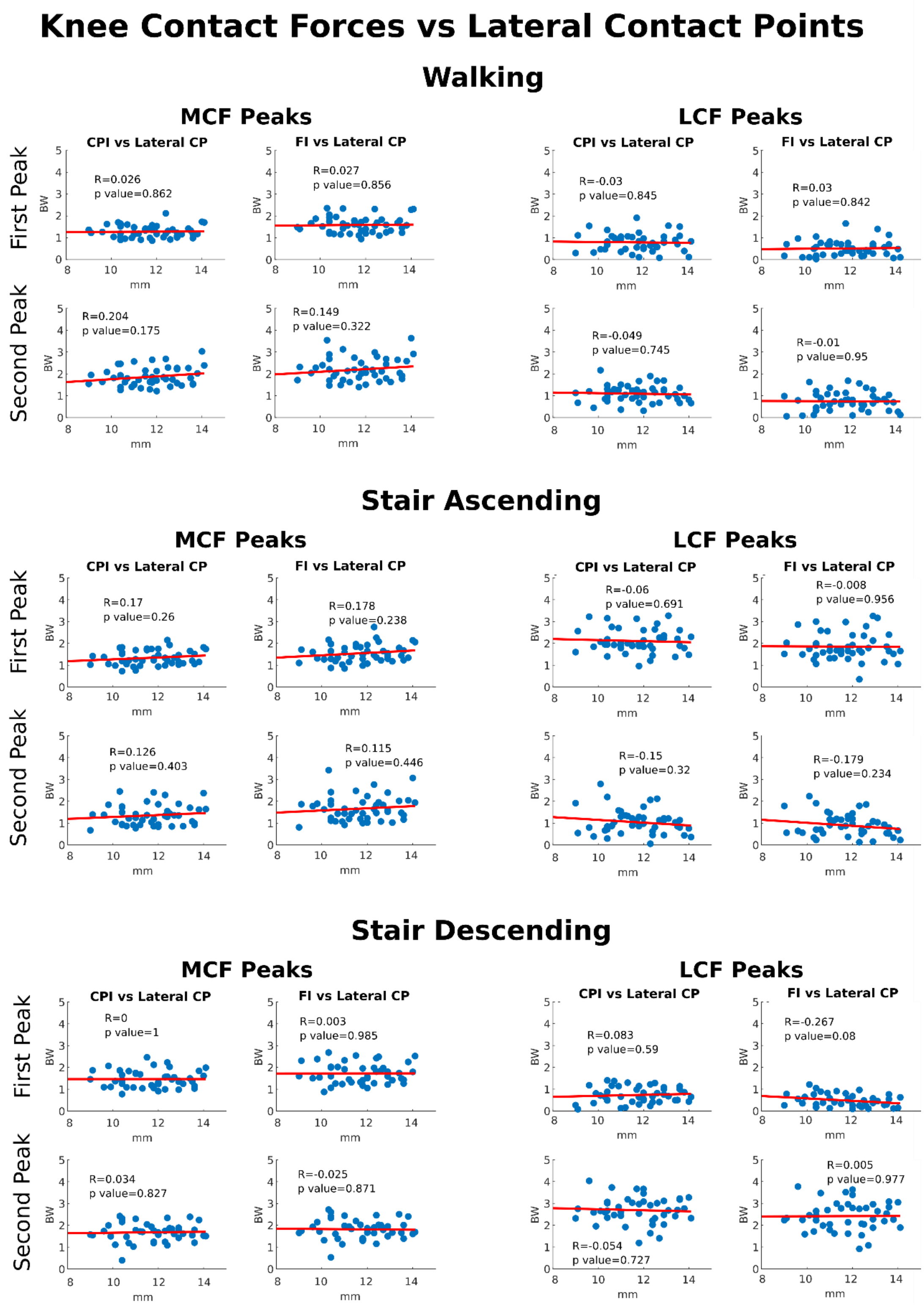

Figure 53: Relationship between both MCFs and LCFs and lateral CPs location in CP informed models. R and p-values are reported as legends in the subplots. Significant correlation, when present, is marked with bold type.

4.3 Indirect validation: EMG vs Activations

Muscle activations estimated using the UI and TFAI models show moderate to strong correlation ($0.351 < R < 0.971$) in all muscles examined for all tasks analyzed, except for a few cases. The Rectus Femoris muscle, during walking, shows moderate inverse correlation ($R=-0.431$, table 7) while during stair ascending no statistically significant correlation was found. During stair descending the gastrocnemius medial head did not find significant correlations, while the Tibialis Anterior muscle showed a strong inverse correlation ($R=-0.806$, table 9).

We found RMSE value in a range between 0.010 and 0.199 among all three tasks considered. It shows the discrepancy between observed data values and the correspondent estimated data. Low RMSE value were calculated, the Activations result similar to the EMGs.

It is not possible to evaluate which of the two models is the best to predict EMGs recorded but, overall, the two models showed very similar behaviour, having comparable RMSE values with respect to all muscles considered in all tasks.

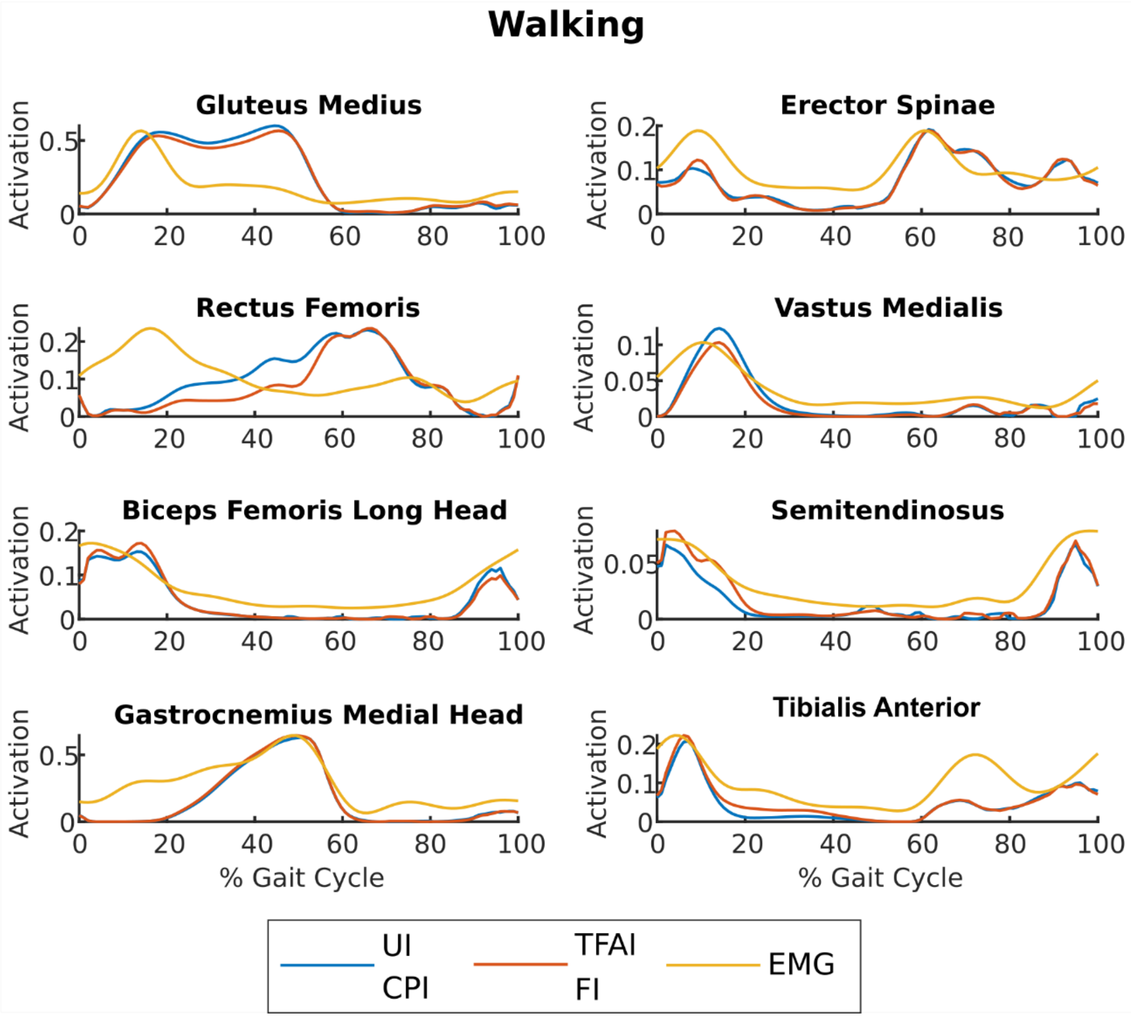

Figure 54: mean of EMGs recorded and activations estimated by TFAI and UI models during walking.

Table 7: table of R, p values and RMSEs evaluated between Activations signals and EMGs recorded during walking.

	Walking					
	UI			**TFAI**		
	R	p-values	RMSE	R	p-values	RMSE
Gluteus Medius	0.581	0.000	0.199	0.581	0.000	0.185
Erector Spinae	0.681	0.000	0.048	0.691	0.000	0.047
Rectus Femoris	-0.431	0.000	0.106	-0.426	0.000	0.109
Vastus Medialis	0.864	0.000	0.027	0.867	0.000	0.023
Biceps Femoris Long Head	0.914	0.000	0.030	0.890	0.000	0.038
Semitendinosus	0.912	0.000	0.014	0.906	0.000	0.017
Gastrocnemius Medial Head	0.909	0.000	0.146	0.914	0.000	0.148
Tibialis Anterior	0.791	0.000	0.057	0.785	0.000	0.058

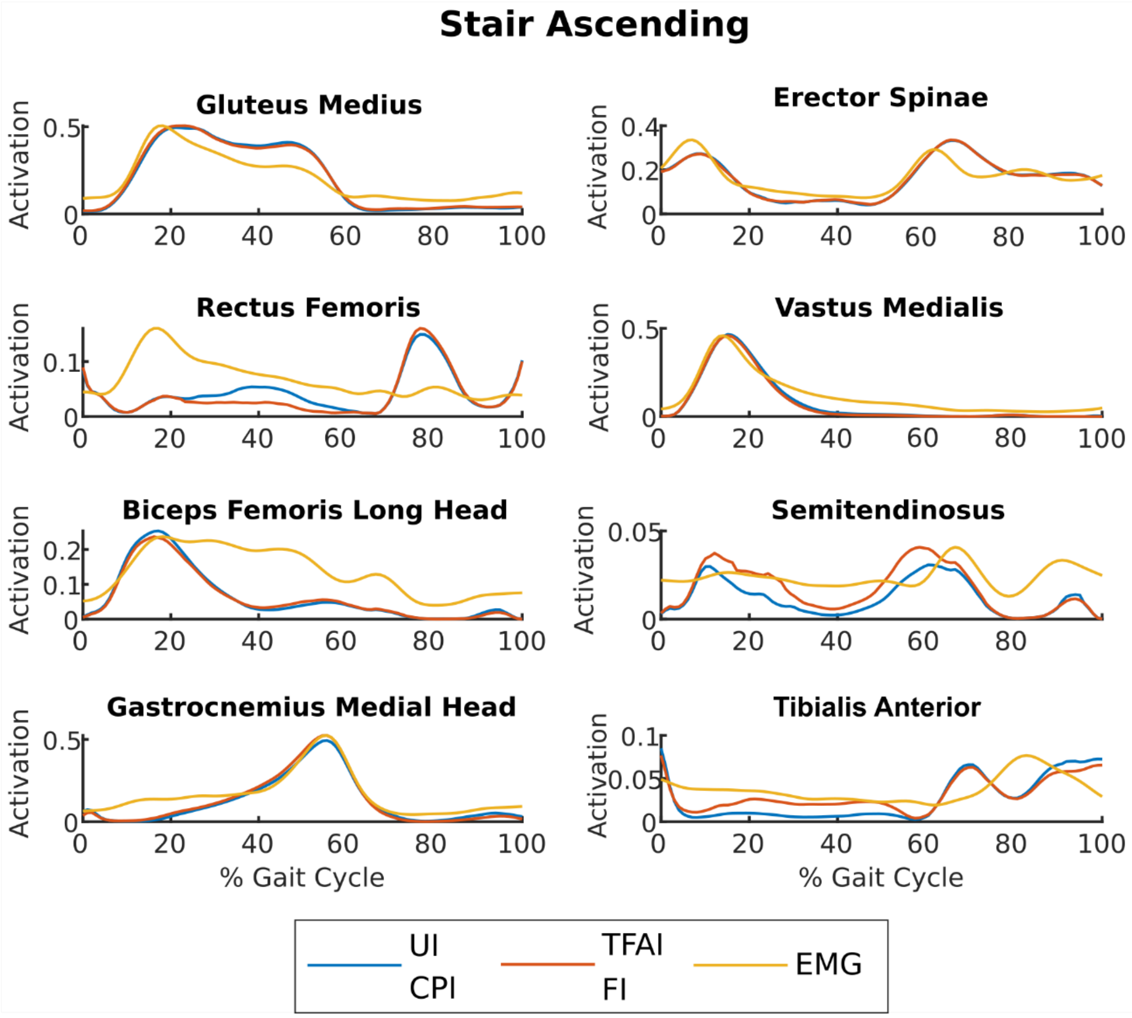

Figure 55: mean of EMGs recorded and activations estimated by TFAI and UI models during stair ascending.

Table 8: table of R, p values and RMSEs evaluated between Activations signals and EMGs recorded during stair ascending.

	Stair ascending					
	UI			**TFAI**		
	R	p-values	RMSE	R	p-values	RMSE
Gluteus Medius	0.931	0.000	0.082	0.944	0.000	0.074
Erector Spinae	0.858	0.000	0.045	0.857	0.000	0.045
Rectus Femoris	-0.175	0.081	0.055	-0.215	0.032	0.065
Vastus Medialis	0.977	0.000	0.050	0.975	0.000	0.053
Biceps Femoris Long Head	0.673	0.000	0.101	0.705	0.000	0.091
Semitendinosus	0.487	0.000	0.010	0.319	0.001	0.014
Gastrocnemius Medial Head	0.962	0.000	0.052	0.971	0.000	0.056
Tibialis Anterior	0.451	0.000	0.028	0.382	0.000	0.020

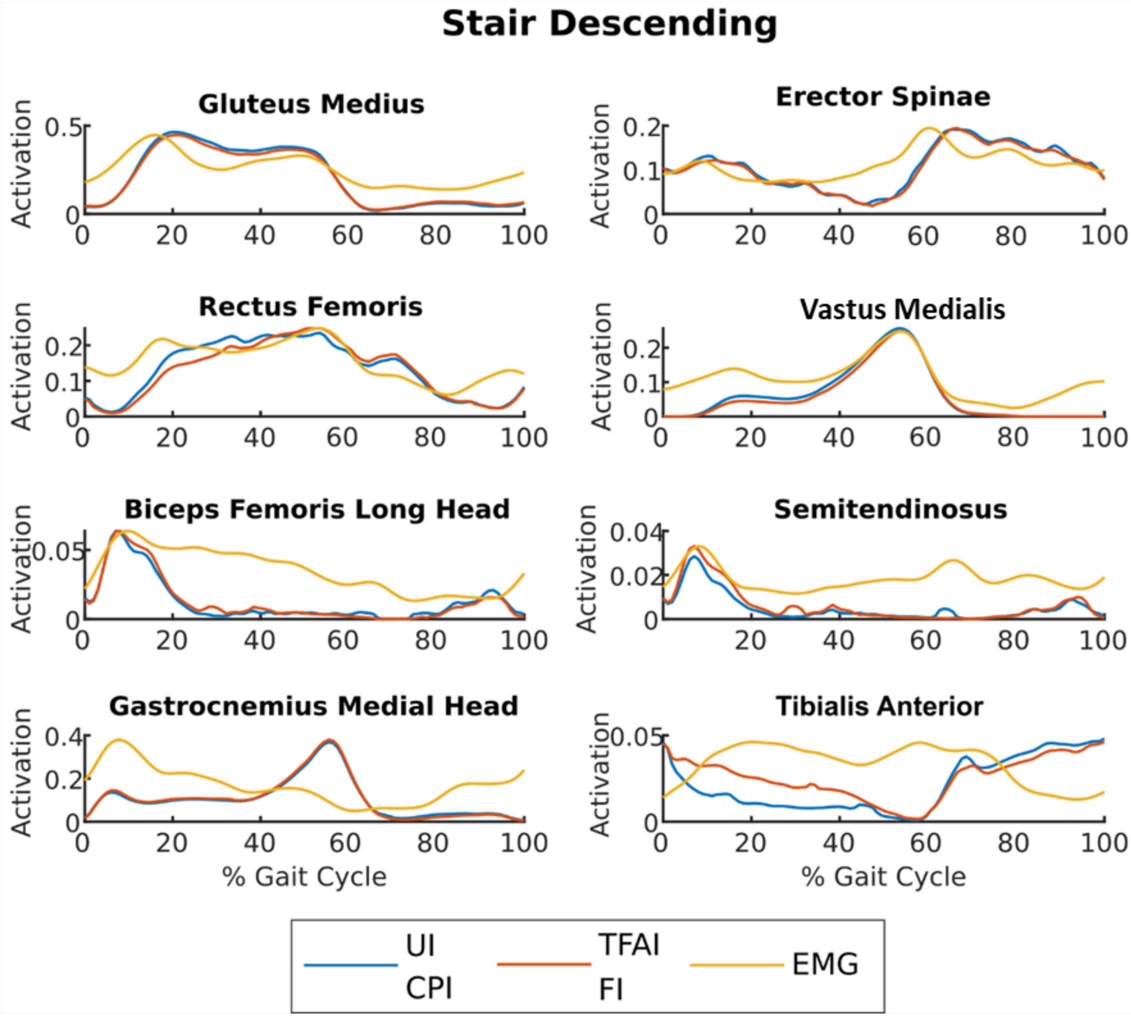

Figure 56: mean of EMGs recorded and activations estimated by TFAI and UI models during stair descending.

Table 9: table of R, p values and RMSEs evaluated between Activations signals and EMGs recorded during stair descending

	Stair Descending					
	UI			**TFAI**		
	R	p-values	RMSE	R	p-values	RMSE
Gluteus Medius	0.816	0.000	0.117	0.816	0.000	0.108
Erector Spinae	0.595	0.000	0.040	0.561	0.000	0.041
Rectus Femoris	0.775	0.000	0.052	0.716	0.000	0.061
Vastus Medialis	0.906	0.000	0.059	0.894	0.000	0.061
Biceps Femoris Long Head	0.531	0.000	0.027	0.626	0.000	0.026
Semitendinosus	0.657	0.000	0.012	0.562	0.000	0.014
Gastrocnemius Medial Head	-0.109	0.281	0.140	-0.078	0.442	0.146
Tibialis Anterior	-0.806	0.000	0.029	-0.719	0.000	0.023

.

Chapter 5

Discussion

The presence of non-physiological stresses may play an important role in the onset and progression of OA. Therefore, accurately characterizing these forces is crucial to assess possible interventions aimed at redistributing loads between the medial and lateral compartments of the knee. One such intervention is HTO, a surgical procedure that aims to realign the tibiofemoral axis to reduce joint load in the medial compartment. Musculoskeletal models are increasingly being used to evaluate joint reaction forces in the knee. Recent studies [35],[42],[43] have shown that that customizing the model using subject-specific geometric parameters such as TFA and CPs can improve the accuracy of force predictions. However, these studies were performed on a smaller cohort of patients than the one available for our study, and many did not estimate KCFs in motor tasks other than walking.

In this thesis work we used musculoskeletal modeling to investigate how CPs and TFA affect the determination of contact loads acting on the medial and lateral compartment of the knee during motor tasks of walking, stair ascending and stair descending. To do so, 50 patients with medial knee OA (K&L <3), previously enrolled for a clinical trial started at Rizzoli Orthopaedic Institute in Bologna aimed at determining effectiveness of HTO for improving the biomechanical environment of the knee joint, were examined. TFAs of the lower limb were determined on weight-bearing anteroposterior radiographs in static conditions. CPs were evaluated using a posteroanterior 45° knee flexion view (Rosenberg view) as the points at the minimum joint space width on the medial and lateral knee compartments.

CPs and TFA were both evaluated using HTO-Rplus, a software developed by the IT team of the BIC laboratory. Known personalization parameters, 4 different models per patient were made from Lerner's validated full-boy model [35]: an uninformed model, a tibiofemoral-informed model, a contact point informed model and finally a fully-informed model. To estimate the MCFs and LCFs, it was necessary to rely on the OpenSim environment, solving in this way the inverse kinematics and dynamics problem from the data obtained during the gait analysis sessions. For each model, 15 full simulations were performed (5 for each repetition of effected motor task), leading us to perform a total of 3000 total simulations and estimate the forces associated with the models of all 50 patients involved in the study. Each simulation involved several sequential steps performed in OpenSim: scaling, inverse kinematics, inverse dynamics, static optimization, and joint reaction analysis. The outputs of the joint reaction analysis were postprocessed in MATLAB to obtain the signals of interest. The outputs of the SO were postprocessed in MATLAB and then compared with the EMG signals recorded during the gait analysis sessions, to validate indirectly our models.

The prediction of medial and lateral knee contact forces was markedly affected by the introduction of TFA and CPs in the musculoskeletal models, and specifically CPs led to more marked variations in KCFs compared to TFA. In fact, our results show that the medial and lateral forces assessed by the different models have statistically significant differences in most part of each task cycle, except for the TFAI and UI models, which showed less differences across the task cycles. The introduction of TFA induces a medial shifting of the contact loads acting on the knee, increasing MCFs and decreasing LCFs. Model customizations using CPs induces an opposite behaviour, decreasing MCFs and increasing LCFs. When studying the distributions of the peaks, it is possible to see how this is also reflected in their amplitudes. In general, there are statistically significant differences for all models in each task analyzed, but the greatest difference was found between the TFAI and CPI models. CPs, among the two personalization parameters, introduce the greatest variation in force estimation. Analysing peak distributions, differences of the medians obtained with CPI models and UI models yields larger values than those obtained by making a difference between the medians of TFAI models and UI models. This allows us to say that CPs are the parameter that most influences the estimation of the knee reaction forces.

To understand which parameters had a higher correlation with the estimated forces, we focused on the correlations between the geometric parameters of model customization and the peak forces obtained. Regarding TFA, linear regressions were performed with force peaks estimated with the TFAI and FI models, the only ones customized with that parameter. Overall, a weak correlation was found in part of the motor tasks between TFA and force peaks considered for both LCFs and MCFs (fig. 51). Linear regressions showed no significant correlation between lateral CPs and KCFs. In contrast, the estimated MCFs show a moderate correlation with medial CPs in almost all motor tasks considered and a weak correlation between LCFs and medial CPs was found during walking and stair descending. The predicted knee contact forces were moderately correlated to the medial CPs, weakly correlated to TFA, and not correlated with lateral CPs. Therefore, medial CPs were highlighted as the parameters that correlate the most with the forces estimated through the custom models, even more than TFA. Overall, the CPs have proved to be the geometric parameter that most influences the force estimates.

The inverse validation process allowed to observe that the predictions of muscle activations obtained through the UI and TFAI models exhibit moderate to strong correlation with the EMG signals taken during the gait analysis sessions, with minor exceptions (table 7,8,9). Even the low RMSE values allow us to say that the models used let us to estimate muscular activations in satisfactory agreement with the EMGs across GC and during all the three tasks considered. We believe that, given the results obtained and reported in section 4.3, the predictions of the models can be considered valid with a good level of confidence.

Given the results obtained from peak analysis and correlations, it is possible to say that using the FI model may be the right choice to study the distribution of KCFs. CPs are found to be more correlated with KCFs, and this leads us to say that customization of baseline musculoskeletal models with this parameter and not just TFA is recommended. A FI model contains both types of customizations and allows to combine the effects introduced by TFA and CPs.

Prior to this work, several studies have been published that aimed to answer the same research questions.

First of all, we have to say that the way we decided to estimate geometric parameters from x-rays is not the only one to find TFA and CPs. A recent study by Zeighami et al. [38] aimed to calculate the knee contact point locations of both healthy subjects and those with osteoarthritis (OA) utilizing bi-planar X-ray images of the knee joint in squat positions. They found that OA subjects had medially located CPs, particularly in the lateral compartment. Also medial and lateral CPs evaluated by us using HTO-Rplus showed a similar behaviour. In other works the distance among medial and lateral CPs was fixed at 40 mm [35] or 50 mm [42] and then both CPs were shifted medially or laterally of the same quantity to perform perturbations and see how the prediction were influenced.

In some of these works, the relationship between TFA and estimated MCFs was investigated. Halder et al [34] showed that the MCFs were linearly correlated with the valgus TFA of the knee joint in five individuals with instrumented knee implants, results in contrast to the findings of our study. MCFs were increased by a larger varus and decreased by a more valgus alignment. Other works as the ones carried out by Kutzner et al. [33] and Trepczynski et al [41] showed a weak correlation instead in single support activities, as in our findings. Zeighami et al. [43], [44] in recent studies evaluated that there is no correlation between TFA and MCFs and LCFs, showing a more marked relationship with CPs instead.

Dumas et al. [63] realized musculoskeletal models informed with CPs trajectories. They compared MCFs and LCFs evaluated among healthy and OA and showed weak correlation between CPs trajectories and force estimated in OA patients. Zeighami et al [43], [44] showed instead a marked correlation between MCFs peaks and CP locations in a cohort of both OA patients and healthy subjects. The correlation between CPs and the resulting KCFs is still a topic debate in research utilizing flexible knee models.

Other studies evaluated the importance of the model personalization with TFA and CPs as we did, obtaining results similar to ours. Smith et al [52] investigated the role of TFA on KCFs in one patient to whom an instrumented knee implant was implanted. They made a musculoskeletal model of the patient under consideration and carried out a perturbation analysis to see how TFA affected the estimated forces. They found out that TFA affects the KCFs distribution among the two compartments: 4 deg varus and 4 deg valgus variation of the TFA leads to 17% and 23% changes in the first peak MCFs. Thelen et al. [64] find out that little variation of TFA as a personalization parameter alters the KCFs distribution by up to 12%, suggesting that the introduction of TFA has an important effect on force estimation and that not taking it into account may lead to overall force estimation bias. One of the Lerner et al [35] goals was to investigate how TFA and CPs affect the KCFs distribution predictions. Their results show that TFA and CPs were both important customization parameters to evaluate a correct prediction of

MCFs and LCFs and should be incorporated as customization parameters into a musculoskeletal model used to investigate this load distributions on the knee compartments. They also demonstrate that their FI model had the best prediction accuracy. Saliba et al [42] performed a study in which they implemented a perturbation of model customization parameters of a scaled models based on anthropometric characteristics of 23 patients with medial knee OA, with a view to quantifying the sensitivity of KCFs predictions with TFA and CPs. Their results show that MCFs increased, and lateral loads decreased, by between 3% and 6% BW for each degree of varus TFA perturbation. Shifting the medial CPs medially increased MCFs and decreased LCFs in a range of 1% and 4% of BW per millimeter.

The literature review highlights, however controversially, the link between TFA, CPs and model-estimated forces. A reason why we did not find a marked correlation between TFA and KCFs might be the fact that a good part of the studies conducted in this area are based on perturbation of personalization parameters but keeping the anthropometric characteristics of the models constant. On the other hand, we had a large patient cohort with high intra-subject variability of physical and anthropometric characteristics. The models we implemented are also subject to some limitations. There are only two subject-specific parameters implemented in our models, CPs and TFA, and it is possible to have additional parameters that have an important influence on the estimation of joint loads. There is also an uncertainty associated with the determinations of TFA and CPs. In fact, the way these are determined can lead to errors that affect the estimation of KCFs. Another aspect concerns the representation of the knee model as a 1 DOF joint in which the CPs appear to be defined only in the frontal plane and that their movement in the anteroposterior direction is not allowed. It is expected that their movement in the anteroposterior direction may have some effects on the determination of total forces but not on the distribution of loads among the knee compartments [36]. This type of modeling also involves that the contact points between the femur and tibia are represented as single points and thus disregard the fact that contact may occur in a distributed portion of bone. Other possible sources of uncertainty that may have affected the estimation of KCFs are, for example, the placement of markers during gait analysis sessions and all the modeling parameters used to build the starting musculoskeletal model (muscle geometry, maximum isometric force, body segments parameters...)

Chapter 6

Conclusions

The objectives of this thesis were twofold: to evaluate how geometric parameters of customization, such as TFA and CPs, influenced the prediction of joint reaction forces by quantifying the differences introduced, and to evaluate the correlation between these parameters and the peak forces obtained.

It has been demonstrated that the inclusion of customization parameters has a significant impact on the forces estimated by musculoskeletal models. Specifically, TFA personalization results in increased loads in the medial compartment, while the introduction of CPs leads to an opposite effect, increasing loads in the lateral compartment. By analyzing peak distributions, it was possible to determine that the largest contribution to the variation of predicted forces is introduced through the customization of models using CPs.

The results indicate that there is no clear correlation between TFA and the forces estimated by the personalized models and complete absence of correlation between lateral CPs and forces may be attributed to the range of measurements obtained from X-ray images, which all fell within a restricted interval. However, medial CPs were found to be the most influential parameter in force estimation. Therefore, we can conclude that our model customization should include CPs in addition to TFA. Moreover, the results obtained from indirect model validation, which compared activations and EMGs, provide a certain level of confidence that the estimated forces from our models are consistent.

The absence of a strong correlation between TFA and MCF, as reported in the literature and supported by our findings, does not necessarily negate the potential benefits of HTO intervention in mitigating the progression of OA. However, our study highlights the importance of customizing CPs in musculoskeletal models to obtain accurate force estimations. Neglecting the inclusion of CPs during model customization may compromise the accuracy of force values and should be avoided.

Possible future developments could be based on:

- Understanding how CPs affect the course of medial unicompartmental knee OA and how these parameters can be used to find new techniques to slow down the disease. Finding a way to establish a connection between CPs and identifiable clinical parameters related to OA development would be valuable. Currently, the varus angle is the primary parameter considered in this context.
- Defining an accurate measurement protocol for TFA, but especially for CPs, to lower the sensitivity of measurements as the operator estimates their positions.
- Making a comparison with the assessed KCFs present in post-operated patients. This would provide insight into whether tibiofemoral realignment has indeed affected the distribution of joint loads.
- Introducing a clinical examination to test maximal isometric contraction in the cohort of selected patients. This would allow us to be more consistent during indirect model validation by comparing EMGs and activations.

References

[1] S. M. Haley *et al.*, 'Late Life Function and Disability Instrument: II. Development and Evaluation of the Function Component', *J. Gerontol. A. Biol. Sci. Med. Sci.*, vol. 57, no. 4, pp. M217–M222, Apr. 2002, doi: 10.1093/gerona/57.4.M217.

[2] D. J. Hunter and S. Bierma-Zeinstra, 'Osteoarthritis', *The Lancet*, vol. 393, no. 10182, pp. 1745–1759, Apr. 2019, doi: 10.1016/S0140-6736(19)30417-9.

[3] A. M. Schwartz, K. X. Farley, G. N. Guild, and T. L. Bradbury, 'Projections and Epidemiology of Revision Hip and Knee Arthroplasty in the United States to 2030', *J. Arthroplasty*, vol. 35, no. 6, pp. S79–S85, Jun. 2020, doi: 10.1016/j.arth.2020.02.030.

[4] S. M. Kurtz *et al.*, 'International survey of primary and revision total knee replacement', *Int. Orthop.*, vol. 35, no. 12, pp. 1783–1789, Dec. 2011, doi: 10.1007/s00264-011-1235-5.

[5] P. Gerus *et al.*, 'Subject-specific knee joint geometry improves predictions of medial tibiofemoral contact forces', *J. Biomech.*, vol. 46, no. 16, pp. 2778–2786, Nov. 2013, doi: 10.1016/j.jbiomech.2013.09.005.

[6] Z. F. Lerner, M. S. DeMers, S. L. Delp, and R. C. Browning, 'How tibiofemoral alignment and contact locations affect predictions of medial and lateral tibiofemoral contact forces', *J. Biomech.*, vol. 48, no. 4, pp. 644–650, Feb. 2015, doi: 10.1016/j.jbiomech.2014.12.049.

[7] S. Meireles, N. D. Reeves, R. K. Jones, C. R. Smith, D. G. Thelen, and I. Jonkers, 'Patients With Medial Knee Osteoarthritis Reduce Medial Knee Contact Forces by Altering Trunk Kinematics, Progression Speed, and Stepping Strategy During Stair Ascent and Descent: A Pilot Study', *J. Appl. Biomech.*, vol. 35, no. 4, pp. 280–289, Aug. 2019, doi: 10.1123/jab.2017-0159.

[8] P. D. B. Price, C. Gissane, and D. J. Cleather, 'The influence of pain on tibiofemoral joint contact force and muscle forces in knee osteoarthritis patients during stair ascent', *Eng. Rep.*, vol. 2, no. 9, Sep. 2020, doi: 10.1002/eng2.12227.

[9] P. S. Chatra, 'Bursae around the knee joints', *Indian J. Radiol. Imaging*, vol. 22, no. 01, pp. 27–30, Jan. 2012, doi: 10.4103/0971-3026.95400.

[10] A. Turkiewicz *et al.*, ‘Current and future impact of osteoarthritis on health care: a population-based study with projections to year 2032’, *Osteoarthritis Cartilage*, vol. 22, no. 11, pp. 1826–1832, Nov. 2014, doi: 10.1016/j.joca.2014.07.015.

[11] J. H. Kellgren and J. S. Lawrence, ‘RADIOLOGICAL ASSESSMENT OF OSTEO-ARTHROSIS’, *Ann. Rheum. Dis.*.

[12] M. D. Kohn, A. A. Sassoon, and N. D. Fernando, ‘Classifications in Brief: Kellgren-Lawrence Classification of Osteoarthritis’, *Clin. Orthop.*, vol. 474, no. 8, pp. 1886–1893, Aug. 2016, doi: 10.1007/s11999-016-4732-4.

[13] D. T. Felson, ‘Osteoarthritis as a disease of mechanics’, *Osteoarthritis Cartilage*, vol. 21, no. 1, pp. 10–15, Jan. 2013, doi: 10.1016/j.joca.2012.09.012.

[14] A. Teichtahl, ‘Abnormal biomechanics: a precursor or result of knee osteoarthritis?’, *Br. J. Sports Med.*, vol. 37, no. 4, pp. 289–290, Aug. 2003, doi: 10.1136/bjsm.37.4.289.

[15] S. Meireles *et al.*, ‘Knee contact forces are not altered in early knee osteoarthritis’, *Gait Posture*, vol. 45, pp. 115–120, Mar. 2016, doi: 10.1016/j.gaitpost.2016.01.016.

[16] A. W-Dahl, S. Toksvig-Larsen, and E. M. Roos, ‘Association between knee alignment and knee pain in patients surgically treated for medial knee osteoarthritis by high tibial osteotomy. A one year follow-up study’, *BMC Musculoskelet. Disord.*, vol. 10, no. 1, p. 154, Dec. 2009, doi: 10.1186/1471-2474-10-154.

[17] M. B. Collier, C. A. Engh, J. P. McAuley, and G. A. Engh, ‘Factors Associated with the Loss of Thickness of Polyethylene Tibial Bearings After Knee Arthroplasty’:, *J. Bone Jt. Surg.*, vol. 89, no. 6, pp. 1306–1314, Jun. 2007, doi: 10.2106/JBJS.F.00667.

[18] A. Srivastava, G. Y. Lee, N. Steklov, C. W. Colwell, K. A. Ezzet, and D. D. D’Lima, ‘Effect of tibial component varus on wear in total knee arthroplasty’, *The Knee*, vol. 19, no. 5, pp. 560–563, Oct. 2012, doi: 10.1016/j.knee.2011.11.003.

[19] A. Guermazi *et al.*, ‘Prevalence of abnormalities in knees detected by MRI in adults without knee osteoarthritis: population based observational study (Framingham Osteoarthritis Study)’, *BMJ*, vol. 345, no. aug29 1, pp. e5339–e5339, Aug. 2012, doi: 10.1136/bmj.e5339.

[20] K. Rönn, N. Reischl, E. Gautier, and M. Jacobi, ‘Current Surgical Treatment of Knee Osteoarthritis’, *Arthritis*, vol. 2011, pp. 1–9, Apr. 2011, doi: 10.1155/2011/454873.

[21] A. Neuprez *et al.*, ‘Total joint replacement improves pain, functional quality of life, and health utilities in patients with late-stage knee and hip osteoarthritis for up to 5 years’, *Clin. Rheumatol.*, vol. 39, no. 3, pp. 861–871, Mar. 2020, doi: 10.1007/s10067-019-04811-y.

[22] S. L. Delp, J. P. Loan, M. G. Hoy, F. E. Zajac, E. L. Topp, and J. M. Rosen, ‘An interactive graphics-based model of the lower extremity to study orthopaedic

surgical procedures', *IEEE Trans Biomed Eng*, vol. 37, no. 8, pp. 757–767, Aug. 1990.

[23] S. L. Delp and J. P. Loan, 'A computational framework for simulating and analyzing human and animal movement', *Comput. Sci. Eng.*, vol. 2, no. 5, pp. 46–55, Oct. 2000, doi: 10.1109/5992.877394.

[24] A. D. Sylvester, S. G. Lautzenheiser, and P. A. Kramer, 'A review of musculoskeletal modelling of human locomotion', *Interface Focus*, vol. 11, no. 5, p. 20200060, Oct. 2021, doi: 10.1098/rsfs.2020.0060.

[25] Hicks, Jennifer L et al., '"Is my model good enough? Best practices for verification and validation of musculoskeletal models and simulations of movement."', *J. Biomech. Eng.*, vol. 137, no. 2 (2015): 020905, doi: 10.1115/1.4029304.

[26] B. J. Fregly *et al.*, 'Grand challenge competition to predict in vivo knee loads: GRAND CHALLENGE COMPETITION', *J. Orthop. Res.*, vol. 30, no. 4, pp. 503–513, Apr. 2012, doi: 10.1002/jor.22023.

[27] D. Zhao, S. A. Banks, D. D. D'Lima, C. W. Colwell, and B. J. Fregly, 'In vivo medial and lateral tibial loads during dynamic and high flexion activities', *J. Orthop. Res.*, vol. 25, no. 5, pp. 593–602, May 2007, doi: 10.1002/jor.20362.

[28] H. J. Kim, J. W. Fernandez, M. Akbarshahi, J. P. Walter, B. J. Fregly, and M. G. Pandy, 'Evaluation of predicted knee-joint muscle forces during gait using an instrumented knee implant', *J. Orthop. Res.*, vol. 27, no. 10, pp. 1326–1331, Oct. 2009, doi: 10.1002/jor.20876.

[29] D. Kumar, K. T. Manal, and K. S. Rudolph, 'Knee joint loading during gait in healthy controls and individuals with knee osteoarthritis', *Osteoarthritis Cartilage*, vol. 21, no. 2, pp. 298–305, Feb. 2013, doi: 10.1016/j.joca.2012.11.008.

[30] A. Trepczynski, I. Kutzner, G. Bergmann, W. R. Taylor, and M. O. Heller, 'Modulation of the Relationship Between External Knee Adduction Moments and Medial Joint Contact Forces Across Subjects and Activities: EAM as a Measure of In Vivo Contact Forces', *Arthritis Rheumatol.*, vol. 66, no. 5, pp. 1218–1227, May 2014, doi: 10.1002/art.38374.

[31] I. Kutzner, A. Trepczynski, M. O. Heller, and G. Bergmann, 'Knee Adduction Moment and Medial Contact Force – Facts about Their Correlation during Gait', *PLoS ONE*, vol. 8, no. 12, p. e81036, Dec. 2013, doi: 10.1371/journal.pone.0081036.

[32] J. P. Walter, N. Korkmaz, B. J. Fregly, and M. G. Pandy, 'Contribution of tibiofemoral joint contact to net loads at the knee in gait: CONTRIBUTION OF TIBIOFEMORAL JOINT CONTACT', *J. Orthop. Res.*, vol. 33, no. 7, pp. 1054–1060, Jul. 2015, doi: 10.1002/jor.22845.

[33] I. Kutzner, A. Bender, J. Dymke, G. Duda, P. von Roth, and G. Bergmann, 'Mediolateral force distribution at the knee joint shifts across activities and is driven

by tibiofemoral alignment', *Bone Jt. J.*, vol. 99-B, no. 6, pp. 779–787, Jun. 2017, doi: 10.1302/0301-620X.99B6.BJJ-2016-0713.R1.

[34] A. Halder, I. Kutzner, F. Graichen, B. Heinlein, A. Beier, and G. Bergmann, 'Influence of Limb Alignment on Mediolateral Loading in Total Knee Replacement: In Vivo Measurements in Five Patients', *J. Bone Jt. Surg.*, vol. 94, no. 11, pp. 1023–1029, Jun. 2012, doi: 10.2106/JBJS.K.00927.

[35] Z. F. Lerner, M. S. DeMers, S. L. Delp, and R. C. Browning, 'How tibiofemoral alignment and contact locations affect predictions of medial and lateral tibiofemoral contact forces', *J. Biomech.*, vol. 48, no. 4, pp. 644–650, Feb. 2015, doi: 10.1016/j.jbiomech.2014.12.049.

[36] C. M. Saliba, S. C. E. Brandon, and K. J. Deluzio, 'Sensitivity of medial and lateral knee contact force predictions to frontal plane alignment and contact locations', *J. Biomech.*, vol. 57, pp. 125–130, May 2017, doi: 10.1016/j.jbiomech.2017.03.005.

[37] S. Van Rossom *et al.*, 'The influence of knee joint geometry and alignment on the tibiofemoral load distribution: A computational study', *The Knee*, vol. 26, no. 4, pp. 813–823, Aug. 2019, doi: 10.1016/j.knee.2019.06.002.

[38] A. Zeighami *et al.*, 'Tibio-femoral joint contact in healthy and osteoarthritic knees during quasi-static squat: A bi-planar X-ray analysis', *J. Biomech.*, vol. 53, pp. 178–184, Feb. 2017, doi: 10.1016/j.jbiomech.2017.01.015.

[39] M. S. Kim, I. J. Koh, K. Y. Choi, B. S. Kim, and Y. In, 'Changes in joint space width over time and risk factors for deterioration of joint space width after medial opening-wedge high tibial osteotomy', *Arch. Orthop. Trauma Surg.*, vol. 142, no. 10, pp. 2513–2524, Mar. 2021, doi: 10.1007/s00402-021-03876-2.

[40] Y. Miura *et al.*, 'Difference in the joint space of the medial knee compartment between full extension and Rosenberg weight-bearing radiographs', *Eur. Radiol.*, vol. 32, no. 3, pp. 1429–1437, Mar. 2022, doi: 10.1007/s00330-021-08253-6.

[41] A. Trepczynski *et al.*, 'Dynamic Knee Joint Line Orientation Is Not Predictive of Tibio-Femoral Load Distribution During Walking', *Front. Bioeng. Biotechnol.*, vol. 9, p. 754715, Nov. 2021, doi: 10.3389/fbioe.2021.754715.

[42] C. M. Saliba, S. C. E. Brandon, and K. J. Deluzio, 'Sensitivity of medial and lateral knee contact force predictions to frontal plane alignment and contact locations', *J. Biomech.*, vol. 57, pp. 125–130, May 2017, doi: 10.1016/j.jbiomech.2017.03.005.

[43] A. Zeighami, R. Dumas, and R. Aissaoui, 'Knee loading in OA subjects is correlated to flexion and adduction moments and to contact point locations', *Sci. Rep.*, vol. 11, no. 1, p. 8594, Dec. 2021, doi: 10.1038/s41598-021-87978-2.

[44] A. Zeighami, R. Aissaoui, and R. Dumas, 'Knee medial and lateral contact forces in a musculoskeletal model with subject-specific contact point trajectories', *J. Biomech.*, vol. 69, pp. 138–145, Mar. 2018, doi: 10.1016/j.jbiomech.2018.01.021.

[45] P. D. B. Price, C. Gissane, and D. J. Cleather, ‘The influence of pain on tibiofemoral joint contact force and muscle forces in knee osteoarthritis patients during stair ascent’, *Eng. Rep.*, vol. 2, no. 9, Sep. 2020, doi: 10.1002/eng2.12227.

[46] N. Marques Luís and R. Varatojo, ‘Radiological assessment of lower limb alignment’, *EFORT Open Rev.*, vol. 6, no. 6, pp. 487–494, Jun. 2021, doi: 10.1302/2058-5241.6.210015.

[47] M. Marsh *et al.*, ‘Differences between X-ray and MRI-determined knee cartilage thickness in weight-bearing and non-weight-bearing conditions’, *Osteoarthritis Cartilage*, vol. 21, no. 12, pp. 1876–1885, Dec. 2013, doi: 10.1016/j.joca.2013.09.006.

[48] A. Leardini, Z. Sawacha, G. Paolini, S. Ingrosso, R. Nativo, and M. G. Benedetti, ‘A new anatomically based protocol for gait analysis in children’, *Gait Posture*, vol. 26, no. 4, pp. 560–571, Oct. 2007, doi: 10.1016/j.gaitpost.2006.12.018.

[49] H. Tankisi *et al.*, ‘Standards of instrumentation of EMG’, *Clin. Neurophysiol.*, vol. 131, no. 1, pp. 243–258, Jan. 2020, doi: 10.1016/j.clinph.2019.07.025.

[50] L. Schmid, T. Klotz, T. Siebert, and O. Röhrle, ‘Characterization of Electromechanical Delay Based on a Biophysical Multi-Scale Skeletal Muscle Model’, *Front. Physiol.*, vol. 10, p. 1270, Oct. 2019, doi: 10.3389/fphys.2019.01270.

[51] A. Nordez, T. Gallot, S. Catheline, A. Guével, C. Cornu, and F. Hug, ‘Electromechanical delay revisited using very high frame rate ultrasound’, *J. Appl. Physiol.*, vol. 106, no. 6, pp. 1970–1975, Jun. 2009, doi: 10.1152/japplphysiol.00221.2009.

[52] J. T. Hopkins, J. B. Feland, and I. Hunter, ‘A COMPARISON OF VOLUNTARY AND INVOLUNTARY MEASURES OF ELECTROMECHANICAL DELAY’, *Int. J. Neurosci.*, vol. 117, no. 5, pp. 597–604, Jan. 2007, doi: 10.1080/00207450600773764.

[53] J. Troy Blackburn, D. R. Bell, M. F. Norcross, J. D. Hudson, and L. A. Engstrom, ‘Comparison of hamstring neuromechanical properties between healthy males and females and the influence of musculotendinous stiffness’, *J. Electromyogr. Kinesiol.*, vol. 19, no. 5, pp. e362–e369, Oct. 2009, doi: 10.1016/j.jelekin.2008.08.005.

[54] J.-F. Grosset, J. Piscione, D. Lambertz, and C. Pérot, ‘Paired changes in electromechanical delay and musculo-tendinous stiffness after endurance or plyometric training’, *Eur. J. Appl. Physiol.*, vol. 105, no. 1, pp. 131–139, Jan. 2009, doi: 10.1007/s00421-008-0882-8.

[55] F. Ateş, B. L. Davies, S. Chopra, K. Coleman-Wood, W. Litchy, and K. R. Kaufman, ‘Intramuscular Pressure of Human Tibialis Anterior Muscle Reflects in vivo Muscular Activity’, *Front. Physiol.*, vol. 10, p. 196, Mar. 2019, doi: 10.3389/fphys.2019.00196.

[56] M. Żuk, M. Syczewska, and C. Pezowicz, ‘Use of the surface electromyography for a quantitative trend validation of estimated muscle forces’, *Biocybern. Biomed. Eng.*, vol. 38, no. 2, pp. 243–250, 2018, doi: 10.1016/j.bbe.2018.02.001.

[57] R. Akhundov *et al.*, ‘Is subject-specific musculoskeletal modelling worth the extra effort or is generic modelling worth the shortcut?’, *PLOS ONE*, vol. 17, no. 1, p. e0262936, Jan. 2022, doi: 10.1371/journal.pone.0262936.

[58] M. S. DeMers, S. Pal, and S. L. Delp, ‘Changes in tibiofemoral forces due to variations in muscle activity during walking: TIBIOFEMORAL FORCES AND MUSCLE ACTIVITY’, *J. Orthop. Res.*, vol. 32, no. 6, pp. 769–776, Jun. 2014, doi: 10.1002/jor.22601.

[59] F. C. Anderson and M. G. Pandy, ‘A Dynamic Optimization Solution for Vertical Jumping in Three Dimensions’, *Comput. Methods Biomech. Biomed. Engin.*, vol. 2, no. 3, pp. 201–231, Jan. 1999, doi: 10.1080/10255849908907988.

[60] J. Ashburner, ‘SPM: A history’, *NeuroImage*, vol. 62, no. 2, pp. 791–800, Aug. 2012, doi: 10.1016/j.neuroimage.2011.10.025.

[61] T. C. Pataky, ‘One-dimensional statistical parametric mapping in Python’, *Comput. Methods Biomech. Biomed. Engin.*, vol. 15, no. 3, pp. 295–301, Mar. 2012, doi: 10.1080/10255842.2010.527837.

[62] T. C. Pataky, M. A. Robinson, and J. Vanrenterghem, ‘Vector field statistical analysis of kinematic and force trajectories’, *J. Biomech.*, vol. 46, no. 14, pp. 2394–2401, Sep. 2013, doi: 10.1016/j.jbiomech.2013.07.031.

[63] R. Dumas, A. Zeighami, and R. Aissaoui, ‘Knee Medial and Lateral Contact Forces Computed Along Subject-Specific Contact Point Trajectories of Healthy Volunteers and Osteoarthritic Patients’, in *Computer Methods, Imaging and Visualization in Biomechanics and Biomedical Engineering*, vol. 36, G. A. Ateshian, K. M. Myers, and J. M. R. S. Tavares, Eds. Cham: Springer International Publishing, 2020, pp. 457–463. doi: 10.1007/978-3-030-43195-2_36.

[64] D. G. Thelen, K. Won Choi, and A. M. Schmitz, ‘Co-Simulation of Neuromuscular Dynamics and Knee Mechanics During Human Walking’, *J. Biomech. Eng.*, vol. 136, no. 2, p. 021033, Feb. 2014, doi: 10.1115/1.4026358.

[65] R. Barone, V. Benagiano, F. Bucchieri, C. Campanella, F. Cappello, and F. Carini, *Anatomia Umana, Basi Anatomiche per la Semiotica*, 1st ed. EdiSES edizioni.

List of figures

List of tables